CONSTITUTIVE MODELING AND EXPERIMENTAL IDENTIFICATION OF MATERIAL PARAMETERS OF VISCOELASTIC MATERIALS BY VARIABLE ORDER NON-INTEGER DERIVATIVES

A THESIS SUBMITTED TO
THE GRADUATE SCHOOL OF NATURAL AND APPLIED SCIENCES
OF
MIDDLE EAST TECHNICAL UNIVERSITY

BY

MUHAMMED ÇAKIR

IN PARTIAL FULFILLMENT OF THE REQUIREMENTS
FOR
THE DEGREE OF DOCTOR OF PHILOSOPHY
IN
MECHANICAL ENGINEERING

MARCH 2025

Approval of the thesis:

CONSTITUTIVE MODELING AND EXPERIMENTAL IDENTIFICATION OF MATERIAL PARAMETERS OF VISCOELASTIC MATERIALS BY VARIABLE ORDER NON-INTEGER DERIVATIVES

submitted by **MUHAMMED ÇAKIR** in partial fulfillment of the requirements for the degree of **Doctor of Philosophy in Mechanical Engineering Department, Middle East Technical University** by,

Prof. Dr. Naci Emre Altun
Dean, Graduate School of **Natural and Applied Sciences** _____

Prof. Dr. Serkan Dağ
Head of Department, **Mechanical Engineering** _____

Assoc. Prof. Dr. Ergin Tönük
Supervisor, **Mechanical Engineering, METU** _____

Prof. Dr. Hamdullah Yücel
Co-supervisor, **Institute of Applied Mathematics, METU** _____

Examining Committee Members:

Prof. Dr. Fevzi Suat Kadıoğlu
Mechanical Engineering, METU _____

Assoc. Prof. Dr. Ergin Tönük
Mechanical Engineering, METU _____

Assoc. Prof. Dr. Mehmet Bülent Özer
Mechanical Engineering, METU _____

Assist. Prof. Dr. Kutluk Bilge Arıkan
Mechanical Engineering, Ankara University _____

Assist. Prof. Dr. Serdar Arıtan
Exercise and Sport Sciences Department, Hacettepe University _____

Date:04.03.2025

I hereby declare that all information in this document has been obtained and presented in accordance with academic rules and ethical conduct. I also declare that, as required by these rules and conduct, I have fully cited and referenced all material and results that are not original to this work.

Name, Surname: Muhammed Çakır

Signature :

ABSTRACT

CONSTITUTIVE MODELING AND EXPERIMENTAL IDENTIFICATION OF MATERIAL PARAMETERS OF VISCOELASTIC MATERIALS BY VARIABLE ORDER NON-INTEGER DERIVATIVES

Çakır, Muhammed
Ph.D., Department of Mechanical Engineering
Supervisor: Assoc. Prof. Dr. Ergin Tönük
Co-Supervisor: Prof. Dr. Hamdullah Yücel

March 2025, 161 pages

Polymeric materials are widely used due to their ease of manufacture, low density, and cost-effectiveness. Their viscoelastic properties, such as stress relaxation and creep, arise from their long molecular chains. Traditional rheological models describing these properties often require numerous parameters, as they rely on multiple springs and dashpots with estimated constants. An alternative approach is fractional calculus, which employs non-integer derivatives and integrals to simplify the modeling process. This method reduces the number of required parameters while providing a more consistent representation of mechanical behavior by allowing the order of differentiation to vary between 0 and 1—representing purely elastic and purely viscous behavior, respectively.

The mechanical properties of viscoelastic materials are strongly influenced by environmental factors and loading/deformation history, necessitating a variable-order fractional model rather than a constant-order one. In this study, fractional-order viscoelastic models are applied to materials such as PE300, PTFE, and EVA, utilizing

tensile test data. Theoretical models and MATLAB-based simulations are validated through comparisons with experimental results and finite element analysis (FEA). To further enhance predictive accuracy, user-defined material subroutines are developed for the commercial finite element solver ABAQUS, incorporating both constant-order and variable-order formulations.

Further verification of the proposed approach is conducted using the tensile test data obtained from a tensile testing machine equipped with non-contact strain measurement devices. The methodology is assessed by simulating tensile tests providing a comprehensive evaluation of the parameter estimation method. Additionally, the effectiveness of the user material subroutine is examined by comparing simulation results with experimental data, ensuring the reliability of the proposed framework.

Keywords: Viscoelasticity, Fractional Calculus, Variable Order

ÖZ

VİSKOELASTİK MALZEMELERİN DEĞİŞKEN-TAM SAYI OLMAYAN TÜREVLERİ İLE KURAMSAL MODELLENMESİ VE DENEYSEL OLARAK MALZEME PARAMETRELERİNİN BELİRLENMESİ

Çakır, Muhammed
Doktora, Makina Mühendisliği Bölümü
Tez Yöneticisi: Doç. Dr. Ergin Tönük
Ortak Tez Yöneticisi: Prof. Dr. Hamdullah Yücel

Mart 2025 , 161 sayfa

Polimerik malzemeler, üretim kolaylıkları, düşük yoğunlukları ve maliyet etkinlikleri nedeniyle yaygın olarak kullanılmaktadır. Gerilme gevşemesi ve sünme gibi viskoelastik özellikleri, uzun moleküler zincirlerinden kaynaklanmaktadır. Bu özellikleri tanımlayan geleneksel reolojik modeller, birden fazla yay ve sönümleyici içeren, tahmini sabit değerler kullanan yapıları nedeniyle genellikle çok sayıda parametre gerektirmektedir. Alternatif bir yaklaşım olarak kesirli türevli hesaplama, modelleme sürecini basitleştirmek amacıyla tam sayı olmayan türevler ve integraller kullanmaktadır. Bu yöntem, türev mertebesinin 0 ile 1 arasında değişmesine olanak tanıyarak gerekli parametre sayısını azaltmakta ve mekanik davranışı daha tutarlı bir biçimde temsil etmektedir; burada 0 mertebe tamamen elastik, 1 mertebe ise tamamen viskoz davranışı simgelemektedir.

Viskoelastik malzemelerin mekanik özellikleri, çevresel faktörler ile yükleme/deformasyon geçmişinden büyük ölçüde etkilendiğinden, sabit mertebeli bir model ye-

rine değişken mertebeli bir kesirli türevli model kullanılması gerekmektedir. Bu çalışmada, PE300, PTFE ve EVA gibi malzemelere çekme testi verileri kullanılarak kesirli mertebeli viskoelastik modeller uygulanmıştır. Teorik modeller ve MATLAB tabanlı benzetimler, deneysel sonuçlar ile sonlu elemanlar analizi karşılaştırmaları yapılarak doğrulanmıştır. Öngörü hassasiyetini daha da artırmak amacıyla, ticari sonlu elemanlar çözücüsü ABAQUS için hem sabit mertebeli hem de değişken mertebeli formulasyonları içeren kullanıcı malzeme alt programları (UMAT) geliştirilmiştir.

Önerilen yaklaşımın ek doğrulaması, temassız gerinim ölçer cihazlarla donatılmış çekme testi makinesinden elde edilen veriler kullanılarak gerçekleştirilmiştir. Ayrıca, kullanıcı malzeme alt programının etkinliği, simülasyon sonuçlarının deneysel verilerle karşılaştırılmasıyla incelenmiş, böylece önerilen yöntemlerin güvenilirliği sağlanmıştır.

Anahtar Kelimeler: Viskoelastisite, Kesirli Türev, Değişken Mertebe

To the always pure-hearted people...

ACKNOWLEDGMENTS

Firstly, the author would like to thank his supervisor Assoc. Prof. Dr. Ergin Tönük for his help, guidance, and mentorship. Without his support and insight, the completion of this dissertation would not have been possible.

I would also like to express my sincere thanks to my co-supervisor, Prof. Dr. Hamdullah Yücel, for his invaluable advice and assistance. Your constructive input and support during the most critical times have greatly contributed to the development and refinement of this thesis.

Hence, working with them was a unique pleasure. Besides them, the author is also obliged to the thesis examining committee members Assoc. Prof. Dr. Bülent Özer and Assist. Prof. Dr. Kutluk Bilge Arıkan for their encouragement and insightful comments in each meeting.

Lastly, I would like to express my deepest gratitude to my beloved wife, Nesibe, my son, Halil İbrahim, and my daughter, Elif. Throughout this challenging process, their patience, understanding, and unwavering support have been nothing short of heroic. During the countless stressful moments when I was absorbed in my thesis work, they tolerated my endless rants and provided me with the strength to continue. Their extraordinary patience and encouragement have been invaluable to me, and words cannot fully express how much I appreciate them. They truly deserve a Nobel Prize for their remarkable patience and support.

TABLE OF CONTENTS

LIST OF TABLES

TABLES

LIST OF FIGURES

FIGURES

LIST OF ABBREVIATIONS

CO	Constant Order
COF	Constant Order Fractional
COFSB	Constant Order Fractional Scott Blair
DIC	Digital Image Correlation
EVA	Ethylene Vinyl Acetate
FEM	Finite Element Method
FE	Finite Element
FEA	Finite Element Analysis
FM	Fractional Maxwell
FKV	Fractional Kelvin-Voigt
FSLS	Fractional Standard Linear Solid
GL	Grünwald-Letnikov
QLV	Quasi-Linear Viscoelasticity
PE	Polyethylene
PMMA	Polymethyl Methacrylate
PTFE	Polytetrafluoroethylene
RL	Riemann-Liouville
SB	Scott-Blair Model
SLS	Standard Linear Solid
UMAT	User Material (Routine)
VO	Variable Order
VOF	Variable Order Fractional
VOFSB	Variable Order Fractional Scott Blair
V-Ext	Video Extensometer (Method)

$\lceil \bullet \rceil$	Ceiling Operator
${}^{C}D\bullet$	Caputo Type Fractional Derivative
${}^{RL}D\bullet$	Riemann-Liouville Type Fractional Derivative
E	Elastic Constant
E_f	Fractional Characteristic Number (Constant Order)
$E_f(t)$	Fractional Characteristic Function (Variable Order)
α	Fractional Constant Order
$\beta(t)$	Fractional Variable Order
β_k	Fractional Variable Order k-Dimensional Vector Array Form

CHAPTER 1

INTRODUCTION

Deformation of viscoelastic materials is path-dependent, i.e., non-conservative. Mainly most polymeric materials and biological tissues are viscoelastic under certain conditions. Their response to load and deformation is dependent on the time and history of deformation. Two major characteristics of viscoelastic materials are creep behavior under constant stress and stress relaxation behavior under constant deformation. The effects of these two basic responses can simultaneously be observed in any case of loading and deformation. Given the expanding use of polymer technology such as in [6], the characterization of viscoelastic materials has become essential, and an accurate description of material behavior is crucial.

The mechanical behavior of viscoelastic materials depends on internal and external variables. Since the viscoelastic materials exhibit memory dependence, their behavior is influenced by the prior history of deformation and/or stress. Information about the strain and stress states is stored in the complex and elongated polymer chains in the form of residual stress and it corresponds to the internal variables. Internal variables are not the only variable affecting the viscoelastic response. The majority of the polymeric materials are greatly affected by external disturbances. These disturbances include temperature fluctuations and changes in the ambient pH level which can promote chemical reactions that affect the mechanical behavior of the material.

1.1 Research Questions and Approach

In this thesis, the mechanical behavior of viscoelastic materials is modeled using a fractional viscoelasticity approach. Specifically, the primary research question ad-

dressed is how to effectively model and determine the mechanical properties of viscoelastic materials. To answer this question, the study encompasses three main components: the theoretical derivation of the mathematical model for the viscoelastic materials, the experimental determination of fractional viscoelasticity parameters, and the development of a user material subroutine in the Abaqus software, which is the well-known finite element software in the engineering [7]. Together, these components aim to provide a comprehensive framework for capturing and analyzing the fractional viscoelastic behavior of materials.

1.2 Structure of the Thesis

The chapters that comprise this thesis are as follows: In Chapter 2, the available literature is presented. Chapter 3 describes the fractional viscoelastic material model for the quasi-static loading. The methods used in Chapter 4 to ascertain the material parameters are presented. The developed concepts are simulated in a commercial finite element software by implementing the developed user material subroutine in Chapter 5, and the experimental studies to obtain the fractional viscoelastic material parameters are presented in Chapter 6. In Chapter 7, a detailed discussion of the findings and presentation of the core results is provided. Also, a comprehensive analysis of the implications of these results is provided.

CHAPTER 2

LITERATURE REVIEW

In this section, it is aimed to present an overview of studies on the fractional viscoelastic behavior of materials. The studies on the non-integer constant-order and variable-order viscoelastic models are visited. We do not limit the scope of this work to a specific class of viscoelastic materials. Yet, a class of materials obeying the fractional-order viscoelastic constitutive law or variable-order fractional viscoelasticity is examined in this study. Therefore the present chapter aims to deliver a broader view of the field.

Many real materials do not follow the same load-deformation path when they are loaded and unloaded. The extent of the difference between the two paths is called hysteresis which tells the energy recovered during the material restoring is less than the energy used during deforming. The materials showing this path-dependent behavior are called viscoelastic materials. Due to the intricate sub-continuum anisotropy of materials, viscoelastic behavior is prominently observed in biological tissues, polymers, concrete, asphalt mixtures, and the Earth's crust. The path dependence adds unique vibration damping property to polymeric materials with considerably low specific weight. It makes also them good candidates for biomechanical applications.

The two basic responses of a viscoelastic material are relaxation and creep. The earliest efforts to model these behaviors generally depend on the utilization of linear springs and dashpots and their various series or parallel arranged combinations. The simplest viscoelastic material models built with the rheological element are the Maxwell fluid [8], the Kelvin solid [9], and Zener's standard linear solid models [10]. Since these models are constructed upon basic ideal mechanical elements, i.e., springs and dashpots, the constitutive models include the integer-order derivatives of stress

or strain. These models only consider the stress and strain as a function of time. Therefore, these models and their variations constitute linear viscoelastic behavior.

Constitutive equations extracted from the utilization of spring–dashpot elements incorporate the ordinary differential equations. Mainardi and Spada [11] presented the formulation of the classical mechanical viscoelastic model and the fractional counterparts. To capture a more realistic behavior, the number of rheological elements used to construct the constitutive behavior should be increased [12]. However, complex rheological models that involve an increased number of parameters complicate the experimental calibration of the necessary material properties. Specifically, as the complexity of the model increases, so does the number of tests required to determine the material properties of each mechanical element [13, 14]. On the contrary, the fractional modeling requires less number of parameters to be tuned. Fractional calculus is a powerful tool for modeling viscoelastic phenomena requiring a considerably small number of parameters. Therefore, the fractional modeling of viscoelastic behavior simplifies the constitutive model with relatively fewer material parameters therein. Sasso et al. [15] experimentally showed the superiority of the fractional model over the generalized Maxwell and generalized Voigt models under small deformations of rubber and polypropylene.

Furthermore, it has been well-established that real materials exhibit behavior that deviates from the exponential decay which is typical of solutions in linear viscoelasticity, instead displaying power-law responses. This deviation is captured by non-integer differential equations, as experimentally demonstrated by Nutting [16]. The ability of fractional calculus to model this non-exponential decay behavior is particularly advantageous, as it more accurately reflects the complex viscoelastic characteristics of real materials, thus providing a more comprehensive framework for capturing material responses under various loading conditions.

There are numerous works on harmonic loading problems, frequency response, and vibration-damping studies of the viscoelastic materials in the literature. In this study, we keep the harmonic loading problems out of the scope and limit our effort to capture viscoelastic behavior under constant rate mechanical loading. Therefore, the studies concerning frequency domain analysis and harmonic problems are almost untouched

in this study.

2.1 Overview of the Methods Employed to Model Viscoelasticity

In this section, we will deliver a short introduction to the classical methods and integral methods in the viscoelastic modeling.

There are several methods proposed to define viscoelastic behavior. The validity of such methods is generally restricted to very narrow conditions. The classical viscoelastic method employs rheological elements, springs, and dashpots, and investigates their effect on the material response. A more analytical method is the integral method which introduces a convolution product of stress or strain function with a properly defined kernel function. In such a method, a proper definition of the kernel plays a crucial role in the stress-strain relationship [17, 18, 19, 20].

Early contributors mainly focused on the linear viscoelastic behavior, which was developed using the simple rheological elements, Hookean linear spring, and Newtonian linear viscous dashpot, and their series, parallel, or other combinations are utilized. For detailed analysis and mathematical background of the classical viscoelastic models, the reader may refer to landmark books of Flügge [9] and Findley [21] on the classical rheological viscoelasticity. Some of the most commonly employed models are the Maxwell model, the Kelvin-Voigt model, Zener's model, the standard linear elastic solid model, Burger's model, and the generalized Maxwell model. The drawbacks of the integer order classical rheological models are discussed by Di Paola et al. [22, 23]. The relaxation and creep tests show that integer-order models cannot precisely describe the creep and relaxation phenomenon for the basic viscoelastic models. In such models, the stress tends to decrease to zero when the time is extended to infinity under the constant deformation which is contrary to numerous experimental data. Irrespective of how many elementary spring dashpot elements have been used, the kernel of the hereditary integral is always an exponential function. From the above properties of classical viscoelastic models, the conclusion can be drawn that they could be suitable only for a short period of loading with considerable inaccuracy. The kernel function in terms of a power-law growth/decay function can

better portray the realistic creep/relaxation behavior as Nutting [16] and Gemant [24] suggested.

Ingman et al. [25] further draw the attention of the researchers to one of the drawbacks of modeling the viscoelasticity with classical rheological tools. That is the material evolution cannot be captured by such a method since the rheological elements do not allow the material change but only allow a load-deformation state.

Given the limitations of classical viscoelastic models, particularly their inability to accurately capture long-term material behavior and evolution, more advanced methodologies are required. One such approach is the hereditary (convolution) integral method, which offers a more nuanced framework for modeling viscoelastic behavior.

2.1.1 Hereditary (Convolution) Integral Method

Volterra introduced the hereditary integral method in the early 1900s as a branch of linear hereditary viscoelasticity [26] by adopting integral equations. In linear viscoelasticity, the stress and strain are directly related to the time variable. One of the notable advantages of the convolution integral method is the flexibility in selecting the kernel function. A properly chosen kernel function enables the modeling of material evolution and enhances accuracy in predicting long-term behavior.

Pipkin et al. [27] extended the study of viscoelasticity to the nonlinear regime using a series integral representation. Unlike linear viscoelasticity, which considers relaxation and creep functions as dependent only on time, their approach incorporated the entire deformation or loading history of the material.

The hereditary integral method, based on the Boltzmann superposition principle, analytically relates stress and strain by incorporating the complete loading or deformation history of the material. Essentially, the Boltzmann superposition principle introduces a memory effect in the stress-strain relationship. This method utilizes a singular kernel function convolved with an independent state variable, such as stress or strain history [28]. A suitable choice of the kernel function can transform the hereditary integral into a fractional differential operator [23]. The general form of the hereditary

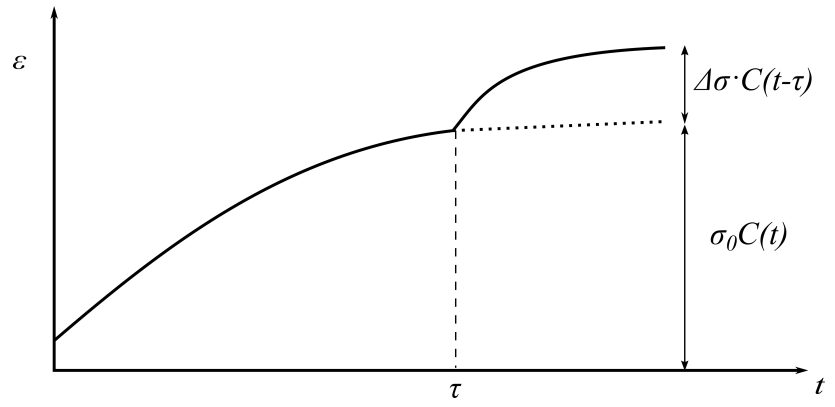

Figure 2.1: Boltzmann Superposition Principle

integral is given by:

$$\text{Stress} = \int_0^t (\text{Relaxation Term}) \times (\text{history of deformation}) \cdot d\tau. \tag{2.1}$$

In linear viscoelasticity, the complete mechanical characterization of a material can be obtained using the creep compliance function or the relaxation modulus. Notably, the creep compliance function does not necessarily require specific spring or dashpot models; instead, it can be directly derived from experimental data, providing a comprehensive description of material behavior. The foundation of linear viscoelasticity can be explained as follows.

For a uniaxial loading case, the strain resulting from an initial constant step load, σ_0, is given by $\varepsilon(t = [0^+, \tau]) = \sigma_0 C(t)$, where $C(t)$ represents the creep function. If an infinitesimally small incremental load $\Delta\sigma$ is applied at a later time, τ, the resulting strain is $\varepsilon(t = [\tau, \infty]) = \Delta\sigma C(t - \tau)$. This process is illustrated in Fig. 2.1. Consequently, the total strain is then expressed as:

$$\varepsilon(t) = \sigma_0 C(t) + \Delta\sigma C(t - \tau). \tag{2.2}$$

The ability to add responses in this manner stems from the linearity of the material, where the combined effect of multiple causes is equivalent to the sum of individual effects. This principle is known as the *Boltzmann Superposition Principle*.

The summation of two loads can be generalized to an infinite number of infinitesimal

loads, each of magnitude $d\sigma_i$. The total response is then given by:

$$\begin{aligned}\varepsilon(t) &= \sigma_0 C(t) + \sum_{i=1}^{\infty} d\sigma_i C(t-\tau_i) \\ &= \sigma_0 C(t) + \int_0^t C(t-\tau)\left(\frac{d\sigma}{dt}\right)_{t=\tau} d\tau.\end{aligned} \tag{2.3}$$

The integral in Eq. 2.3 is referred to as the *hereditary integral*. By following a similar approach and utilizing the relaxation function $R(t)$ and incremental strain $\Delta\varepsilon$, the stress function can be formulated as:

$$\sigma(t) = \varepsilon_0 R(t) + \int_0^t R(t-\tau)\left(\frac{d\varepsilon}{dt}\right)_{t=\tau} d\tau. \tag{2.4}$$

The functions $C(t)$ and $R(t)$ appearing in Eqs. 2.3-2.4 represent the creep and relaxation functions, respectively. Assuming the material is initially stress- and strain-free, the initial terms vanish. The fundamental relations of linear viscoelasticity are thus given as:

$$\sigma(t) = \int_0^t R(t-\tau)\dot{\varepsilon}(\tau)d\tau, \tag{2.5a}$$

$$\varepsilon(t) = \int_0^t C(t-\tau)\dot{\sigma}(\tau)d\tau. \tag{2.5b}$$

The equation set above represents the convolution integral formulation of the viscoelastic constitutive model. The first terms inside the integral, which serve as kernel functions, play a crucial role in viscoelastic modeling [29].

The kernels of the Eq. 2.5, creep and stress relaxation functions, are not entirely independent. Their relationship can be derived using the Laplace transform of Eq. 2.5. The product of the creep and relaxation functions in the Laplace domain is expressed as:

$$\tilde{C}(s)\tilde{R}(s) = \frac{1}{s^2}. \tag{2.6}$$

2.1.2 Fractional Viscoelasticity

The constitutive model based on simple rheological elements typically incorporates ordinary derivatives (i.e., integer-order) of stress or strain. Therefore, the solutions of

such governing equations yield stress-strain responses that are exponential functions of time. However, experimental observations by Nutting [16] on viscoelastic materials revealed that their stress-strain relationships are better represented by power functions of time rather than exponential functions. To capture intermediate modes of creep or relaxation more accurately, an increased number of rheological elements must be used in the model. This, however, introduces a significant limitation: the physical properties of each added element must be determined experimentally, often requiring multiple experiments to accurately characterize the material response. As the complexity of the model increases, the determination of necessary parameters becomes increasingly challenging, potentially making the process impractical.

This limitation of integer-order models underscores the need for a more sophisticated approach, specifically the incorporation of fractional derivatives. It is crucial to emphasize that the concept of material memory cannot be adequately captured by integer-order, local differential operators. Unlike ordinary derivatives, fractional derivatives are non-local operators that depend not only on the value of the function at a specific point and its immediate vicinity but also on the entire history of the function [30]. This memory-dependent characteristic of fractional derivatives makes them particularly well-suited for modeling time- and history-dependent phenomena, such as creep and relaxation, which are commonly observed in viscoelastic materials. As such, fractional derivatives offer a more comprehensive and accurate framework for describing the stress-strain relationship in viscoelastic materials, effectively addressing the shortcomings of integer-order models by incorporating the full history of material response.

2.2 Studies on Fractional Order Viscoelasticity

The idea of non-integer order calculus emerged from correspondence between Leibniz and L'Hôpital in 1695. The question was the foundation of the non-integer order calculus: How should one take the half derivative of a function x? The answer of Leibniz was as inspiring as the question itself: "... One day useful consequences will be drawn".

Following their perspective, numerous great scientists have contributed to the field of non-integer order calculus, commonly known as fractional calculus. However, it was not until the 1930s that fractional calculus began to be employed as a tool for solving real-world problems rather than being regarded solely as an abstract mathematical concept. To the best of our knowledge, the pioneering application of fractional calculus to the study of viscoelastic behavior was introduced by Gemant [24], building upon the earlier observations of Nutting [16]. Nutting proposed that the stress-strain relationship for a viscoelastic material subjected to a constant stress should follow a power-law behavior, formulated as

$$\varepsilon(t) = k\sigma_0 t^n, \tag{2.7}$$

where k and n are material constants, and σ_0 represents the applied constant stress. However, a fundamental limitation of this formulation emerges as $t \to \infty$, leading to an unbounded strain $\varepsilon \to \infty$. This contradicts the observed behavior of most solid continua, which exhibit finite deformation under sustained loading.

In real materials, deviations from purely linear elastic behavior are often observed, particularly under prolonged loading or displacement. Prior to the advent of fractional viscoelasticity, modeling such behavior was primarily based on two approaches: classical rheological models and the introduction of time effects within the linear stress-strain relationship. The latter approach, grounded in the Boltzmann superposition principle, inherently accounts for the history dependence of the material. That is, the mechanical response of the material is influenced by its prior deformation history. This approach introduces a time-dependent fading memory effect, characterized by a suitable kernel function, leading to the hereditary integral formulation of Volterra type:

$$\varepsilon(t) = \int_0^t C(t-\tau)\dot{\sigma}(\tau)d\tau, \tag{2.8a}$$

$$\sigma(t) = \int_0^t R(t-\tau)\dot{\varepsilon}(\tau)d\tau. \tag{2.8b}$$

The hereditary integrals in Eq. 2.8 are analogous to the fractional derivative when a

power-law kernel function is selected.

The first known application of fractional calculus to mechanical problems was proposed by Gemant in 1936 [24]. Gemant suggested that, contrary to previous beliefs, experimental evidence indicates that viscoelastic materials such as rubber and polymers obey a power-law decay rather than an exponential decay. Scott Blair et al. [31] argued that fractional calculus represents a powerful framework for modeling the viscoelastic behavior of real materials. Since viscoelastic materials exhibit mechanical behavior that is intermediate between purely elastic and purely viscous responses, they proposed that the order of differentiation should assume a value between 0 and 1. Based on this hypothesis, they introduced the first non-integer order differentiation model for viscoelastic problems.

The development of fractional viscoelasticity has evolved through a series of significant contributions that have progressively refined the understanding of complex material behavior. Early work by Slonimsky [32] provided a theoretical investigation of the relaxation process in polymeric molecules, demonstrating that a viscoelastic polymer chain constitutes an intermediate state between purely elastic and purely viscous behavior. This insight laid an early foundation for the field.

Building on these ideas, Smit and de Vries [1] introduced rheological models that incorporated fractional derivatives. They successfully formulated a stress–strain relationship for a fractional viscoelastic material subjected to a constant strain rate, $\dot{\varepsilon} = \epsilon$, and derived expressions for stress relaxation and creep in terms of non-integer derivative orders:

$$\sigma(t) = \frac{E\theta^{\alpha}}{\Gamma(2-\alpha)}\,\dot{\epsilon}^{\alpha}\,\varepsilon^{1-\alpha}, \tag{2.9a}$$

$$\varepsilon(t) = \frac{\sigma_0}{E\theta^{\alpha}\Gamma(1+\alpha)}\,t^{\alpha}, \tag{2.9b}$$

where $\Gamma(\bullet)$ is the gamma function, α is the fractional order, and E and θ denote the elastic and viscous material parameters, respectively. Under constant stress σ_0, the creep function obtained in Eq. 2.9a replicates the power-law form originally suggested by Nutting. However, experiments on the nylon yarns revealed that the linear non-integer order model could not capture the entire deformation spectrum; the fractional order was observed to depend not only on time but also implicitly on the de-

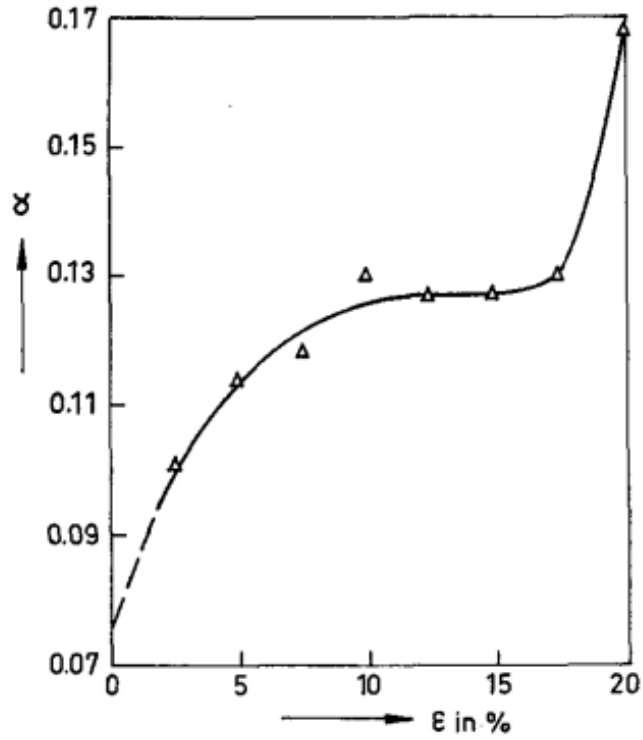

Figure 2.2: Fitted Fractional Order to Nylon Yarns by Smit and de Vries [1]

formation. Figure 2.2 (adapted from [1, Fig. 8a]) illustrates this dependency, thereby establishing Smit and de Vries as early pioneers of variable-order fractional viscoelasticity.

Caputo and Mainardi [33] extended Zener's standard linear solid model [10]—which consists of a Maxwell arm connected in parallel with a Kelvin branch—by converting the integer-order formulation to a fractional-order one. Their four-parameter model is expressed as

$$\sigma(t) + a\frac{d^\alpha \sigma}{dt^\alpha} = m\varepsilon(t) + b\frac{d^\alpha \varepsilon}{dt^\alpha}. \tag{2.10}$$

This formulation permits the derivation of various material models by appropriately adjusting the parameters a, b, m, and α. For example, setting $a = m = 0$ reduces the model to the fractional Scott–Blair model, whereas choosing $a = 0$ or $m = 0$ yields the fractional Voigt or fractional Maxwell models, respectively [26, 34]. In addition, Caputo and Mainardi introduced an alternative fractional derivative definition, leading

to the widely used Caputo-type fractional derivative operator:

$$ {}^{C}Df(t) = \frac{1}{\Gamma(1-\alpha)} \int_0^t \frac{f^{(n)}(\tau)}{(t-\tau)^{\alpha}}\, d\tau, \quad 0 < \alpha < 1, \quad n = \lceil \alpha \rceil, \tag{2.11} $$

where the prescript, ${}^{C}D\bullet$, denotes the Caputo type derivative.

Subsequent work by Bagley and Torvik [35] generalized the standard linear solid model further by proposing a five-parameter viscoelastic model. They reformulated the model in a general form:

$$ \sigma(t) + \sum_{m=1}^{M} b_m D_m^{\beta}\big[\sigma(t)\big] = E_0\epsilon(t) + \sum_{n=1}^{N} E_n D_n^{\alpha}\big[\epsilon(t)\big], \tag{2.12} $$

noting that higher-order derivatives are not required since a first-order approximation sufficiently portrays the mechanical properties of many viscoelastic materials. Under the condition that α and β are equal—a requirement proven by Heymans et al. [36] based on thermodynamic admissibility—the model reduces to a four-parameter form with parameters b, E_0, E_1, and α [37].

Lion et al. [38] further investigated the thermodynamical properties of various fractional viscoelastic constitutive models, studying the Clausius–Duhem inequality in three-dimensional formulations. Ezzat et al. [39] developed a coupled fractional thermo-viscoelastic constitutive model that incorporates a point heat source. This model is based on a governing equation that includes both stress relaxation and thermal relaxation terms, following the formulation of Christensen [8]:

$$ \sigma_{ij} = \int_0^t R_{ijkl}(t-\tau)\frac{\partial \varepsilon_{kl}}{\partial \tau}\, d\tau - \int_0^t \gamma_{ij}(t-\tau)\frac{\partial \theta}{\partial \tau}\, d\tau. \tag{2.13} $$

Subsequently, Ezzat et al. [40] developed a model in which stress relaxation time and thermal relaxation time are treated separately using a Rabotnov-type constitutive equation. The resulting stress–strain relationship is expressed as

$$ \sigma_{ij} = \hat{R}_{\beta}\Big(\varepsilon_{ij} - \frac{e}{3}\delta_{ij}\Big) + \hat{R}_{\alpha}\Big(e - 3\alpha_T \hat{T}\Big)\delta_{ij}, \tag{2.14} $$

where $\hat{R}_{\beta}$ represents the structural relaxation function, $\hat{R}_{\alpha}$ denotes the thermal relaxation function, $e = \varepsilon_{ii}$ is the volumetric strain, α_T is the coefficient of thermal expansion, and $\hat{T}$ is a function that characterizes the thermal difference relative to a reference temperature.

Some researchers have examined the interconnection between linear viscoelasticity and fractional viscoelasticity. For instance, the physical basis of fractional models has been linked to hierarchical arrangements of springs and dashpots. This connection is illustrated by the work of Schiessel et al. [12, 41] and Heymans et al. [42]. They demonstrated the physical connection between fractional modeling and hierarchically arranged ladder or tree models composed of springs and dashpots. In such viscoelastic models, an infinite number of parallel spring-dashpot branches ultimately converge to a formulation based on fractional calculus.

Other noteworthy contributions include the unification of n–fold integration with integer-order numerical differentiation using strip matrices as proposed by Podlubny [43]. These studies underscore the relevance of fractional models in capturing complex mechanical behavior.

Koeller also [19] established a link between linear viscoelasticity and fractional calculus by starting from Volterra's integral equation for materials with memory. In his work, the creep and relaxation functions are expressed in terms of the Mittag–Leffler function, and the idea of substituting dashpot elements with spring–pot elements in classical models was introduced. Koeller further advanced the field by proposing a tensor representation of stress and strain based on the Riesz representation. Sun et al. [44] compared the memory properties of constant- and variable-order models, concluding that while integer-order models may suffice for systems with short-time memory, constant-order fractional models are required to capture long-term memory effects. They also noted that an inappropriately chosen trigonometric order function may yield unrealistic system responses.

Su et al. [45] adopted using transfer function idea in the fractional viscoelastic models. The authors demonstrate that generalized fractional models can be constructed by integrating two selected viscoelastic models, thereby facilitating the development of models with fewer parameters. This approach enhances the flexibility and efficiency of viscoelastic modeling. The proposed methodology is validated through the application of the transfer function to experimental data from various materials, confirming its effectiveness in capturing complex viscoelastic behaviors. Furthermore, the study establishes a clear connection between the transfer function and viscoelas-

tic responses, providing a foundation for future research aimed at refining modeling techniques and expanding their applicability to a broader range of materials. They suggested that the method is suitable for time-varying viscosity fluids such as printer ink, and hydrogenated castor oil. Su et al. [46] proposed an atlas for viscoelastic models. The atlas shown in Fig. 2.3 may be quite guiding on how to start modeling the viscoelastic materials.

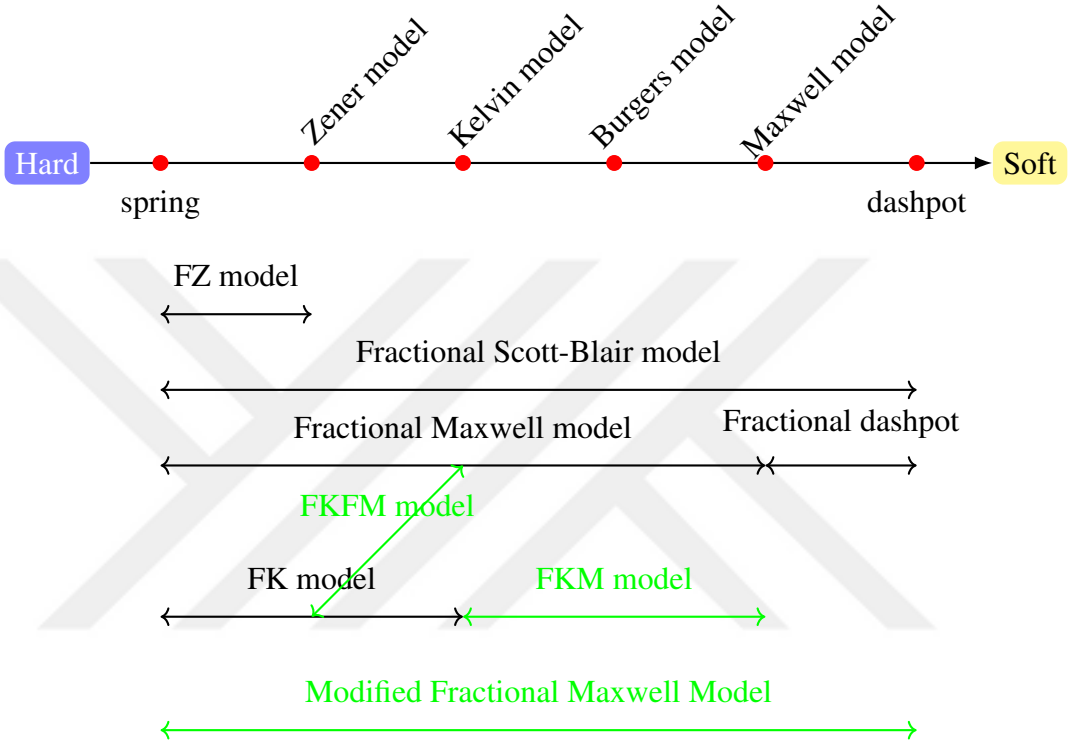

Figure 2.3: An Atlas for Viscoelastic Modeling

These advances provide a natural transition from the classical viscoelastic formulations to the variable order models that capture evolving material states under load. In this context, researchers have begun linking the fractional order directly to material response.

Samko & Ross [47] extended the fractional constant order problems to the variable order in 1993. Thus the variable-order fractional calculus has emerged from their study. Generally speaking, the fractional derivative order can be a function of time,

space, or both [48, 49]. Furthermore, some common differentiation and integration properties, i.e., semi-group property, may no longer hold if the fractional order becomes a function rather than a constant number [47]. This property further complicates the numerical handling of the problems. The variable-order fractional calculus is the direct extension of the constant-order fractional calculus. They also showed the relation between the Riemann-Liouville and Marchaud-type variable-order fractional derivatives,

$$ {}^{RL}_{0}D_{t}^{\beta(t)} f(t) = \frac{1}{\Gamma(1-\beta(t))} \frac{d}{dt} \int_0^t (t-\tau)^{-\beta(t)} f(\tau) d\tau, \tag{2.15} $$

$$ {}^{M}_{0}\mathrm{D}_{t}^{\beta(t)} f(t) = \frac{f(t)}{\Gamma(1-\beta(t)) t^{\beta(t)}} + \frac{\beta(t)}{\Gamma(1-\beta(t))} \int_0^t \frac{f(t)-f(\tau)}{(t-\tau)^{1+\beta(t)}} d\tau, \tag{2.16} $$

$$ {}^{RL}_{0}D^{\beta(t)} f(t) = {}^{M}_{0}\mathrm{D}_{t}{}^{\beta(t)} f(t) + \frac{\beta'(t)}{\Gamma(1-\beta(t)} \int_0^t \frac{f(\tau) \ln{(t-\tau)}}{(t-\tau)^{\beta(t)}} d\tau. \tag{2.17} $$

Di Paola et al. [50] provided the discretization of the Scott-Blair constitutive model by the Grünwald-Letkinov method in the matrix form of the stresses and strains. The same method was also employed by Podlubny [43]. The stress-strain relation is presented by,

$$ \sigma(t) = E_\alpha(t) ({}^{C}_{0}D_{t}^{\alpha(t)} \varepsilon)(t), \tag{2.18} $$

which is then written in two alternative forms,

$$ \sigma(t) = \int_0^t \frac{E_\alpha(t)}{\Gamma(1-\alpha(t))} (t-\tau)^{-\alpha(t)} \dot{\varepsilon}(\tau) d\tau, \tag{2.19a} $$

$$ \sigma(t) = \int_0^t \frac{E_\alpha(\tau)}{\Gamma(1-\alpha(\tau))} (t-\tau)^{-\alpha(\tau)} \dot{\varepsilon}(\tau) d\tau. \tag{2.19b} $$

It is clear from Eq. 2.19, that the material parameter E_α and derivative order α are expressed as a function of integration variable τ and time variable. They presented a step-by-step approach to predict the response of variable-order and material parameters of viscoelastic PET.

A novel approach to the variable fractional order viscoelastic models was presented by Ingman et al. [25], who defined the fractional order parameter as a state function, $S(t)$. This dynamic order, expressed as

$$ \sigma(t) = D^{\alpha(S(t))} \varepsilon(t), \tag{2.20} $$

reflects the variable interplay between elastic and viscous effects during loading. Their work on modeling the contact problem of a hard spherical object indenting a viscoelastic body demonstrated that the fractional order may be a power function of time, for instance, $\alpha(t) = 1 - 2^{-t}$, with the corresponding contact radius and pressure dependent on the applied load.

Lorenzo and Hartley [51] conceptualized the variable-order fractional operators in the spirit of previous experimental studies that Lorenzo performed, which reveals the dependence of the fractional order on the temperature, which was generally taken as a constant number until that time. They offered three different fractional operators in terms of the fractional order as,

$$\begin{aligned}
&\text{C1 type :} \qquad {}_0D_t^{-\alpha(t)} f(t) = \int_0^t \frac{(t-\tau)^{\alpha(t)-1}}{\Gamma(\alpha(t))} f(\tau) d\tau, \\
&\text{C2 type :} \qquad {}_0D_t^{-\alpha(t)} f(t) = \int_0^t \frac{(t-\tau)^{\alpha(\tau)-1}}{\Gamma(\alpha(\tau))} f(\tau) d\tau, \\
&\text{C3 type :} \qquad {}_0D_t^{-\alpha(t)} f(t) = \int_0^t \frac{(t-\tau)^{\alpha(t-\tau)-1}}{\Gamma(\alpha(t-\tau))} f(\tau) d\tau.
\end{aligned} \tag{2.21}$$

The order function is formed as $\alpha(t, \tau)$, where t is the time variable and τ is the integration variable. The main difference between the proposed variable order types is the contribution of the history of the order itself. They used transfer blocks and switching structures to indicate the differences between the models. From the above models, the first model (C1) loses the memory of the order of the past steps, while the second model (C2) remembers the past history of the order with a fading memory of the distant past of the order as the time increases. The last model (C3) completely remembers the past history of the order.

These theoretical studies, along with the establishment of a solid mathematical foundation, significantly accelerated further research in the field. As a result, researchers focused on analyzing the analytical solutions to both small and finite strain problems incorporating the fractional viscoelastic material models.

To advance this motivation, Drapaca et al. [52] introduced continuum mechanics formulations within the framework of fractional calculus. Similarly, Di Paola et al. [22] derived an analytical expression for the fractional Euler-Bernoulli viscoelastic beam under various loading conditions. Also Sumelka et al. [53, 54, 55] formulated frac-

tional elasticity under the continuum mechanics framework in their three subsequent papers. Sumelka and Blaszczyk [53] developed the fractional continua concept with the generalization of the classical continuum approach.

Xiao et al. [56] extended the fractional viscoelastic Zener model to the fractional viscoplastic model. They developed a finite deformation fractional model to describe the viscoplastic behavior of amorphous polymers near the glass transition temperature.

Adolfson and Enelund [57] studied the fractional viscoelastic model for large deformation. Starting from the deformation kinematics, they formulated the stress and strain definitions by using Lagrangian kinematics. The elastic formulations were converted to inelastic descriptions of stress and strains. They calculated the viscoelastic response of two example cases. A tube is subjected to constant internal pressure, and a viscoelastic bar is subjected to step-wise defined three different load levels. Their investigations showed that the material response was highly affected by the viscoelastic order.

Malesza et al. [58] developed an analytical solution to the differential equations containing variable order operators. The numerical solutions of variable order differential equations were compared with the analytical solutions developed using the switching order scheme method. The transfer functions of the derivative order were either connected by a series or parallel arrangement in various configurations. By the time the switch between the order transfer functions was changed, thus, at each time step, the derivative order took up a new value depending on the state of the switches.

The application of fractional calculus extends beyond quasi-static loading conditions. Numerous studies in the literature have explored its effectiveness in dynamic loading scenarios, demonstrating its broad applicability in modeling complex mechanical behavior. For example, several researchers have investigated fractional-order models to describe the response of materials subjected to oscillatory, impact, and other time-dependent loading conditions. To illustrate this, we cite several notable works here.

Makris et al. [59] used a two-parameter fractional rheological model by converting the Maxwell and Kelvin-Voigt model using spring–pot elements. They allowed the

derivative of the fractional element to change between (0,2). At the limit values, the Scott-Blair element (spring–pot) behaves like either a spring for the case of $\alpha = 0$ or an inerter (for vibration isolation purposes) for the case of $\alpha = 2$. This property allows to capture of the inertial effects alone. We remark that in such a case, a unit analysis in the constitutive equation is needed. It is physically unclear what material actually represents the behavior modeled in this study.

Eldred et al. [60] developed a mathematical model for a viscoelastic bar subjected to a sinusoidal axial load. They solved the problem numerically using a three-parameter Kelvin–Voigt model and obtained the numerical solution by adopting the Grünwald finite difference scheme proposed by Oldham and Spanier [61]. In addition, they compared the computational performance of the Grünwald finite difference scheme with that of a scheme derived from the Riemann–Liouville fractional derivative definition.

2.2.1 Applications in the Field of Finite Element Method

Building upon these theoretical advancements, fractional viscoelasticity has also been incorporated into finite element (FE) formulations and their applications to analyze complex structures. In this context, various studies have explored the implementation of fractional constitutive models within the FE framework to better capture the time-dependent behavior of viscoelastic materials.

Wei and Shimizu [62] studied the time-domain FE formulation of a viscoelastic continuum considering the structural dynamics. The Riemann-Liouville fractional operator was considered as a special case of Stieltjes convolution in their study. They constructed the FE model based on the fractional Kelvin-Voigt model by treating the elastic volumetric deformation and viscoelastic volumetric deformation cases separately.

From a numerical standpoint, Eldred et al. [60] modeled a viscoelastic bar under sinusoidal axial load using a three-parameter Kelvin–Voigt model. They employed Grünwald finite difference scheme [61] proposed by Oldham and Spanier. They compared its performance with schemes based on the Riemann–Liouville definition.

Schmidt and Gaul [63] extracted the finite element formulation for Delrin (polyacetal) material converting the integer order 3-parameter model to the fractional form for the dynamic loading cases. They demonstrated that fractional modeling provides a better fit with the experimental results obtained in the frequency domain.

The torsional deformation of viscoelastic beams was also studied by Colinas-Armijo et al. [64]. The labeled line elementless method (LEM) was used to eliminate the requirement of discretization of the domain as an alternative to the boundary element method (BEM) and finite element method (FEM). The analytical formulation for the fractional viscoelastic beams was presented in their work.

A fractional viscoelastic Timoshenko beam under static load was modeled by Pirrotta et al. [65]. The beam material was taken as a single fractional spring–pot element. The numerical solution for the time response of deformation was developed. Sumelka et al. [66] studied the fractional Euler-Bernoulli beams, which find a significant area of applications in micro and nano electromechanical (MEMS) devices. The continuum mechanics approach was adapted to the fractional viscoelastic beam deflection problem.

A FEM application of fractional viscoelasticity was made by Alotta et al. [67]. They present a brief formulation of the fractional viscoelastic creep and stress relaxation behavior of a fractional Kelvin-Voigt model. They implemented their formulation to the UMAT subroutine in commercial FEA code Abaqus [7]. They also showed the correspondence between the analytical and FEA results.

Alotta et al. [68] split the volumetric and deviatoric contributions of the relaxation term by additive decomposition of the relaxation modulus,

$$R_{ijkl}(t) = \left(K_R(t) - \frac{2}{3} G_R(t) \right) \delta_{ij}\delta_{kh} + G_R(t)(\delta_{ik}\delta_{jh} + \delta_{ih}\delta_{jk}), \tag{2.22}$$

where $G_R(t)$ is the deviatoric relaxation function and $K_R(t)$ is the volumetric relaxation functions, respectively. Both relaxation functions were defined as power-law functions with different parameters. The key aspect of their work is that when the relaxation modulus is decomposed to the volumetric and deviatoric components, the Poisson's ratio can be expressed as a time-dependent function. From the expressions of the stress and strain tensors, they obtained the viscoelastic Poisson's ratio. They

have reported that when directional anisotropy holds for the material single relaxation/creep function does not suffice. Therefore multiple Poisson's ratio definitions are always required for the anisotropic materials. An important feature of the viscoelastic Poisson's ratio is that it exhibits different behavior under creep and relaxation tests.

Alotta et al. [69] stated that the significance of fractional viscoelasticity over the other methods employed in the viscoelastic modeling is reducing the mechanical parameters. They also reported that the mechanical model of the spring–pot element could be obtained through the classical viscoelasticity by an infinite sequence of elements connected in a proper sequence with the serial or parallel arrangement [70]. The authors defined the relaxation modulus composed of volumetric and deviatoric contributions, which the same authors developed previously [68, 71]. The authors outline a remarkable feature of fractional viscoelasticity. The spring–pot element alone cannot precisely capture the viscoelastic response of different materials. For example, when the shear creep of some soils is considered, the FKV model should be employed. Certain types of polyethylene, such as ultra-high molecular weight polyethylene (UHMWPE), are effectively modeled using the fractional model (FM), while biological tissues are best represented by the fractional-standard linear solid (FSLS) model. They discretized the fractional derivative using the Grünwald-Letkinov procedure. They developed a UMAT subroutine and its formulation for the fractional viscoelastic models for 3D FEA. Alotta et al. [72] estimated the UHMWPE wear rate used in the osteoarthritic prosthesis application using the fractional-order model. The wear predicted by the fractional viscoelastic model was found almost tenfold higher than the one estimated by the elastoplastic wear model.

After reviewing the theoretical foundations of fractional viscoelasticity, it becomes imperative to examine the experimental studies that both validate and extend these models. Experimental investigations offer invaluable insights into the practical behavior of viscoelastic materials and serve to bridge the gap between theoretical predictions and real-world applications. In the following discussion, key experimental studies are reviewed that demonstrate the applicability of the theoretical models and open new avenues for future research in the field.

2.2.2 Experimental Studies in the Literature

Advancements in the theoretical material models have paved the way for more comprehensive investigations into material behavior. As a result, researchers have increasingly focused on exploring the applicability of fractional-order viscoelasticity to a wide range of materials. This research spans diverse fields, encompassing materials that exhibit complex mechanical responses. Notably, studies have been conducted on biological tissues, where viscoelastic properties play a crucial role in physiological functions. Similarly, investigations have extended to synthetic viscoelastic materials such as polymeric materials, adhesives, and even geological materials, including the Earth's crust. These developments highlight the growing significance of fractional-order viscoelasticity in understanding the mechanical behavior of various natural and engineered materials.

Glöckle et al. [73] studied the relaxation characteristics of protein chains which are modeled with fractional differential equations based on Zener's model. The fractional order of differentiation shows an apparent sensitivity to the thermal disturbances [74]. In another study [75] of the same authors the relaxation function of the fractional differential equation presented in H-fox functions.

Makris [76] contributed by examining the constitutive behavior of fractional viscoelastic models and by introducing viscoelastic compressibility, notably expressing the viscoelastic Poisson function via Mittag–Leffler functions.

Heymans et al. [36] demonstrated the effectiveness of the Zener model containing a fractional order damping element (spring–pot) for tensile loading of amorphous polycarbonate at various temperatures. According to the authors, Zener's model can better describe the rubbery glassy transition of a viscoelastic material. They demonstrated the contributions of the strain softening (rejuvenation) and temperature to the non-linear fractional viscoelastic model.

Ramirez and Coimbra [77] studied the constitutive relation for linear viscoelastic materials with the help of variable-order fractional calculus. A critical point underlined in their study is that unlike the integer-order models or constant-order models, variable-order elements eliminate the need for more elements in series or parallel

combinations. The reason for that is that the variation freedom of the derivative order helps to capture any intermediate equivalent value between 0 and 1. They developed a statistical mechanical model under the constant strain rate compression deformation of composite and epoxy resins. However, it is important to note that the fractional-order parameter is considered as a function of dimensionless time, specifically $\bar{t} \cdot \ln(\bar{t})$. This assumption becomes unrealistic as the order approaches zero, making it inconsistent with the actual physical phenomena.

Di Paola et al. [23] studied the two polymers designated as Aerstop CN20 and Aerstop VX5 for their stress relaxation and creep behavior. They used a two-parameter fractional-order model, which is derived from the well-known Boltzmann stress superposition principle. The material parameters, the fractional order, and the relaxation term are determined from the fit procedure. The specimens are loaded under isothermal conditions until their 10 percent and 30 percent ultimate tensile strength. The creep and stress relaxation responses are sufficiently well estimated by the two-parameter fractional order viscoelastic model.

Müller et al. [2] experimentally investigated the viscoelastic properties of polypropylene. They developed an experimental procedure including monotonic loading, cyclic loading, and relaxation tests as shown in the Figs. 2.4 and 2.5.

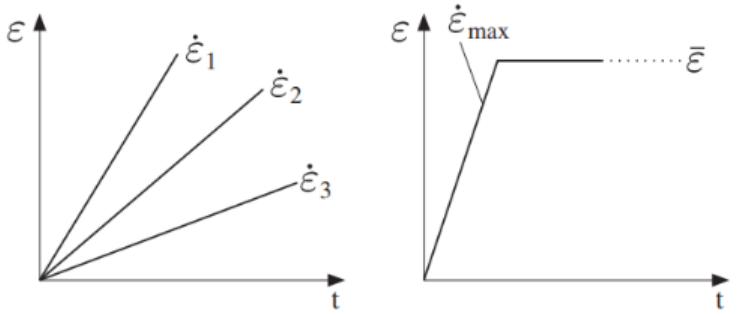

Figure 2.4: Monotonic Loading and Relaxation Tests [2]

They performed the experimental studies at three strain rate levels to reveal the strain rate dependence of the material. All the experiments were done at a constant temperature of 296 K, slightly above the glass transition temperature of polypropylene, 271 K. They modeled the constitutive behavior of the PP with fractional standard linear

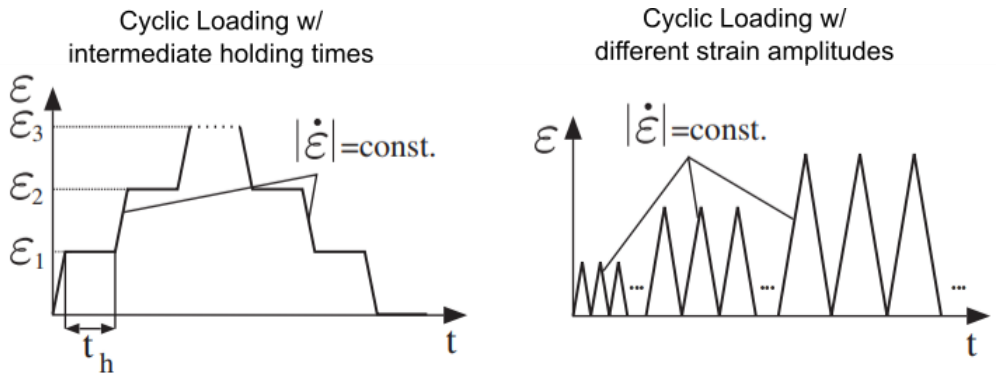

Figure 2.5: Cyclic Loading Tests [2]

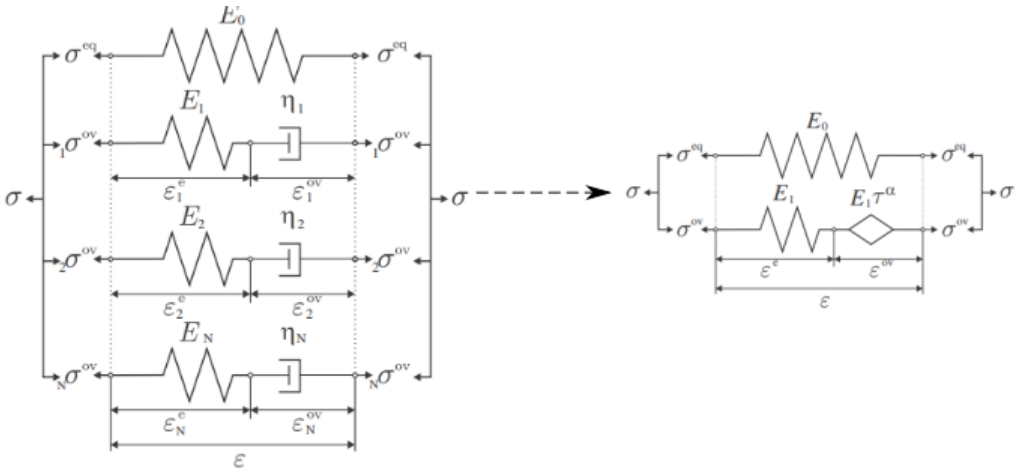

Figure 2.6: Interconversion of Generalized Maxwell Model to Fractional SLS Model [2]

solid model by converting the Weichert model [78]. To capture the long-term and short-term relaxation response of the material, a second fractional Maxwell arm was attached to the fractional SLS model as shown in Fig. 2.6. With this modification, the four-parameter viscoelastic model was extended to the six-parameter one. The developed nonlinear viscoelastic model was adapted to FE code Marc with a generalization to multi-dimension.

The thermomechanical behavior of amorphous thermoplastics was described by Lei et al. [3]. They developed two Maxwell models as shown in Fig. 2.7 having two parallel fractional elements to capture the glassy and the rubbery regimes at once for various thermoplastics such as PMMA, PMA, and PPP near and above the glass

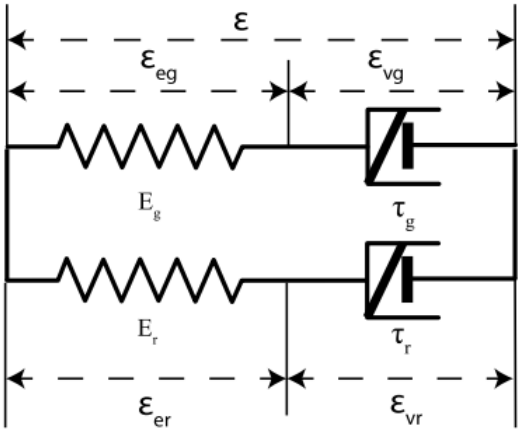

Figure 2.7: Lei's Fractional Model [3]

transition temperature under the small strain setting. They stated that the fractional Zener model can better describe the relaxation modulus of thermosetting polymers. They also estimated the storage and loss modulus of the same materials with the proposed model. The stress-strain relationship is then expressed as,

$$\sigma = \underbrace{E_g \epsilon_{eg}}_{\sigma_g} + \underbrace{E_r \epsilon_{er}}_{\sigma_r}, \tag{2.23}$$

where, E_g, E_r denote the glassy and rubbery moduli, respectively. Subscripts $\bullet_r$ and $\bullet_r$, denote the rubbery and glassy properties, respectively.

The stress relaxation behavior of glassy polymers was studied by Xiang et al. [79]. They developed a constitutive model based on Marchaud's fractional derivative definition,

$${}^{M}D_c^{\alpha(t)} f(t) = \frac{f(t)}{\Gamma(1-\alpha(t))(t-c)^{\alpha(t)}} + \frac{\alpha(t)}{\Gamma(1-\alpha(t))} \int_c^t \frac{f(t)-f(\tau)}{(t-\tau)^{1+\alpha(t)}} d\tau. \tag{2.24}$$

PETG specimens were subjected to compressive strains of $\varepsilon = 0.15$, 0.35, and 0.60 at 40, 55, and 70 $^{\circ}C$ temperatures, all of which below the glass transition temperature of $T_g = 80\ ^{\circ}C$ after 30 minutes heat treatment above the glass transition temperature. Deformations for each specimen were kept constant for 30 minutes. They adopted four different definitions for variable fractional order; piecewise constant, linear, trigonometric, and exponential functions of time. The variable order models

are detailed in Eq. 2.25:

$$
\begin{aligned}
V1: \qquad & \alpha(t) = \begin{cases} a, & t \in [0,1], \\ b, & t \in (1,30], \end{cases} \\
V2: \qquad & \alpha(t) = at + b, \\
V3: \qquad & \alpha(t) = a \cdot sin(bt) + c \cdot cos(bt), \\
V4: \qquad & \alpha(t) = a \cdot e^{bt}.
\end{aligned}
\tag{2.25}
$$

Under the constant temperature, the order function was best approximated by the V2 model since temperature increases the polymer chain mobility. Therefore, the stress-strain relationship for their model was expressed as

$$\sigma(t) = E\theta^{at+b}\frac{\varepsilon_0 t^{-at-b}}{\Gamma(1-at-b)}. \tag{2.26}$$

The developed variable order constitutive model and experimental study were compared with Sweeney's [80], Fancy's [81], and Nutting's [16] models. The variable order constitutive model can better estimate the stress relaxation behavior under different strain levels and temperatures.

Experimental studies have primarily been conducted on synthetic materials, limiting the scope of investigation. However, biological tissues have also become a significant focus in fractional viscoelasticity research. Due to their complex mechanical properties, including time-dependent deformation and stress relaxation, fractional-order models have been increasingly applied to better understand their behavior.

The quasilinear viscoelastic (QLV) model was proposed by Fung [82]. QLV as a special case of fully nonlinear viscoelastic theory [83]. Although the rheological viscoelastic models and Fung's QLV model were widely used in experimental studies until 2005, Doehring et al. [84] may be the first who apply the fractional calculus on biological tissues successfully. They applied fractional calculus to model heart valve tissue for 1D uniaxial tension loading cases. They used both QLV theory and fractional order viscoelasticity and compared results for the same tissue. The FOV model was found better at modeling the aortic heart valve than the QLV model according to experimental evidence. Fung's QLV model is described by

$$\sigma(t) = \int_{-\infty}^{t} R(t-\tau)\frac{\partial \sigma^e(\varepsilon)}{\partial \varepsilon} d\varepsilon(\tau), \tag{2.27}$$

where $\sigma^e(\varepsilon)$ is defined as the instantaneous elastic response and $R(t)$ is the reduced relaxation function. Here, a proper assumption for the relaxation function plays a crucial role in the correct estimation of the stress function. Craiem et al. [85] assumed the kernel function appearing in Fung's QLV model in the form of a power function as follows,

$$R(t) = C_1 + C_2 \cdot t^{-\alpha}. \tag{2.28}$$

Freed and Diethelm [86, 87] investigated the human heel pad using fractional viscoelasticity in their two consecutive works. They showed that fractional calculus has excellent potential for modeling the relaxation and creep behavior of isotropic soft tissue.

Craiem et al. [85] and Craiem et al. [88] studied arterial viscoelasticity in two different works. They reported that the QLV modeling can successfully display the arterial mechanics. However, the FOV modeling is reportedly superior to the integer-order models and the QLV model in terms of prediction of actual material response. They used the fractional order Kelvin-Voigt model and standard linear elastic solid model with fractional spring–pot element to model the stress relaxation of the human aorta.

Grahovac and Zigic [89] modeled the muscle force relaxation of the hamstring muscle group based on Zener's model. The muscle extension was characterized by ramp extension in 16 seconds with a holding time of 100 seconds. The fractional differential equation was solved by Laplace transform. Grünwald's finite difference method was adopted to handle the fractional differentiation numerically. The experimental data was approximated by the seven-term exponential Prony series. The fractional model showed better confidence with the experimental results.

Libertaux and Pascon [90] studied the test results of an unconfined brain tissue compression from a previous work of others. They modeled the tissue with both convolution-based hyperviscoelasticity and fractional differential viscoelasticity. The parameters of the models are determined with stochastic optimization. The primary outcomes of their study are as follows. The single Mittag-Leffler function does not suffice to characterize the relaxation process of the brain tissue. However, adding another Mittag-Leffler function with different characteristic time and order would burden the computational speed. The fractional differential model is better at capturing the re-

laxation process.

Meral et al. [91] studied two tissue-mimicking materials under harmonic loading and compared the fractional and integer order viscoelastic models. Ramirez and Coimbra [92] compared different definitions of variable order derivative operators for the dynamic properties of a viscoelastic oscillator. Rossikhin and Shitikova [93] presented an extensive review study on the applications of fractional dynamic problems of solid mechanics. In a most recent review study on the variable-order fractional operators and some of their applications are presented by Patnaik et al. in [49].

An experimental investigation of postmortem brain tissue of an animal was performed by Bentil and Dupaix [94]. They modeled the brain tissue by a fractional Zener viscoelastic constitutive model. They conducted unconfined compressive stress relaxation tests on the brain tissue with different postmortem ages at 1 mm/min and 5 mm/min deformation rates. One of the research questions in their work is whether the fractional order can portray tissue degradation. They concluded that brain tissue degradation can be related to stiffness constants of the fractional Zener model. To that extent, they could not correlate tissue degeneration with postmortem age of the tissue with the fractional order.

Petekkaya & Tönük [95] conducted an experimental investigation on the viscoelastic properties of living human compound tissue. They measured the force-displacement response of the forearm bulk soft tissue with a hemispherical indentor assuming the isotropic tissue behavior. The constitutive behavior was modeled with a fractional Zener model by Demirci & Tönük [96], and material parameters were extracted. The accuracy of the model predictions for relaxation and creep behaviors was compared with the solutions obtained using the Prony series. A better agreement was reported in the case of fractional Zener-type viscoelastic modeling of the material behavior.

The viscoelastic properties of cancerous breast tissue are investigated by Carmichael et al. [97]. Breast tissue cells isolated from the highly-invasive and non-invasive stages of breast cancer were tested with an atomic force microscope at about $9 \pm 3\, mN$ load, which corresponds to a $2 - 3\ \mu m$ indentation of the corresponding cells. They modeled the Hertz contact force both by the SLS model and the fractional Zener model. The least-squares fitting procedure revealed that the fractional Zener model

could reflect the actual force response better than the former when the human breast cells are considered.

Dai et al. [98] compared experimental and numerical stress relaxation curve fit results of a mammal lung. For the modeling of the lung tissue, the fractional standard linear solid, standard linear solid, and generalized Maxwell models are utilized, and material parameters are extracted. The stress relaxation experiments are performed with a cylindrical indentor geometry. The fractional standard linear solid model was better at modeling the stress relaxation behavior though it requires fewer parameters to be determined.

The creep and relaxation behavior of the human knee ligaments and tendons (hamstring and patellar) are investigated by Bologna et al. [99]. As a critical result presented by the authors is that the numerical values of fractional orders are different in relaxation and creep modes of loading. This observation is commented as "relaxation runs faster than creep".

Traver et al. [100] used linear elastic, Kelvin-Voigt, Zener's standard linear elastic model, and fractional Kelvin Voigt model to capture in-vivo flexural behavior of the toenail plates for clinical purposes. Force relaxation and creep data of the twenty subjects showed that fractional-order modeling is superior to the other models when the root mean squared error (RMSE) value of the curve fit results is considered.

Fractional viscoelastic modeling further finds a good basis for most rock-based materials, earth crust geophysics, and soil-based materials such as clay. For instance, Peng et al. [101] simulated the wellbore creep behavior, and Wu et al. [102] developed a variable fractional order creep model for rock-based materials. Xu et al. [103] investigated the creep behavior of soils. Han et al. [104] adopted a variable-order fractional viscoelastic model based on the Scott-Blair model for the stress relaxation behavior of rock. The order function and the mechanical parameters are determined through analysis of the log-log stress-strain data. This approach involves fitting the model to the experimental data by examining the relationship between stress and strain on a logarithmic scale, which facilitates the accurate determination of the fractional order function and relevant mechanical parameters. They proposed the order function to be

an exponential decay function of the normalized function of strain as follows,

$$\alpha(t) = e^{-\frac{\varepsilon(t)}{\varepsilon_0}}, \tag{2.29}$$

where ε_0 is the normalization factor of strain, and $\varepsilon(t)$ is the strain function.

They unveiled that the rock materials represent different material behaviors at different deformation levels. The derivative order shifts its form at each deformation level, making it a piece-wise varying order function. Wu et al. [105] studied the creep behavior of the salt rock. They developed a short-memory approach to the problem. The creep behavior of the salt rock was split into three stages, namely, transient creep, steady creep, and accelerated creep. The model remembers only the strain in the current stage of creep. They assumed the fractional-order $\alpha(t)$ is constant at every stage. Also, they used the strain information at the previous stage. The parameters in the viscoelastic constitutive model were obtained from curve fitting results by taking the logarithm of strain and time data.

Xu and Jiang [106] studied the time-dependent creep behavior of polymer and rock. The authors employed an interior-point algorithm for inverse identification of material parameters contained in the fractional model, despite there being possible other alternatives such as the Levenberg-Marquardt method, the genetic algorithm, and the Bayesian method.

Bouras et al. [107] studied the non-linear creep behavior of concrete both under different constant temperatures and increasing temperatures based on the variable order fractional viscoelastic models. They obtained curve fit expressions of the fractional order in terms of temperature data. The model they developed showed a good agreement with the experimental evidence, especially at elevated temperatures. However, near room temperature, the model weakly displayed the exact behavior for different concrete mixtures.

Fractional viscoelasticity serves as a versatile tool for modeling a wide range of materials, including adhesives, shape memory polymers, and propellants. Its ability to capture complex time-dependent mechanical behavior makes it particularly useful for materials that exhibit both elastic and viscous characteristics. By providing a more accurate representation of material responses, fractional viscoelasticity has gained

increasing attention in various engineering and scientific applications.

Li et al. [108] proposed a variable-order fractional viscoelasticity model for shape memory polymers. The physical properties of such materials undergo a dramatic shift under the effect of the internal structure changes. Such changes are always triggered by an external stimulus such as light or temperature exposure. Based on the fractional Zener model, they benefited from Lorenzo's [51] C1 type of derivative definition. Their material model consists only of time-fractional-order differential equations. If the spatially non-homogeneity is considered and long-term spatial contribution is sought, a partial fractional differential equation with a space-time fractional differential operator would be employed as per their suggestion. They used the Levenberg-Marquardt regularization method to find the variable order with an iterative process.

Colinas-Armijo et al. [109] investigated epoxy resin subjected to random temperature changes. They employed the fractional Maxwell model and adopted the time-temperature superposition principle. The experimental data were taken from the previous work of the first author. They obtained the material parameters, including the fractional order in terms of the temperature. The fractional order was expressed as a power function of the temperature, while the other material parameters were shown as a linear function of temperature.

Esmonde and Holm [110] investigated the dynamic fractional viscoelastic properties of the two adhesive substances, cyanoacrylate adhesive, and methacrylate resin. They adopted a method that assumes a change from a particular fractional rheological model to another appropriate model during the curing process. For instance, the Maxwell model is selected as a starting model of methacrylate at the beginning of cure, the end of cure is modeled with the SLS model. The transition between the two models is governed by a transition function formulated by the ratio of the final state to the initial state.

Fang et al. [4] applied the fractional calculus to obtain the viscoelastic material behavior of the solid propellants used in solid rocket motors. Although the mechanical behavior of the solid propellants is highly affected by side factors such as strain rate, load type, temperature, humidity, and aging, they did not include these factors in their

study. They proposed a generalized Maxwell model consisting of an equilibrium part and a non-equilibrium part. The equilibrium part is represented by a linear spring. The non-equilibrium part comprises two Maxwell branches connected in parallel, one of which is used to model rubbery behavior. The other one is used to capture the glassy behavior of the propellant; see Fig. 2.8.

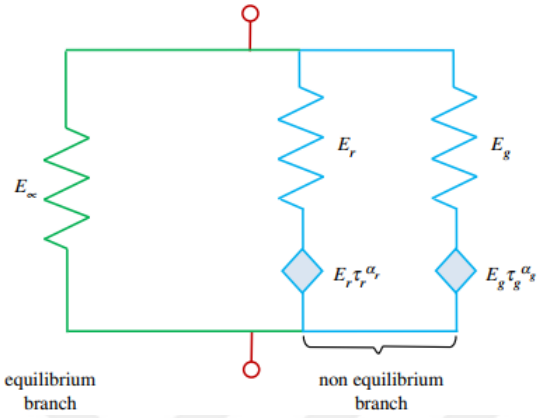

Figure 2.8: Fang's Model [4]

They obtained the dynamic material properties experimentally. The stress relaxation and its fractional counterpart are compared with the seven-term Prony series solution. Dynamic experiments revealed that the fractional model could accurately portray the glass transition region and the stress relaxation behavior.

2.2.3 Parameter Estimation Studies in the Literature

Because the behavior of the viscoelastic material highly depends on the order function, a precise definition of the order is always a key characteristic. Tabatabaei et al. [5] studied the order identification process in soft tissue. They adopted an adaptive method to determine the value of the fractional-order and other parameters in the fractional-order viscoelastic material model. To test their algorithm they produced synthetic data on the fractional order. Subsequently, Gaussian white noise was added to the fractional order. Then, they tested their algorithm on the noisy fractional order data. Fig. 2.9 illustrates the Gaussian noise added synthetically produced fractional order data (dashed line) and the fractional order determined by their algorithm (continuous line).

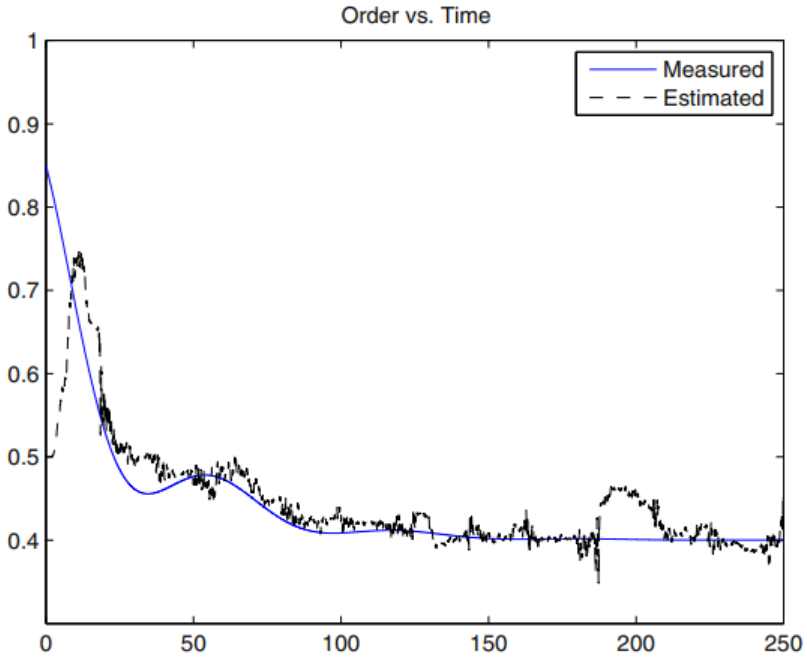

Figure 2.9: Gaussian White Noise Data on Fractional Order [5]

The developed method was experimentally verified with an indentation test apparatus with collected force-displacement data. The measured strain and model estimate is presented in Fig. 2.10.

The top of Fig. 2.10 shows the discrepancy between the measured and inversely calculated strain response of the soft tissue, whereas the corresponding estimates for the fractional order are shown at the bottom of Fig. 2.10.

Meng et al. [111] used variable-order fractional calculus to model the post-yield phase of some ductile metallic materials and soil. They successfully showed that the variable-order fractional modeling can simulate strain hardening and softening at constant strain rates tension and compression tests. The derivative order is found to be zero near the small strains, but it portrays a linear dependence on the strain level. It is observed from the obtained results in [111], that the order function is triggered when the deformation exceeds a certain level.

Meng et al. [112] formulated the variable order Scott-Blair model and its strain dependence under a constant rate of deformation. The fractional order was assumed to

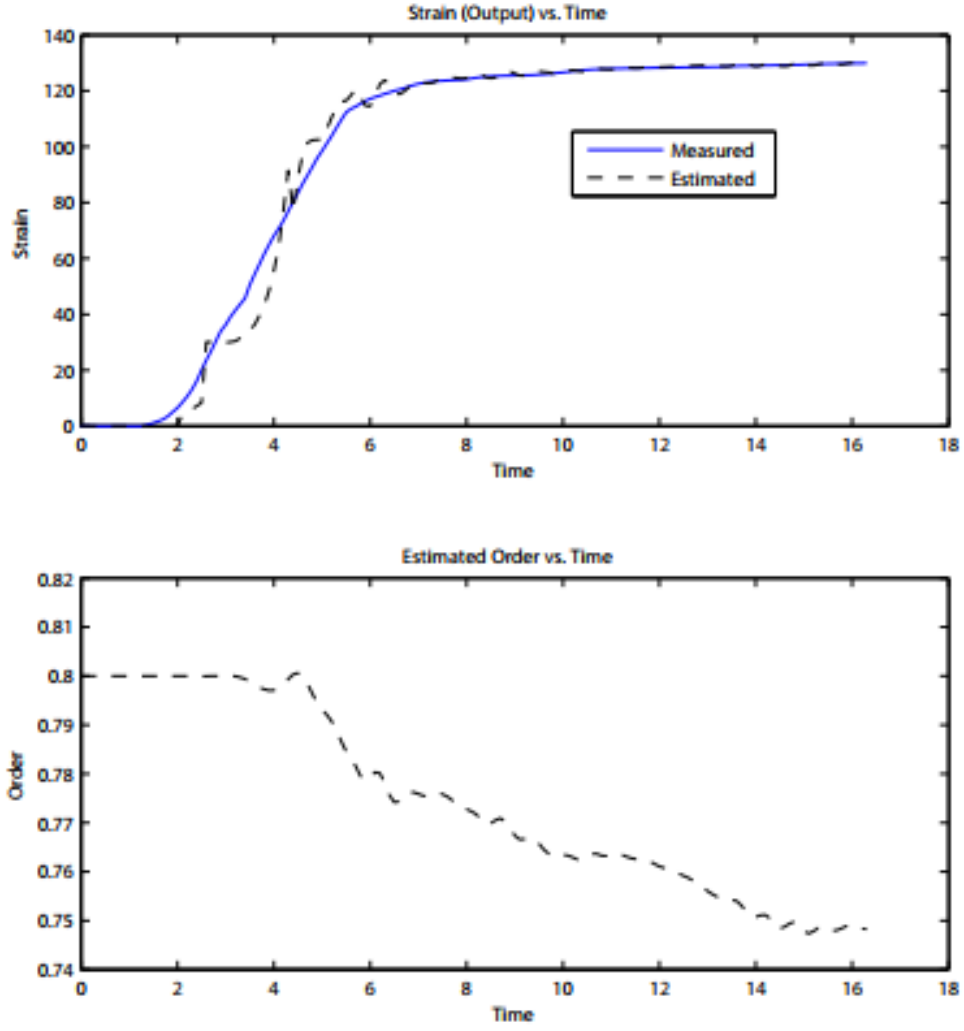

Figure 2.10: Measured Strain (Top) and VO-Viscoelastic Model Estimates (Bottom) [5]

be linearly dependent on time and strain. The model parameters were extracted at different temperatures and strain rates for PC material. To eliminate the physical aging and reset the thermal history, the specimens were held at $150\ ^{\circ}C$ temperature for 30 min. The test temperatures are chosen between $20\ ^{\circ}C$ and $140\ ^{\circ}C$. The specimens were kept at the test temperature for 30 minutes prior to the experiment to ensure thermal equilibrium. The compression tests were performed at two different strain rates. The material parameters are extracted to simulate the strain hardening behavior above the strain $\varepsilon = 0.5$.

Meng et al. [113] used a piece-wise definition for the variable fractional order for the constitutive model of polymeric materials under uni-axial loading cases for constant strain rates. They assumed the fractional order takes up a new value at each time increment. The parameters, including the fractional order of the material described by a spring–pot element (Scott-Blair model), were found from the curve fit of logarithmic stress and logarithmic strain data. The method was tested with small and large strain settings at low to mid strain rates under tension (Polyurea) and compression (PET). The constant fractional-order model was not found effective for the specimens under large deformation. However, under small deformations, the constant-order fractional viscoelastic model captured the material behavior well enough. The experimental evidence showed that the fractional order changes its behavior after a certain strain level is reached for a particular material at different deformation speeds. The variable fractional order from the applied strain is determined from the formulation presented in their work. Meng et al. [114] also investigated the description of the fractional-order amorphous glassy polymers under compressive strain. The function for the variable order was proposed as a linear function of time. The fractional orders of PETG and PMMA materials undergo three regimes during the deformations.

2.2.4 Numerical Studies in the Literature

Although many of the studies mentioned earlier primarily focus on strong numerical solutions, this section is dedicated to exploring various numerical approaches.

The studies addressing the numerical aspects of fractional differential equations can broadly be classified into three primary areas: (1) solving fractional differential equa-

tions using various numerical methods, (2) efforts on optimizing numerical solvers by efficiently managing memory properties and reducing computational costs, and (3) determining the physical parameters of the fractional system.

One of the early contributions to numerical methods was made by Oldham and Spanier [61], who introduced techniques for numerical differentiation and integration. Building upon this, Diethelm [115] developed an algorithm for solving fractional generic differential equations of constant fractional orders, and later, Diethelm et al. [116] extended this work by employing a predictor-corrector algorithm. This approach generalized the Adams integrator, a method commonly used for solving first-order problems numerically. In a similar vein, Adolfsson et al. [117] utilized an internal variable formulation of stress. To manage the high computational cost associated with the growing and accessing of stored data at each time step, and to reduce the memory requirements needed for numerical computations, they introduced sparse quadrature.

Diethelm et al. [118] further contributed by presenting a variety of numerical algorithms aimed at solving different fractional differential equations. Their work also included a scheme for the computation of the Mittag-Leffler function and its derivatives. Valerio and da Costa [119] provided numerical approximations for different variable-order fractional derivatives, utilizing a fuzzy interference engine to approximate the derivatives of functions with variable orders. Additionally, Li [120] proposed a highly efficient method for numerically solving fractional differential equations, specifically by analytically expressing Caputo derivatives through cubic B-spline wavelets, in conjunction with a generalized wavelet collocation method.

In parallel, researchers have continually sought ways to reduce computational costs, often focusing on optimizing memory usage. Several studies have addressed this challenge with innovative techniques. For instance, Podlubny [121] introduced the fixed memory principle, which helps streamline memory usage. Similarly, Ford & Simpson [122] and Diethelm & Freed [123] adopted logarithmic memory, a technique that further optimizes computational resources. Deng [124] proposed the short memory method, which was later explored by Libertiaux [90]. More recently, Tavasani et al. [125] applied shifted Chebyshev polynomials to solve the Caputo-Prabhakar-like fractional derivative of varying order.

In the same line of thought, El Hamidi & Tfayli [126] investigated the identification of order in the fractional differential equations, while Beltempo et al. [127] focused on the aging behavior of materials. They developed a numerical scheme for fractional viscoelastic materials, which accounts for hereditary aging effects. Du & Liang [128] introduced two new approximations for fractional derivatives of variable order, offering further improvements in computational accuracy. Similarly, Tavares et al. [129] developed a numerical solution for variable-order fractional partial differential equations. Another notable contribution was made by Bhrawy et al. [130], who developed a numerical algorithm for solving fractional differential equations involving variable-order Caputo derivatives.

For more extensive theoretical analysis, the reader may refer to the comprehensive works of Lai et al. [131] and Anastassiou et al. [132], which provide in-depth details on numerical methods applied to constant and variable-order fractional differential equations.

2.2.5 Review Studies

The first comprehensive review study on the field was published by Freed [28] under NASA. The theory of fractional viscoelasticity, mathematical and numerical tools developed until their time included in their work. The formulations of the isotropic and transversely isotropic viscoelastic models are presented. Surguladze [133] published another review with a mathematics point of view, including certain applications on the topic.

Samko [134] conducted a review study on the mathematical framework of variable-order fractional modeling. Chen et al. [78] presented an overview study of the simple rheological models and their formulations.

Comprehensive review studies by Freed [28] and Surguladze [133] summarized the theoretical and numerical tools developed in the field, while Lorenzo and Hartley [51] advanced the concept of variable-order fractional operators by relating the fractional order to temperature variations.

References [135] and [136] present further details on the mathematical background

of the theory, applications, and even more details. A recent review study is presented by Bonfanti et al. [137] provided a summary table of studies concerning the studies on the real materials. Also, they have provided benchmark material data for each of the traditional and fractional models. Yang et al. [138] recently published a book containing in-depth mathematical analysis. It also discusses the existing fractional operators, their derivations, many features, and the theoretical basis of the field.

As a concluding remark for this section, several key insights can be drawn from the literature survey:

- Most polymeric materials undergo significant changes in their properties once the glass transition temperature is reached. As such, temperature change plays a crucial role in variable fractional-order viscoelasticity.
- A noticeable gap in the literature exists regarding the characterization of fractional-order behavior based on real experimental data.
- Variable-order fractional viscoelasticity shows great potential for accurately capturing the mechanical behavior of viscoelastic materials, particularly by considering both internal and external variables simultaneously.
- The application of the variable fractional-order viscoelasticity concept to commercial finite element analysis software, specifically using user material subroutines, remains largely unexplored.

This study will specifically focus on the last three outcomes listed above. By delving into these areas, we aim to provide a detailed analysis and deeper insights into their implications for practical applications.

In the following chapters, we will address the material characterization, parameter estimation, and finite element analysis (FEA) applications of the proposed concepts.

CHAPTER 3

MODELING OF THE VISCOELASTIC BEHAVIOR BY FRACTIONAL CALCULUS

The general fractional viscoelastic model is Scott-Blair's single spring-pot model. The model represents an intermediate behavior between linear elastic solid and viscous fluid. The variable fractional order model has the substantial property of continuous adaptability from a purely linear elastic case to a purely viscous state and vice versa. For such states the adaptation of the fractional order permits it may take up values between 0 and 1 which could continuously change by internal and/or external variables. The adaptation property inherent in the variable fractional-order viscoelastic model significantly simplifies the formulation of the mechanical model. In contrast, a model with multiple rheological elements would typically require complex configurations of springs and dashpots. Such configurations demand accurate estimation of each individual parameter, which is much more challenging. The variable fractional order viscoelastic model is superior in these aspects over classical rheological and constant fractional order viscoelastic models.

The rheological model representing the constant fractional order spring-pot element is illustrated by a square element, as shown in Fig. 3.1. This constitutive model involves three material constants: E (elasticity constant), θ (viscous parameter), and α (fractional order). In the literature, the fractional characteristic number E_f is commonly employed, which denotes the product of these three material parameters. To denote the variability on the fractional order an arrow is put on the square element as shown in Fig. 3.2.

The model itself is a single mechanical element capable of capturing the elastic and viscous behavior at the same time. Similar to the rheological viscoelasticity, the use

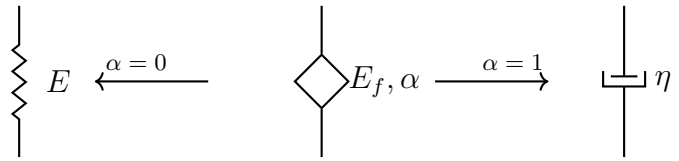

$$\sigma(t) = E\frac{d^0}{dt^0}\varepsilon(t) \qquad \sigma(t) = E_f\frac{d^\alpha}{dt^\alpha}\varepsilon(t) \qquad \sigma(t) = \eta\frac{d^1}{dt^1}\varepsilon(t)$$

Figure 3.1: Fractional Spring-pot Element

of Scott-Blair's spring-pot element can be used in combination with the linear elastic springs and dashpots in series and parallel branches to construct complicated models. However, adding extra mechanical elements in the rheological models causes complicated mathematical models to be solved to obtain accurate mechanical responses. Furthermore, rheological models comprising springs and dashpots are capable of producing mechanical responses which are exponential functions of time [14, 96]. Nutting's [16] observation suggests that viscoelastic materials show mechanical responses that could be better represented by decaying or growing functions of time.

Since the derivation, finite element analysis applications, and parameter estimation get even more complicated, we limit the complexity of the viscoelastic model in this study by a single Scott-Blair's spring-pot element and add variability property on the fractional order. Variable order spring-pot element has three material properties as shown in Fig. 3.2. Those properties are elastic constant E [MPa], viscous parameter θ $[s^{-\beta}]$, and fractional variable order $\beta(t)$.

The fractional characteristic function, $E_f(t)$, is derived from the elasticity constant, the viscous constant, and the fractional order sequence.

In this chapter, we present the methods we adopted to calculate the stress and strain responses of the viscoelastic material. The method is introduced starting with the constant-order case and then extended to the variable-order material model. Analytical solutions of the constant-order viscoelastic model to the proposed problems are

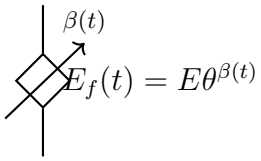

$$\sigma(t) = E\theta^{\beta(t)} \frac{d^{\beta(t)}}{dt^{\beta(t)}} \varepsilon(t)$$

Figure 3.2: Variable Order Spring-pot Element

also derived. The suggested loading conditions form the foundation for the experimental problems, providing the theoretical framework upon which the experimental setup and analysis are built. These problems serve as a basis for validating the models and methodologies used in the study.

3.1 Modeling the Constant Fractional Order Viscoelastic Behavior

The analytical solution of the constant-order fractional Scott-Blair viscoelasticity model can be easily derived for mathematically simple, easy-to-apply, and well-behaved strain histories. In this section, the mathematical tools used to extract the stress-strain responses of the constant fractional-order viscoelastic Scott-Blair model will be presented in the context of practical application. These methods can also be applied to other detailed material models, such as the Fractional Kelvin-Voigt Model, the Fractional Maxwell Model, and similar. During the development of analytical solutions, the Caputo definition of fractional derivatives, differentiation with the Riemann-Liouville operator of fractional derivatives, and integral transformations can be employed whenever necessary.

In the following section, we will present the mathematical tools and derivations required to obtain the stress or strain histories for several simple load/deformation histories, to extract the material responses.

3.1.1 Ramp Stress Problem

In a load-controlled test, the mechanical load is applied via a feedback-controlled mechanism. Now we investigate an application of a ramp load as a case study and its analytical solution is derived.

A ramp load with a load rate of S is applied as a function of time, $\sigma(t) = S \cdot t$,

$$S \cdot t = E\theta^{\alpha} D^{\alpha} \varepsilon(t). \tag{3.1}$$

Writing out in the expanded form gives us,

$$S \cdot t = E\theta^{\alpha} \int_0^t (t-\tau)^{-\alpha} \dot{\varepsilon}(\tau) d\tau. \tag{3.2}$$

The unknown, $\varepsilon(t)$, can be obtained through Laplace transformation. Using the Laplace transform of a constant order fractional derivative of a generic function, $f(t)$,

$$\mathcal{L}({}_0^C D_t^{\alpha} f(t); s) = s^{\alpha} F(s) - s^{\alpha-1} f(0), \tag{3.3}$$

where s denotes the Laplace variable [139]. The stress-strain relation can be expressed in the Laplace domain as follows,

$$\frac{S}{E\theta^{\alpha}} \frac{1}{s^2} = s^{-\alpha} \tilde{\varepsilon}(s). \tag{3.4}$$

Solving for strain and taking the inverse Laplace transform, we obtain,

$$\varepsilon(t) = \frac{S}{E\theta^{\alpha}} \frac{t^{\alpha+1}}{\Gamma(2+\alpha)} = \frac{\sigma(t) t^{\alpha}}{E\theta^{\alpha} \Gamma(2+\alpha)}. \tag{3.5}$$

Here, $\sigma(t)$ represents the stress at time t, E is the elastic modulus, ε denotes the strain the material is subjected to, α is the constant fractional order, and θ is the viscous parameter.

3.1.2 Stress Relaxation Problem

Stress relaxation is one of the important phenomena observed in the viscoelastic materials. The relaxation characteristics are evaluated by applying a constant deformation on the material. This implies that the strain function is constant in time, meaning that $\varepsilon(t) = \epsilon$ and we have,

$$\sigma(t) = E\theta^{\alpha} ({}_0^C D_t^{\alpha} \varepsilon)(t) = E\theta^{\alpha} \frac{1}{\Gamma(1-\alpha)} \int_0^t (t-\tau)^{-\alpha} \underbrace{\dot{\varepsilon}(\tau)}_{\varepsilon(t)=\epsilon} d\tau = 0. \tag{3.6}$$

If this is the case, Caputo definition of the fractional derivative does not work. This is due to the derivative term appearing in the integral producing zero value when differentiated as shown in Eq. 2.11, thereby indicating an absence of stress relaxation in the material. This limitation represents a drawback of the Caputo definition. Consequently, the Riemann-Liouville (RL) definition should be employed. RL definition involves computing the derivative outside the integral rather than inside the integration. The solution is obtained as

$$\sigma(t) = E\theta^{\alpha}({}^{RL}_{0}D^{\alpha}_{t}\varepsilon)(t) = E\theta^{\alpha}\frac{1}{\Gamma(1-\alpha)}\frac{d}{dt}\int_{0}^{t}(t-\tau)^{-\alpha}\epsilon d\tau. \tag{3.7}$$

After appropriately changing the variable $t - \tau = u$ and $-d\tau = du$, and solving for the stress, the solution is derived as follows,

$$\sigma(t) = \frac{E\epsilon}{\Gamma(1-\alpha)}\left(\frac{t}{\theta}\right)^{-\alpha}. \tag{3.8}$$

3.1.3 Ramp Strain Loading Problem

The mechanical testing equipment allows position-controlled tests. Such equipment applies load by controlling the displacement exerted on the material. The simplest position-controlled test is the ramp load. The ramp load can be defined as

$$\varepsilon(t) = \epsilon \cdot t, \tag{3.9}$$

where ϵ is the constant strain rate. Writing out the stress-strain relationship, we get

$$\sigma(t) = E\theta^{\alpha}\,{}^{C}_{0}D^{\alpha}_{t}\varepsilon(t). \tag{3.10}$$

and

$$\begin{aligned} {}^{C}_{0}D^{\alpha}_{t}\varepsilon(t) &= \frac{1}{\Gamma(1-\alpha)}\int_{0}^{t}(t-\tau)^{-\alpha}\dot{\varepsilon}(\tau)d\tau \\ &= \frac{1}{\Gamma(1-\alpha)}\int_{0}^{t}(t-\tau)^{-\alpha}\epsilon d\tau \\ &= \frac{\epsilon t^{-\alpha+1}}{\Gamma(2-\alpha)}. \end{aligned} \tag{3.11}$$

The above solution is obtained by proper change of variables $t - \tau = u$, and $-d\tau = du$. Then the stress-time relation is obtained as follows

$$\sigma(t) = E\epsilon\theta^{\alpha}\frac{t^{1-\alpha}}{\Gamma(2-\alpha)}. \tag{3.12}$$

If the RL definition of fractional derivative is applied, we obtain,

$$\begin{aligned}\sigma(t) &= E\theta^{\alpha}\, {}^{RL}_{0}D^{\alpha}_{t}\varepsilon(t) \\ &= E\theta^{\alpha}\frac{1}{\Gamma(1-\alpha)}\frac{d}{dt}\int_0^t (t-\tau)^{-\alpha}\epsilon d\tau \\ &= \frac{E\theta^{\alpha}\epsilon t^{-\alpha+1}}{\Gamma(2-\alpha)} = \frac{E\theta^{\alpha}\varepsilon(t)t^{-\alpha}}{\Gamma(2-\alpha)},\end{aligned} \tag{3.13}$$

as expected.

3.1.4 Creep Problem

The creep test is one of the most commonly employed tests in the viscoelastic materials. The test is performed at constant load while deformation on the specimen is being recorded. Assuming the material is subjected to a uniform stress with $\sigma(t) = S$, recalling the material model,

$$\sigma(t) = E\theta^{\alpha}D^{\alpha}\varepsilon(t) \tag{3.14}$$

and setting the stress function to a constant value $\sigma(t) = S$,

$$\frac{S}{E\theta^{\alpha}} = D^{\alpha}\varepsilon(t), \tag{3.15}$$

Laplace transformation gives us,

$$\mathcal{L}\left(\frac{S}{E\theta^{\alpha}}; s\right) = \mathcal{L}(D^{\alpha}\varepsilon(t); s), \tag{3.16}$$

$$\frac{S}{E\theta^{\alpha}}\frac{1}{s} = s^{\alpha}\tilde{\varepsilon}(s). \tag{3.17}$$

Then rearranging and solving for the strain in the Laplace domain, we get

$$\tilde{\varepsilon}(s) = \frac{1}{s^{\alpha+1}}\frac{S}{E\theta^{\alpha}} \rightarrow \frac{\Gamma(\alpha+1)}{s^{\alpha+1}}\frac{S}{\Gamma(\alpha+1)E\theta^{\alpha}}. \tag{3.18}$$

Last, inverse Laplace transform produces the strain solution in the time domain as,

$$\varepsilon(t) = \frac{t^{\alpha}S}{\Gamma(\alpha+1)E\theta^{\alpha}}. \tag{3.19}$$

Alternatively, the inversion of the derivative operator will yield the same result,

$$I^{\alpha}S = E\theta^{\alpha}D^{-\alpha}D^{\alpha}\varepsilon(t), \tag{3.20}$$

$$\varepsilon(t) = \frac{S}{E\theta^{\alpha}} \frac{t^{\alpha}}{\Gamma(\alpha)\alpha} = \frac{St^{\alpha}}{E\theta^{\alpha}\Gamma(\alpha+1)}. \tag{3.21}$$

Note that, an important relation between the creep compliance and stress relaxation modulus in the Laplace domain is

$$\tilde{R}(s)\tilde{C}(s) = \frac{1}{s^2}. \tag{3.22}$$

The creep compliance is then expressed as

$$C(t) = \frac{t^{\alpha}}{E\theta^{\alpha}\Gamma(1+\alpha)}. \tag{3.23}$$

3.1.5 Generic Strain History

The stress-strain behavior of a fractional viscoelastic material can be calculated by the Grünwald-Letnikov fractional derivative. The method uses a backward difference scheme to calculate the stress response for a prescribed strain history [140].

The stress and strain response of a viscoelastic material is calculated by Eq. 3.24,

$$\begin{aligned} \sigma(t) &= E_f({}^{C}D^{\alpha}\varepsilon)(t) \\ \varepsilon(t) &= E_f^{-1}({}^{C}D^{-\alpha}\sigma)(t) \end{aligned}, \qquad 0 \leq \alpha \leq 1, \tag{3.24}$$

where E_f is the fractional constant number denoting for $E\theta^{\alpha}$, the symbol D stands for the fractional derivative operator, and the $D^{-\alpha}$ is the fractional integration operator. For the constant fractional-order mathematical model, the fractional derivative operator is mathematically inverse of the fractional integral operator. It is essential here to provide a mathematical description of the constant fractional order derivative and fractional integral operators, respectively by,

$${}^{C}D^{\alpha}f(t) = \int_0^t \frac{(t-\tau)^{-\alpha}}{\Gamma(1-\alpha)} \dot{f}(\tau)d\tau \ , \quad \alpha = [0,1] \tag{3.25}$$

and

$$I^{\alpha}f(t) = D^{-\alpha}f(t) = \int_0^t \frac{(t-\tau)^{\alpha-1}}{\Gamma(\alpha)} f(\tau)d\tau \ , \quad \alpha = [0,1]. \tag{3.26}$$

As one may recognize, Eq. 3.25 looks like an integral operation rather than a classical-integer order derivative operation.

If the fractional derivative concept is applied to the COFSB model viscoelasticity stress-strain relationship, it reads

$$\begin{aligned}\sigma(t) &= \frac{E_f}{\Gamma(1-\alpha)}\int_0^t (t-\tau)^{-\alpha}\dot{\varepsilon}(\tau)d\tau,\\ \varepsilon(t) &= \frac{1}{E_f\Gamma(\alpha)}\int_0^t (t-\tau)^{\alpha-1}\sigma(\tau)d\tau.\end{aligned} \tag{3.27}$$

For the mathematically simple functions, the stress-strain relationship can easily be derived from the Eq. 3.27. Riemann-Liouville and Caputo-type fractional operators can be expressed in discretized form by employing the Grünwald-Letnikov finite difference scheme. Recalling the Riemann-Liouville (1850) and Caputo (1967) definitions of the fractional derivative,

$${}^{RL}D^{\alpha}f(t) = \begin{cases} \dfrac{1}{\Gamma(m-\alpha)}\dfrac{d^m}{dt^m}\displaystyle\int_0^t \frac{f(\tau)}{(t-\tau)^{\alpha+1-m}}d\tau\ ; & m-1\le\alpha<m,\\ \dfrac{d^m f}{dt^m}\ ; & \alpha=m.\end{cases} \tag{3.28}$$

$${}^{C}D^{\alpha}f(t) = \begin{cases} \dfrac{1}{\Gamma(m-\alpha)}\displaystyle\int_0^t \frac{f^{(m)}(\tau)}{(t-\tau)^{\alpha+1-m}}d\tau\ ; & m-1\le\alpha<m,\\ \dfrac{d^m f(t)}{dt^m}; & \alpha=m,\end{cases} \tag{3.29}$$

where m is the next integer greater than α so that, $m = \lceil\alpha\rceil$.

The backward difference Grünwald-Letnikov (1868) derivative is expressed as

$${}^{GL}Df(t) = \lim_{N\to\infty}\left(\frac{t}{N}\right)^{-\alpha}\sum_{j=0}^{N-1} A_{j+1} f\left(t - j\frac{t}{N}\right), \tag{3.30}$$

where A_{j+1} are the Grünwald coefficients expressed by the recursive formula

$$A_{j+1} = \frac{\Gamma(j-\alpha)}{\Gamma(-\alpha)\Gamma(j+1)}. \tag{3.31}$$

Application of these generic definitions to the stress-strain relationship of a viscoelastic continuum subjected to a strain history of ε_n reads [141]

$$\sigma_n = E_f\,{}^{GL}D^{\alpha}\varepsilon_n = E_f\Delta t^{-\alpha}\mathbf{\Omega}_{(n\times n)}(\alpha)\varepsilon_n, \tag{3.32}$$

where ${}^{GL}D^{\alpha}(\bullet)$ is the constant order Grünwald-Letnikov fractional derivative operator. The matrix appearing in Eq. 3.32 stores the Grünwald coefficients and is

expressed as,

$$\mathbf{\Omega}_{(n\times n)}(\alpha) = \begin{bmatrix} \omega_1(\alpha) & 0 & \dots & & 0 \\ \omega_2(\alpha) & \omega_1(\alpha) & 0 & \ddots & \\ \vdots & & & \ddots & 0 \\ \omega_n(\alpha) & \omega_{n-1}(\alpha) & \dots & \omega_2(\alpha) & \omega_1(\alpha) \end{bmatrix}. \tag{3.33}$$

The entries that appeared in the lower band triangular strip matrix, $\mathbf{\Omega}(\alpha)$, used to calculate the Grünwald-Letnikov fractional derivative can be found by using the recursion formula,

$$\begin{aligned} \omega_1(\alpha) &= 1\,; \quad j = 1, \\ \omega_2(\alpha) &= \alpha\,; \quad j = 2, \\ \omega_{j+1}(\alpha) &= \omega_j(\alpha)\frac{j-1-\alpha}{j}\,; \quad j > 2. \end{aligned} \tag{3.34}$$

In the above description of the formulation of the stress using the strain, the history of deformation is divided into n time steps so that,

$$\sigma(t), \varepsilon(t) = 0 \quad \text{for} \quad t \leq 0. \tag{3.35}$$

Constant time step discretization is assumed, meaning that the time progression occurs in uniform intervals. Specifically, the time steps are defined as:

$$t_j = j\Delta t \quad \text{for} \quad j = 1, 2, 3, \dots, n. \tag{3.36}$$

This approach assumes a constant time increment, Δt, between each discrete time point. The use of constant time steps ensures a straightforward numerical implementation. While this method simplifies the formulation, it may also introduce certain limitations in terms of capturing transient behaviors that could require finer time resolution in specific cases.

Thus, the stresses at every time step $\sigma_n^T = [\sigma_1,\ \sigma_2, \dots,\ \sigma_n]$ are calculated using the strain history $\varepsilon_n^T = [\varepsilon_1,\ \varepsilon_2, \dots,\ \varepsilon_n]$ expressed as one-dimensional arrays. We underline that the validity of the above model is limited by the following cases;

- Material should be initially stress/strain-free. The model loses its validity in the multi-step problems.
- The model is developed for the fixed time step problems. The formulation may not maintain its accuracy in cases involving non-uniform or adaptive time increments.

3.2 Modeling the Variable Fractional Order Viscoelastic Behavior

As discussed in Chapter 2, different variable order fractional viscoelasticity models are proposed in the literature. The VO fractional viscoelastic model adopted in this study is as follows,

$$\sigma(t) = E_f(t)({}^{C}D^{\beta(t)}\varepsilon)(t) = E_f(t)\int_0^t \frac{(t-\tau)^{-\beta(t)}}{\Gamma(1-\beta(t))}\dot{\varepsilon}(\tau)d\tau. \tag{3.37}$$

The VOF viscoelastic model adopted in this study readily portrays the fading memory property of viscoelastic material. The other alternative forms of VOF viscoelastic models discussed previously should add the contribution of the history of the past parameters. Since there is no known mechanical example of such a material remembering the past states of the material parameters, those models are excluded from this work.

The adopted model portrays the memory of the past strain history only. The above form of fractional viscoelasticity is the generalization of the constant order fractional spring-pot element.

For the mathematically simple strain functions (i.e., strain history) and description of the fractional order, it is easy to calculate the stress response. A comparable method to constant order fractional viscoelasticity is needed to calculate the stress response for the generic strain history. The variable order Grünwald matrix shall be denoted by $\mathbf{\Psi}(\beta(t))$ to distinguish it from the constant order Grünwald coefficients matrix $\mathbf{\Omega}(\alpha)$ to prevent confusion. For the same reason, the notation used to denote fractional order is switched to another symbol, β with a variability notifier for the time, $\beta(t)$. Similar to the constant order fractional viscoelastic model, $\mathbf{\Psi}_{(n\times n)}(\beta(t))$ is an n size square lower triangular strip matrix that is described by Podlubny in [43, 142],

$$\sigma_n = \mathbf{\Psi}_{(n\times n)}(\beta(t))\varepsilon_n. \tag{3.38}$$

Since the fractional order does not have a constant number in the course of analysis, the fractional characteristic number is no longer constant but is an explicit function of fractional order or an implicit function of time. Therefore, expressing the fractional characteristic number at every increment,

$$\eta_i = E_{f_i}\Delta t_i^{-\beta_i} \quad \text{for} \quad E_{f_i} = E\theta^{\beta_i} \tag{3.39}$$

the Grünwald-Letnikov derivative in matrix form reads

$$\boldsymbol{\Psi}(\beta(t)) = \begin{bmatrix} \eta_1\omega_1(\beta_1) & 0 & \dots & & 0 \\ \eta_2\omega_2(\beta_2) & \eta_2\omega_1(\beta_2) & 0 & \ddots & \\ \vdots & & & \ddots & 0 \\ \eta_n\omega_n(\beta_n) & \eta_n\omega_{n-1}(\beta_n) & \dots & \eta_n\omega_2(\beta_n) & \eta_n\omega_1(\beta_n) \end{bmatrix}. \tag{3.40}$$

Then, the stress is then formulated by

$$\sigma(t) = \begin{bmatrix} \eta_1\omega_1(\beta_1) & 0 & \dots & & 0 \\ \eta_2\omega_2(\beta_2) & \eta_2\omega_1(\beta_2) & 0 & \ddots & \\ \vdots & & & \ddots & 0 \\ \eta_n\omega_n(\beta_n) & \eta_n\omega_{n-1}(\beta_n) & \dots & \eta_n\omega_2(\beta_n) & \eta_n\omega_1(\beta_n) \end{bmatrix} \begin{bmatrix} \varepsilon_1 \\ \varepsilon_2 \\ \vdots \\ \varepsilon_n \end{bmatrix}. \tag{3.41}$$

We note that although the constant order fractional derivative is the inverse of the fractional integration operator of the constant order, the same is not valid for the variable order model [47, 143].

The algorithms used to calculate the stress response of a variable fractional order viscoelastic continuum under a generic strain history are presented as Alg.1 and Alg.2.

Algorithm 1 Calculation of VO Grünwald Coefficients

Require:

$n \geq 1$, ▷ Length of the discretized time data defined as 1D vector array

$\beta(i)$, ▷ $\beta(i)$ is the stored/calculated values of variable fractional order for every time step i, expressed in a vector array form

Ensure: Dimensional conformity

length$(T) = n$, ▷ T is total time

length$(\beta) = n$,

Initialize:

$\omega(1) = 1$ ▷ First term of the Grünwald coefficients

if $n \geq 1$ **then**

for $j = 1 : n$ **do**

$\omega(j+1) = \omega(j)\dfrac{j - 1 - \beta(i)}{j}$ ▷ $\beta(i)$ corresponds the fractional order at i^{th} time step

if $j + 1 > n - 1$ **then break**

end if

end for

end if

Algorithm 2 Calculation of Stress Response of a VOFSB Viscoelastic Model

Require:

$E, \theta, \beta_j, t, dt, T, \epsilon, \varepsilon$

Compute:

$\varepsilon = \epsilon t$, ▷ Strain history

$[t]_{1\times n} = [0 : dt : T]$, ▷ Time discretization

$E_{\beta_j} = E\theta^{\beta_j}$, ▷ Fractional characteristic numbers at each time increment

Initialize: Grünwald Coefficient Matrix

$[\mathbf{\Psi}]_{n\times n} = \mathbf{zeros}(n)$,

for $k = 1 : n$ **do** ▷ Row

Compute: Grünwald Coefficients as n length vector arrays

$[\omega]_{1\times n}$ = using, ALGORITHM 1 $\leftarrow (\beta(k), n)$ ▷ Algorithm uses β_k and n to compute n size vector array containing Grünwald coefficients

for $i = 1 : k$ **do** ▷ Column

$\eta(k) = E_\beta(k) dt^{-\beta(k)}$

$\mathbf{\Psi}(k, i) = \omega(k - i + 1)\eta(k)$ ▷ Constructing Grünwald Matrix

end for

end for

$[\sigma]_{n\times 1} = [\mathbf{\Psi}]_{n\times n} [\varepsilon]_{n\times 1}$ ▷ Stress response obtained as a 1D vector array containing the stress values corresponding to every time/strain increments

The flowchart of Algs. 1 and 2 is also depicted in Figure 3.3.

The presented algorithms are used to calculate the stress response of the viscoelastic material from generic material parameters. The same algorithm is valid for both CO and VO fractional viscoelastic material if the fractional order is provided properly. Then, these parameters are determined back from the synthetic experimental test data. The generic material data is not required to match the real material parameters except a natural condition on the definition of the fractional order, $0 \leq \beta(t) \leq 1$. Therefore, algorithms are tested with simple strain histories and physically reasonable material parameters.

It should be emphasized that deriving an analytical solution for the variable order fractional viscoelastic Scott-Blair model is challenging, even when considering simple strain history. The Laplace transformation is also another alternative method for solving variable fractional order differential equations. However, because the mathematical complexity of the fractional order adds highly complex relations in the Laplace domain when adopted, it becomes non-invertible in terms of algebraically known functions. The Laplace transform of a variable fractional order derivative of a function is derived by Scarpi [139]

$$\mathcal{L}({}_0^S D_t^{\beta(t)}) f(t); s) = s^{sA(s)} F(s) - s^{sA(s)-1} f(0), \tag{3.42}$$

where

$$A(s) = \mathcal{L}(\beta(t); s) = \int_0^\infty e^{-st} \beta(t) dt. \tag{3.43}$$

Recent studies have focused on variable fractional-order viscoelasticity, with several researchers following Scarpi's formulation based on the use of Laplace transforms [144, 145]. However, to the best of our knowledge, parameter estimation studies based on experimental data have not yet been addressed.

In the next chapter, parameter estimation studies and the obtaining the fractional orders from the synthetic test data will be discussed in detail.

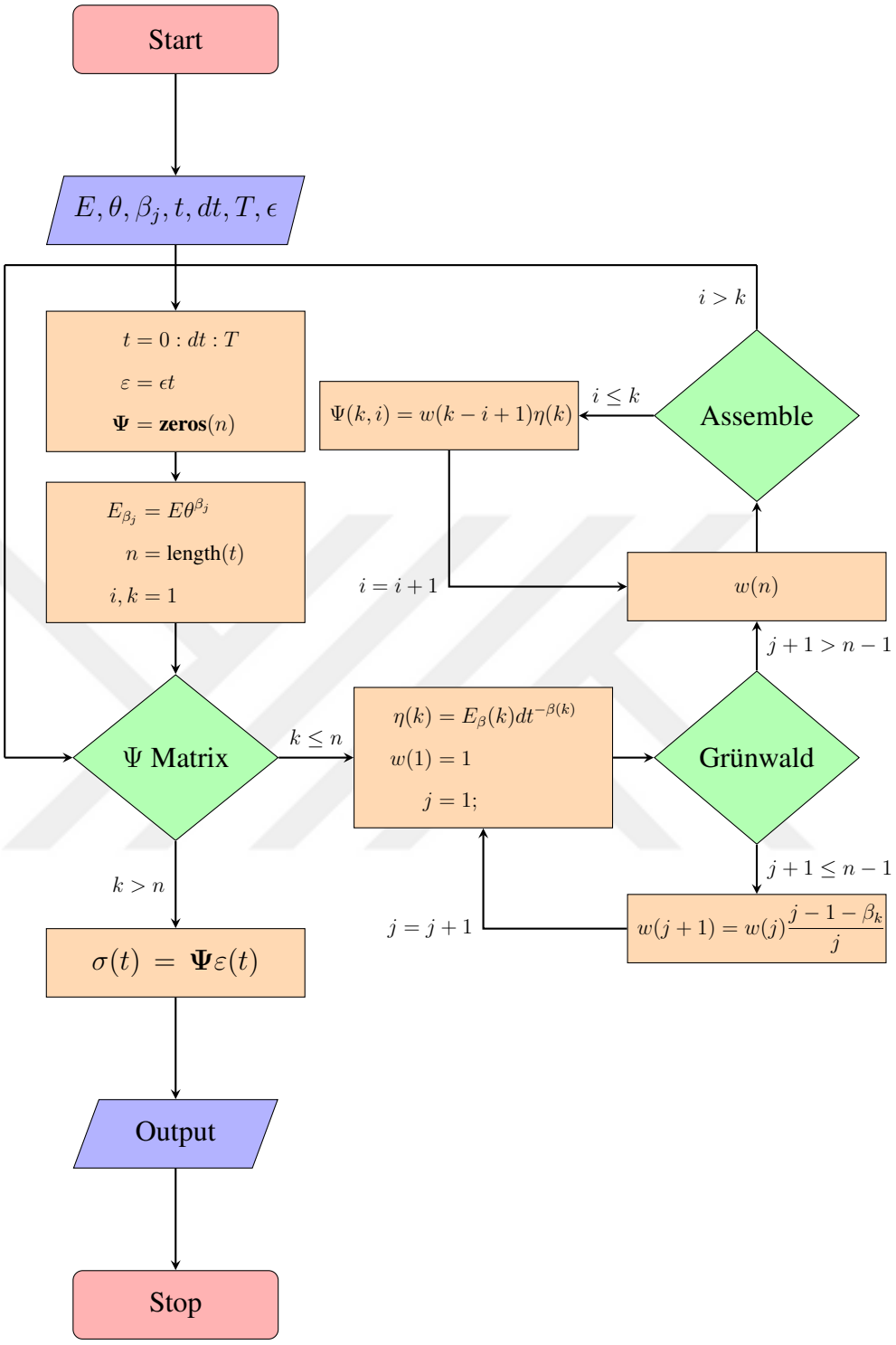

Figure 3.3: Flow Chart of Stress Calculation of a VOF Viscoelastic Material

CHAPTER 4

MATERIAL PARAMETER ESTIMATION STUDIES

Obtaining the material parameters from conventional mechanical tests is the key stage in this study. The main viscoelastic material parameters to be determined are the fractional order, $\beta(t)$, and viscoelastic characteristic function, $E_f(t)$. The material parameter $E_f(t)$ is the viscoelastic fractional material parameter function expressed as a function of time. The fractional viscoelastic characteristic function is defined as the product of the elastic constant and instantaneous fractional power of the viscous parameter. The variability of the fractional order provides a good mathematical model that can adapt the material parameters to the altering conditions [145]. This property gives flexibility to the material model. Therefore, the combined effect of internal and external variables can be accurately assessed through the variable fractional viscoelastic modeling technique providing a comprehensive understanding of their interplay and impact on the overall system response. The spectrum of fractional order variation spans from purely viscous behavior to purely linear elastic behavior. This adaptive behavior of the material model allows for the reduction of mathematical complexity by reducing the number of parameters to be tuned experimentally as compared to the integer-order viscoelastic rheology models.

$$\sigma(t) = E\theta^{\beta(t)}\, {}^{C}D^{\beta(t)}\varepsilon(t) = E_f(t)\, {}^{C}D^{\beta(t)}\varepsilon(t)\,, \quad 0 \leq \beta(t) \leq 1. \tag{4.1}$$

Eq. 4.1 implies that there are only three material parameters when $\beta(t)$ is constant, i.e., $\beta(t) = \alpha$, which simplifies the model to the constant-order fractional viscoelastic model. However, if variable-order fractional viscoelasticity is considered the unknowns are E, θ, β_i. It is important to note that when considering the entire dataset, the number of unknown material parameters for a discrete dataset of size n increases to $n + 2$. This increase arises because the fractional order is independent of strain,

stress, or prior load state fractional orders.

Internal or external variables may have an impact on the variability of the fractional order. The amount of strain, strain rate, and temperature changes, independently or in combination, can change the variable order in any range between 0 and 1. In this chapter, we present our approach to how the trend of order can be captured.

4.1 Constant Order Parameter Estimation Study

The viscoelastic materials represent constant order fractional viscoelastic behavior under certain conditions. As an example to this phenomenon, around room temperature polymeric chains are so-called frozen, and especially at small strains most of the viscoelastic materials exhibit linear elastic behavior [146]. Increasing the strain on the material causes a slip in intermolecular chains and even strengthens the polymeric chains. In these two states of deformation, an observable change in the material behavior takes place. Because of this phenomenon, the constant order fractional viscoelastic model does not suffice to represent the material behavior. The stress is calculated for a COFSB model as long as the strain and fractional characteristic number, E_f, are known,

$$\sigma(t) = E_f \, {}^{C}D^{\alpha}\varepsilon(t). \tag{4.2}$$

As suggested in [113], assuming a constant strain rate loading subjected to the specimen with the following relation $\varepsilon(t) = \epsilon t$, reduces the effort in parameter estimation greatly, since the time rate of change of strain appearing in the constant order fractional model produces a constant number, $\dot{\varepsilon}(t) = \epsilon$. Other forms of strain function will complicate the form of stress function, also it is even harder to obtain experimentally. Therefore, we adopt a constant rate deformation load to perform parameter estimation studies. Recalling the stress-strain relation by Eq. 4.3

$$\sigma(t) = E_f \int_0^t \frac{(t-\tau)^{-\alpha}}{\Gamma(1-\alpha)} \dot{\varepsilon}(\tau) d\tau \tag{4.3}$$

for a constant rate of deformation load, the strain can be expressed as a function of time as

$$\varepsilon(t) = \epsilon t, \tag{4.4}$$

and inserting the strain rate into the Eq. 4.3, the stress response of COFSB viscoelastic material is obtained as

$$\sigma(t) = \frac{E_f \epsilon}{\Gamma(2-\alpha)} t^{1-\alpha}. \tag{4.5}$$

This presents an analytical method for constant strain rate loading that can be executed using a displacement-controlled universal tension testing apparatus. Using Eq. 4.4, the stress in terms of strain is calculated in an alternative form

$$\sigma(\varepsilon) = \frac{E_f \epsilon^{\alpha}}{\Gamma(2-\alpha)} \varepsilon^{1-\alpha}, \tag{4.6}$$

where the material parameters E_f and α can be determined by curve fitting the experimental data to the Eq. 4.5 or Eq. 4.6.

4.2 Variable Order Parameter Estimation Study

The variation of the fractional order needs to be handled in a different strategy. We first recall the stress-strain relation given in the VOFSB model

$$\sigma(t) = \int_0^t \frac{E\theta^{\beta(t)}}{\Gamma(1-\beta(t))} (t-\tau)^{-\beta(t)} \dot{\varepsilon}(\tau) d\tau, \tag{4.7}$$

under the generic strain and fractional order history.

The derivative order is assumed to be constant within a time increment for sufficiently small time intervals. In other words, after every time increment, the derivative order takes a new value as given in Table 4.1, while it is constant during a particular time increment.

Table 4.1: Description of the Variation of Fractional Order Over Time

Order	Time
β_1	$0 < t < t_1$
β_2	$t_1 < t < t_2$
$\vdots$	$\vdots$
β_n	$t_{n-1} < t < t_n$

Determining material parameters under arbitrary or random strain histories poses significant challenges due to the considerable nonlinearity of the problem. Hence, a

methodological approach is adopted for parameter estimation studies under constant strain rate deformation. Opting for constant strain rate deformation simplifies the complexity of the problem, as the rate of the strain yields a straightforward quantity: the crosshead displacement velocity of the uniaxial simple tension test apparatus divided by the gage length of the tensile test specimen. Imposing the constant strain rate in the Eq. 4.3 stress-strain relation for a VOFSB viscoelastic model becomes,

$$\sigma(t) = \int_0^t \left(\frac{E\theta^{\beta(t)}}{\Gamma(1-\beta(t))}\epsilon \right) (t-\tau)^{-\beta(t)} d\tau. \tag{4.8}$$

The expression enclosed in brackets, $\left(\frac{E\theta^{\beta(t)}}{\Gamma(1-\beta(t))}\epsilon\right)$, in Eq. 4.8 remains unaffected by the integration variable, τ, yet it still remains dependent on both order and time. Upon integration, it takes the following form:

$$\sigma(t) = \frac{E\theta^{\beta(t)}\epsilon}{\Gamma(2-\beta(t))} t^{1-\beta(t)}. \tag{4.9}$$

This represents the analytical representation of stress in terms of time. The progression of the fractional order β is not ascertainable unless it is defined as a constant order. To obtain the sequential pattern of the fractional order, we need to solve a nonlinear regression problem. The details of the approach are as follows.

Since the bracketed term in Eq. 4.8 is independent of the integration kernel and is a power function, $(t-\tau)^{-\beta(t)}$, its integration will produce a power function, as well. Therefore, the solution should be sought in the form of a power function of time as shown in Eq. 4.10,

$$S_k(t) = \kappa_k t^{(1-\beta_k)}. \tag{4.10}$$

Moreover, the bracketed term in Eq. 4.8 should behave like a penalty term, κ_k, as shown in Eq. 4.10, adjusting the curve fit for each time increment.

To implement this concept, first, the stress-time data is fitted using the nonlinear least squares method to obtain the sequence of the fractional order. Afterwards, a nonlinear constrained optimization approach is employed to determine the material parameters E and θ, ensuring that the solution satisfies the given constraints. This optimization process allows for the precise calibration of the material properties, which are crucial for the accuracy of the model.

Given that the fractional order is permitted to vary at each time increment, and stress is influenced by the history of previous load states, curve fitting is conducted for each

time increment using the stress-time data from the onset of the stress history up to that specific increment.

We minimize the following nonlinear regression problem,

$$\min \left(\sum \parallel F(x_k) - y_k \parallel^2 \right). \tag{4.11}$$

Here, y_k represents the stress values at each data point, and the objective is to fit $F(x_k)$ to these observed stress values at each discrete time increment. At every increment of the computation, the solver takes up a new β value and proceeds the computation to minimize the sum of squares of the error.

The function denoted as $F(x_k)$, presented in Eq. 4.11 is a nonlinear function defined in MATLAB as,

$$\sigma(t) = \kappa t^{1-\beta}, \tag{4.12}$$

which is used to model the data by Eq. 4.10.

The method also takes into account the long-term fading memory property of the fractional viscoelasticity by shifting the starting point of the curve fitting data. The contribution of the distant past of the strain to the current stress is less dominant than the recent past history of the strain. This is evident from the Grünwald constants when the Eq. 3.34 is expanded. If the time is taken long enough the direct contribution of the distant past strain history tends to lose its significance to the calculation of the current stress. Nevertheless, the contribution of the distant past strains still remains in the more recent past stress history implicitly.

In the scope of the above explanation, the negligible contribution of the far past history of the load states is excluded from the parameter estimation study. The negligible contribution of the distant past can be explained as follows. Considering the Eqs. 3.32, 3.33, and 3.34, for a generic value of fractional order, $\omega_i(\alpha)$ approaches to the zero as index i grows. As the index grows and ω_i gets even smaller the contribution of the

earliest strains, for instance $\varepsilon_1, \varepsilon_2, ...$, loses its significance.

$$\begin{aligned} \sigma_1 &= \omega_1 \varepsilon_1 \\ \sigma_2 &= \omega_2 \varepsilon_1 + \omega_1 \varepsilon_2 \\ \sigma_3 &= \omega_3 \varepsilon_1 + \omega_2 \varepsilon_2 + \omega_1 \varepsilon_3 \\ &\vdots \end{aligned} \tag{4.13}$$

Eq. 4.13 illustrates the forgetting property of the distant past of the deformation. On this basis, during the parameter estimation study, we propose a window-shifting method.

However, the method does inherit some limitations. As the curve fitting technique necessitates more than two data points, obtaining fractional orders from the very last several data points becomes impractical. Moreover, theoretically, the extensive deformation history should still influence the subsequent load state. Nonetheless, our method truncates the earliest data of the load states, implicitly representing their existence through the shifted data points. The fractional order estimation method is based on the sliding window method. The method uses a data window of size h to fit the data to the power function of time. The size of the window should be a minimum of three because curve fitting requires a minimum of three points. The data window is then shifted some distance to calculate a new fit to find the next value of the fractional order. Both the window size and the shift length are two important parameters impacting the fractional order estimation study. The curve fitting method is schematically illustrated in Fig. 4.1.

Once the sequence of fractional orders is determined through nonlinear regression, a subsequent nonlinear constrained optimization is performed to find the remaining material properties, E and θ.

In this subsequent process, the fractional orders obtained from the previous step are used to prepare an objective function. The function to be minimized is given by:

$$f = |\tilde{\sigma}_n(E, \theta, \varepsilon_n, \beta_n) - \sigma_n|, \tag{4.14}$$

where $\tilde{\sigma}_n$ represents the estimated stress history, and σ_n is the original stress history.

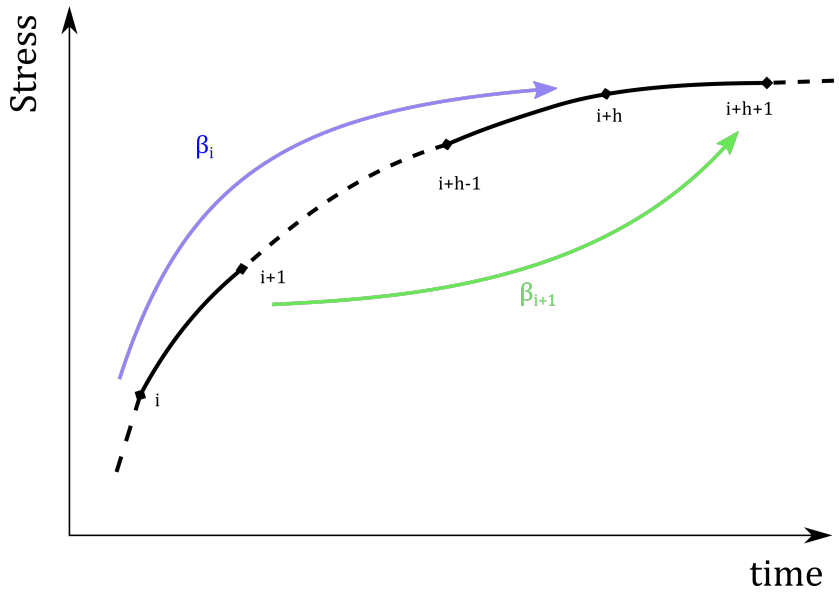

Figure 4.1: Illustration of the Fractional Order Estimation Method

The optimization code finds the best values for the material parameters by minimizing the objective function, 4.14.

This approach ensures that the material properties E and θ are optimized by minimizing the discrepancy between the predicted and actual stress histories, thereby providing the best fit to the data.

To solve the nonlinear constrained optimization problem, the `fmincon` function, a standard solver in MATLAB, is employed. `fmincon` is designed to handle problems where the objective function and constraints are nonlinear, providing robust solutions through built-in algorithms. The function iteratively updates the solution by minimizing the objective function while ensuring that the constraints are satisfied. The optimization code is prepared as follows:

An anonymous function, Eq. 4.14, is defined to compute the norm of the difference between the predicted values of the model and the imposed (measured) data. The norm of the difference between these predictions and the imposed data represents the error to be minimized.

Then, the error function with the constraints is defined as follows:

$$\text{Error}(\boldsymbol{\phi}) = \begin{cases} \|SS(\boldsymbol{\phi}, t) - S\|_2 \\ [E, \theta] \geq [0, 0] \end{cases}, \tag{4.15}$$

where $SS(\boldsymbol{\phi}, t)$ represents the predicted values from the model (Eq. 4.12), dependent on the parameter vector $\boldsymbol{\phi} = [E, \theta]$, and time t, while S is the vector of observed values of stress at every time increment. The term $\| \cdot \|_2$ denotes the Euclidean norm, which quantifies the magnitude of the discrepancy between the predicted and actual values. The objective of the optimization process is to minimize this error. To solve the constrained optimization problem, the interior-point method is employed.

The algorithm and parameters therein that MATLAB uses are described as follows,

$$\min_x f(x); \begin{cases} c(x) \leq 0 \\ ceq(x) = 0 \\ A \cdot x \leq b \\ Aeq \cdot x = beq \\ l_b \leq x \leq u_b \end{cases}, \tag{4.16}$$

where $f(x)$ is the definite function to be minimized or maximized which returns a scalar. ub, lb are upper and lower bounds respectively, b and beq are vectors containing the parameters to define the inequality and equality constraints, A and Aeq are inequality and equality matrices, $c(x)$ and $ceq(x)$ are functions that return vectors, $f(x), c(x)$, and $ceq(x)$ can be nonlinear functions. Since there are no linear equality or inequality constraints the constraint terms are defined as empty sets, [].

Since the model requires mechanical material parameters, a lower bound constraint is imposed on the solver to ensure physical feasibility. Specifically, the two-parameter lower bounds are set to non-negative values, reflecting the inherent non-negativity of material properties. Thefore, the lower bound constraints are imposed in the solver as zero.

Unlike other constrained optimization problems, where parameters such as A, b, c define linear and nonlinear constraints, the present study deals only with parameter estimation subject to simple bounds. The optimization is performed solely on param-

eter estimation with bounds without enforcing additional constraints. Thus, matrix A and vectors b, c are not required for this approach.

This constraint is incorporated into the optimization problem to prevent the solver from exploring parameter values that are mechanically unrealistic. By enforcing these bounds, the solution space is restricted to values that are both feasible and meaningful within the context of mechanical material modeling. This approach enhances the robustness of the optimization process and ensures that the resulting parameter estimates are consistent with the physical principles.

Given that the structure of the stress function is pre-established, the unidentified fractional orders are substituted with the determined orders obtained in the previous step. Consequently, the remaining unknown parameters, namely E and θ, are then deduced through a nonlinear constrained optimization. Upon completing the identification of the material parameters, the stress response of the material is calculated from the identified parameters and the imposed strain history.

4.2.1 Verification of the Parameter Estimation Method from Synthetic Test Data

In the preceding section, we outline the methodology for determining material properties. To validate this approach, we consider seven possible scenarios for the fractional order. Synthetic test data is then generated using these fractional order and the generic material properties. Subsequently, we apply our methodology to the synthetic test data to inversely derive the pattern of the fractional order, which is imposed on the model to calculate the stress response of the hypothetical material.

During the generation of the synthetic test data, the material parameters are hypothetically selected as $E = 1$ MPa, $\theta = 0.05$ s$^{-\beta}$, and a strain rate of $\epsilon = 0.1$ s^{-1}. The stress response of the hypothetical material is then calculated from Eq. 3.24 for each synthetic dataset, utilizing the fractional order models constructed in Table 4.2.

The following fractional order models are proposed for investigating fractional order estimation studies, as summarized in Table 4.2. Each model represents a different approach to varying the fractional order over time, allowing for a comprehensive

analysis of material behavior. These models are crucial for understanding the impact of fractional order variations on material responses, which are integral to accurate parameter estimation in viscoelastic systems.

Table 4.2: Overview of Different Fractional Order Models

Model Description	**Variable Order Model**
Constant order	$\beta(t) = 0.5$
Constant then linearly increasing in time	$\beta(\hat{t}[0, 0.5]) = 0;\ \beta(\hat{t}[0.5, 1]) = [0, 0.7]$
Linearly varying order	$\beta(\hat{t}[0, 1]) = [0, 0.3]$
Order quadratic in time	$\beta(t) = 0.001t^2 + 0.05t$
Order harmonic in time (sine function)	$\beta(t) = 0.5 + \sin\left(\frac{3\pi}{4}t - \frac{\pi}{2}\right)/2$
Order harmonic in time (cosine function)	$\beta(t) = 0.5 + \cos\left(\frac{3\pi}{4}t - \frac{\pi}{2}\right)/2$
Constant then linearly decreasing in time	$\beta(\hat{t}[0, 0.5]) = 0.3;\ \beta(\hat{t}[0.5, 1]) = [0.3, 0.1]$

The $\hat{t}$ used in the Table 4.2 denotes normalized time variable.

The parameter estimation study is conducted by examining seven cases of hypothetical variable fractional order forms. The sequence of the fractional orders is generated to test the efficiency of the method. Subsequently, the material parameters E, θ are inserted into the model to calculate the stress response for the ramp deformation. By following the method developed in this study the imposed material parameters can be precisely obtained for the constant order and piece-wise constant order models.

However, the sudden changes in the fractional order cannot be captured well in relatively short times. Because the finite difference method employed in this study utilizes Grünwald constants. The Grünwald constants do not approximate the value of the fractional order instantly. It is clear from the Fig. 4.2, several data points are required to converge to the constant fractional order. In the early times of the deformation, there is a slight difference between the imposed and predicted values of the fractional order, and it converges slowly, as shown in Fig. 4.2.

The algorithm demonstrates limited adaptability to abrupt shifts in the fractional order. This behavior can be attributed to the stress calculation technique employed, namely the Grünwald-Letnikov (GL) method. In other words, there should be enough

increments to find the target value. In the variable order model, the target value of the fractional order changes as well.

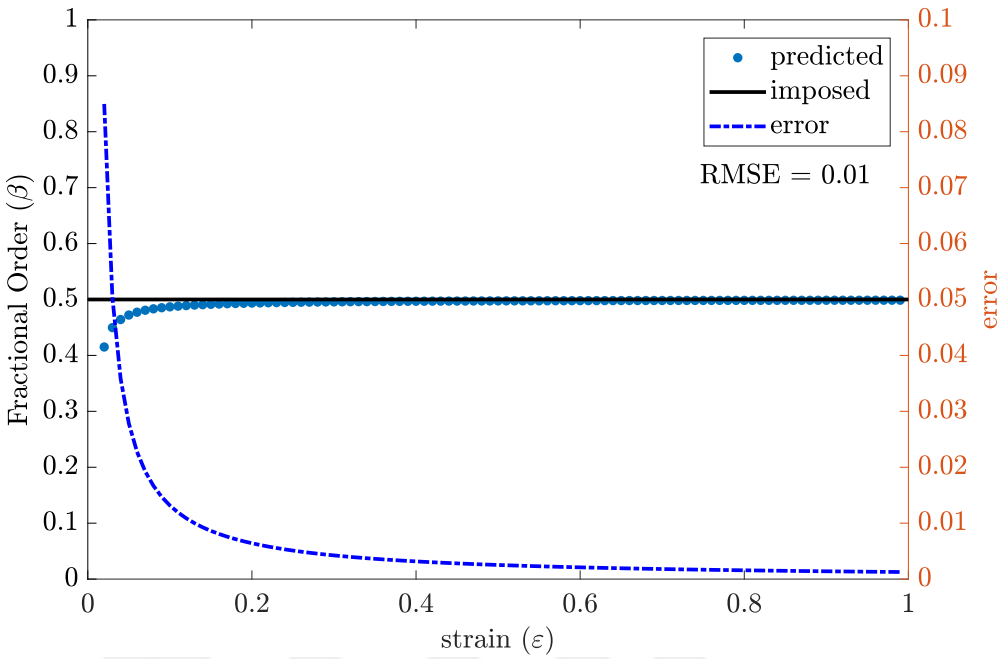

Figure 4.2: Constant Order Estimation Study

The same phenomenon is also observable in Fig. 4.3 and Fig. 4.4. Order estimation slightly adapts the updated value of the fractional order as observed from the figures. The model could predict the orders with considerable accuracy when the initially constant and the linearly changing fractional order as seen in Fig. 4.3 – Fig. 4.8.

Figs. 4.3 and 4.4 suggest that during the linear change in the fractional order, the parameter estimation exhibits both undershooting and overshooting behaviors as the deformation progresses.

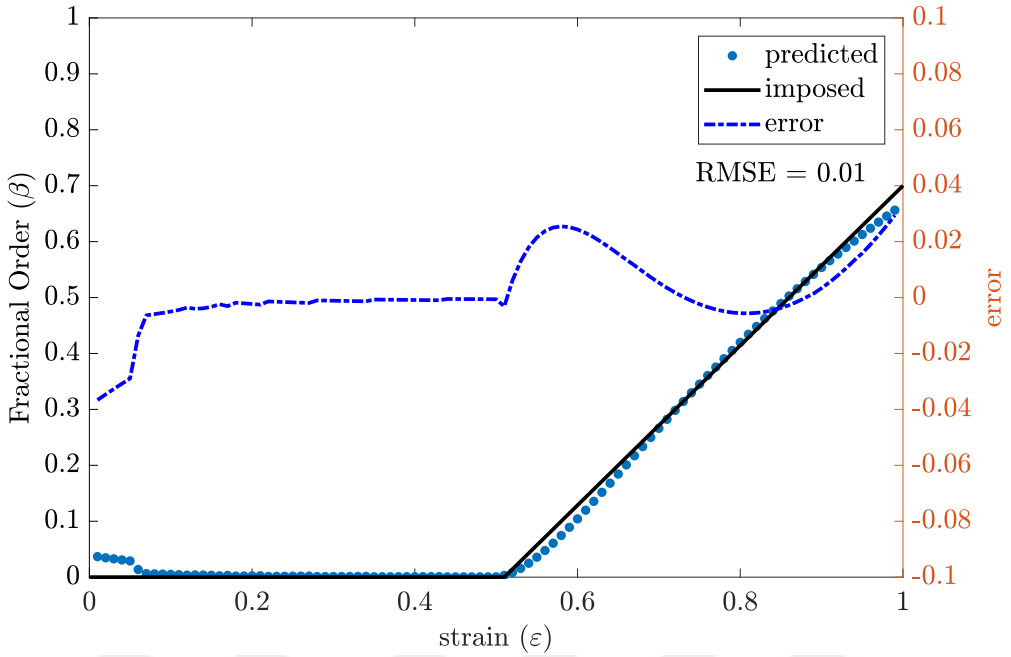

Figure 4.3: Piecewise Constant Order Estimation Study

In terms of the trend of the fractional order, Case 3 and Case 7 have somewhat opposite behaviors. In Case 3, the fractional order increases from 0 to 0.7 after half of the deformation has occurred, as shown in Fig. 4.4. In contrast, Case 7 starts with a constant order, 0.3, and then decreases to 0.1, as illustrated in Fig. 4.8. In these two opposite cases, the performance of the determination of the fractional order displays a similar performance. The RMSE error is calculated as 0.03 for both of the two cases.

In Case 3, which differs from Case 1 and Case 7 due to its initial fractional order value, the estimation converges to the imposed value more rapidly compared to the scenario where the fractional order remains constant and non-zero. This suggests that the deviation from the purely elastic region, which initiates the nonlinearity in the stress response, influences the convergence time of the parameter estimation.

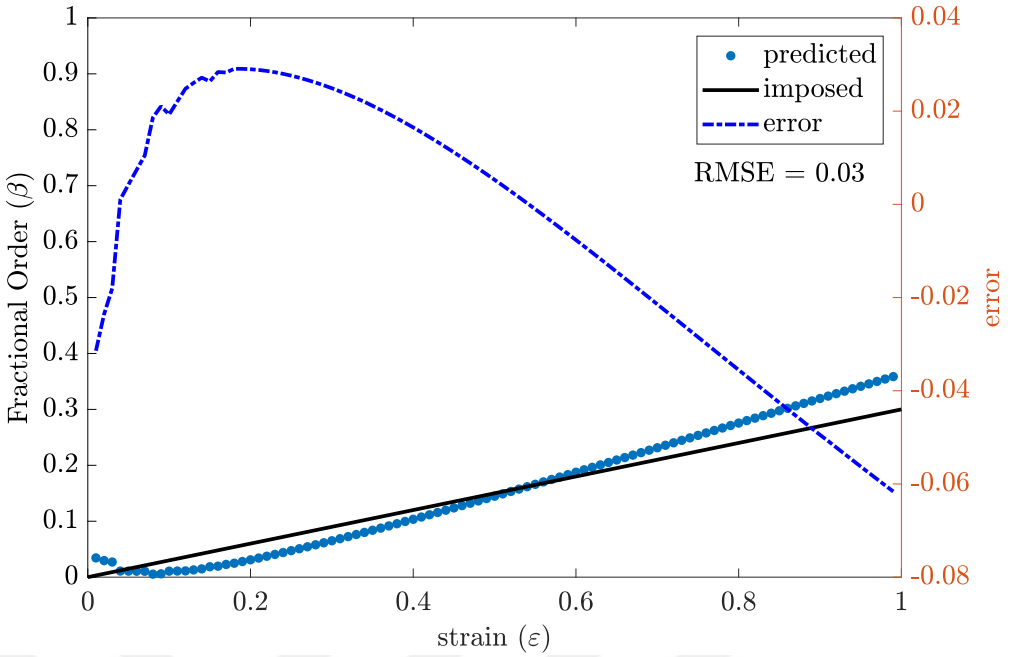

Figure 4.4: Linearly Varying Order Estimation Study

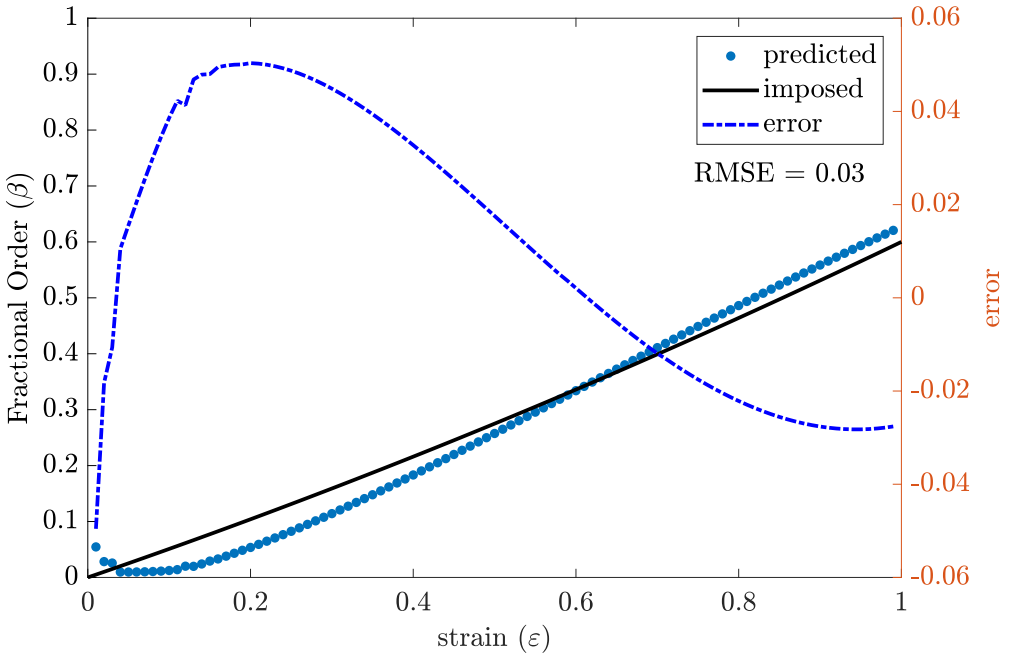

Figure 4.5: Quadratic in Time Order Estimation Study

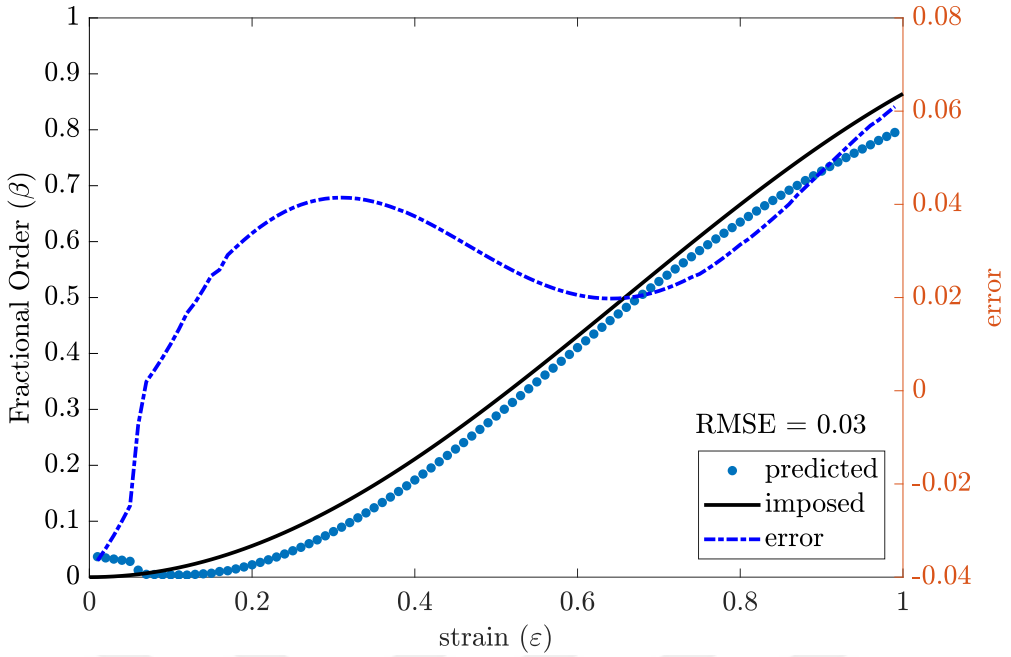

Figure 4.6: Harmonic in Time Order Estimation Study

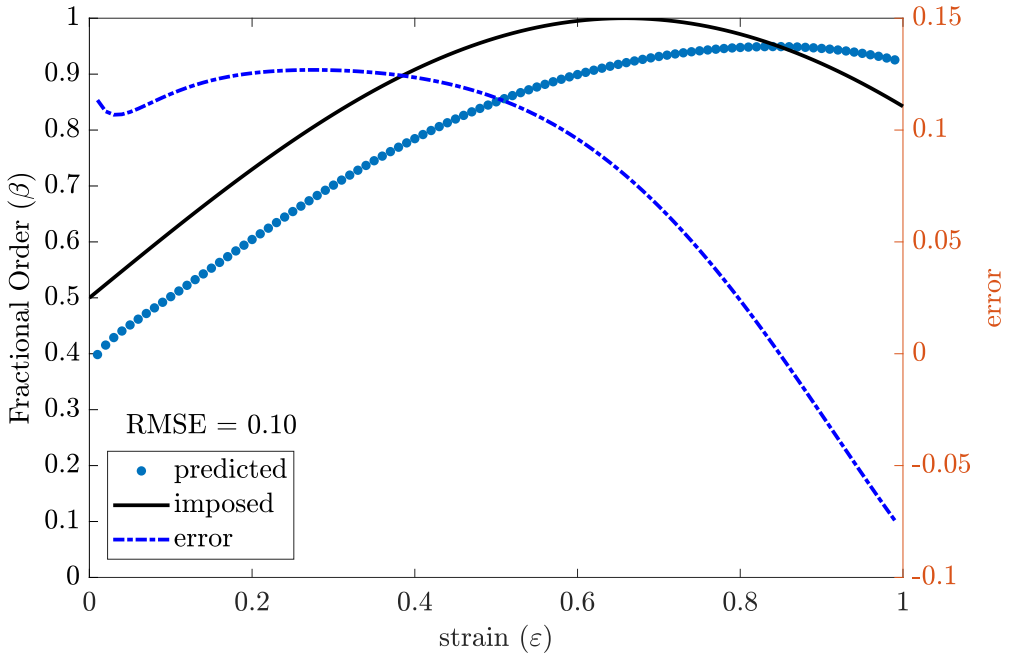

Figure 4.7: Harmonic in Time Order Estimation Study

Among the investigated cases, the least consistent behavior is observed in Case 6 as

seen in Fig. 4.7. This case stands out as the most unique among the other models. The fractional order starts at 0.5 and then rises harmonically to 1 before decreasing to a value of 0.8. Throughout this trend, the lowest correlation is observed between the imposed and predicted fractional order values. However, it is noteworthy that the difference between the estimated and imposed values remains nearly constant until approaching the inflection point of the imposed data curve. The estimation curve follows a phase-lag trend relative to the imposed values of the fractional orders.

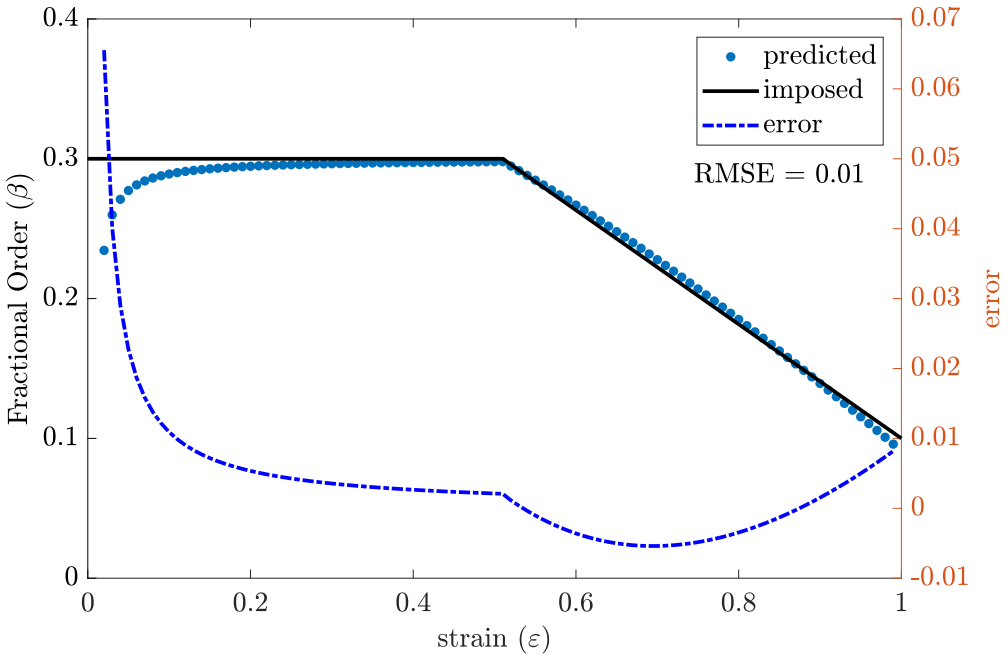

Figure 4.8: Constant Linearly Decreasing in Time Order Estimation Study

The parameter estimation study from the synthetic test data results indicates that if the change in the fractional order is linear in time, the root mean squared error between the imposed stress, y_i in Eq. 4.17, and predicted stress, $\hat{y}_i$ in Eq. 4.17, from the determined fractional order is on the order of 0.01. Higher-order nonlinearity impairs the performance of the parameter estimation study.

$$\text{RMSE} = \sqrt{\sum_{i=1}^{n} \frac{(\hat{y}_i - y_i)^2}{n}}. \tag{4.17}$$

In the synthetic test data, the time increment for the Grünwald step size is selected as $\Delta t = 0.1$ s, resulting in a data size of $n = 101$ for a 10 s analysis.

4.2.2 Parameter Estimation Studies Other Potential Approaches

The parameter estimation method we developed works effectively, except for the fractional orders that are defined to change harmonically over time. However, to reduce the uncertainty associated with this method, we explored alternative approaches for identifying material parameters. Our efforts primarily focused on finding an analytical method to generate the sequence of fractional orders. Below, we present the two approaches we pursued.

In the first method, we followed Meng et al.'s [114] formulation, the CO fractional derivative of a function is expressed as,

$$D^{\alpha} f(t) = g(t, \alpha). \tag{4.18}$$

It can be expressed by the finite sum for $t_0 = 0$ and total time is equally divided by n increments,

$$D^{\alpha} f(t) = \sum_{k=1}^{n} [g(t_k, \alpha) - g(t_{k-1}, \alpha)] + g(0, \alpha). \tag{4.19}$$

The material is assumed to be initially stress and strain-free. Upon this assumption, the last term vanishes. Extending this formulation to the variable order formulation needs updating the resultant function,

$$D^{\beta(t)} f(t) = \sum_{k=1}^{n} [g(t_k, \beta_k) - g(t_{k-1}, \beta_k)], \tag{4.20}$$

such that,

$$D^{\beta_k} f(t) = g(t_k, \beta_k). \tag{4.21}$$

The stress is then computed from,

$$\sigma(t) = E\theta^{\beta(t)} D^{\beta(t)} \varepsilon(t) = E\theta^{\beta_k} D^{\beta_k} \varepsilon(t) = \sum_{k=1}^{n} [\sigma(t_k, \beta_k) - \sigma(t_{k-1}, \beta_k)]. \tag{4.22}$$

Upon application of the strain history as $\varepsilon(t) = \epsilon t$, we get,

$$\sigma(\varepsilon) = \sum_{k=1}^{n} E(\epsilon\theta)^{\beta_k} \frac{\varepsilon_k^{1-\beta_k} - \varepsilon_{k-1}^{1-\beta_k}}{\Gamma(2-\beta_k)}. \tag{4.23}$$

Meng et al. [113] expressed the stress as a finite sum of the strain difference for constant strain rate deformation,

$$\sigma(\varepsilon) = \sum_{k=1}^{n} E(\epsilon\theta)^{\beta_k} \frac{\varepsilon_k^{1-\beta_k} - \varepsilon_{k-1}^{1-\beta_k}}{\Gamma(2-\beta_k)}. \tag{4.24}$$

The stress increment at two subsequent increments is obtained as,

$$\sigma(\varepsilon_k) - \sigma(\varepsilon_{k-1}) = E(\epsilon\theta)^{\beta_k} \frac{\varepsilon_k^{1-\beta_k} - \varepsilon_{k-1}^{1-\beta_k}}{\Gamma(2-\beta_k)}. \tag{4.25}$$

For $k = 1$, we have,

$$\sigma(\varepsilon_1) = E(\epsilon\theta)^{\beta_1} \frac{\varepsilon^{1-\beta_1}}{\Gamma(2-\beta_1)} = \eta\varepsilon_1^{1-\beta_1}. \tag{4.26}$$

Taking the logarithm of both sides, we obtain,

$$\ln\sigma(\varepsilon) = \ln\eta + (1-\beta_1)\ln\varepsilon. \tag{4.27}$$

As reported by Meng et al. in [113], after computing the $\ln\sigma - \ln\varepsilon$ data from the experimentally obtained $\sigma - \varepsilon$ data, logarithmic data is fitted to a straight line at every increment. Then β_k is obtained for the entire time history. However, the method did not work well in either synthetic or experimental data. Because the fractional order cannot be determined from the stress difference at two subsequent strain data. Meaning that,

$$\log(\sigma(\varepsilon_k) - \sigma(\varepsilon_{k-1})) = \log\left(E(\epsilon\theta)^{\beta_k} \frac{\varepsilon_k^{1-\beta_k} - \varepsilon_{k-1}^{1-\beta_k}}{\Gamma(2-\beta_k)}\right), \tag{4.28}$$

$$\log(\Delta\sigma_k) = \log\left(\frac{E(\epsilon\theta)^{\beta_k}}{\Gamma(2-\beta_k)}\right) + \log(\varepsilon_k^{1-\beta_k} - \varepsilon_{k-1}^{1-\beta_k}). \tag{4.29}$$

In Eq. 4.29, the latter term on the right-hand side of the equation includes two strain values corresponding to the k^{th} and $k-1^{th}$ increments. Unlike Meng's method, the ε_{k-1} terms are found to be significant values that cannot be disregarded after the first step anymore because $\varepsilon(0) = 0$ and $\varepsilon(t \geq 0) \neq 0$. Therefore taking the logarithm of the Eq. 4.29 does not work to produce the straight line fitting between the two data points.

Another alternative potential method can be developed by following Burlon et al.'s [141] stress formulation for the variable order viscoelastic material subjected to a generic strain history,

$$\sigma_n = \eta_n\omega_n(\beta_n)\varepsilon_1 + \eta_n\omega_{n-1}(\beta_n)\varepsilon_2 + \cdots + \eta_n\omega_1(\beta_n)\varepsilon_n. \tag{4.30}$$

For $n = 1$,

$$\sigma_1 = \eta_1\omega_1(\beta_1)\varepsilon_1. \tag{4.31}$$

For $n = 2$,

$$\sigma_2 = \eta_2\omega_2(\beta_2)\varepsilon_1 + \eta_2\omega_1(\beta_2)\varepsilon_2. \tag{4.32}$$

and for $n = 3$,

$$\sigma_3 = \eta_3\omega_3(\beta_3)\varepsilon_1 + \eta_3\omega_2(\beta_3)\varepsilon_2 + \eta_3\omega_1(\beta_3)\varepsilon_3. \tag{4.33}$$

For the subsequent stress increments,

$$\begin{aligned}\Delta\sigma_n &= \sigma_n - \sigma_{n-1} \\ &= \eta_n\omega_n(\beta_n)\varepsilon_1 + \eta_n\omega_{n-1}(\beta_n)\varepsilon_2 + \cdots + \eta_n\omega_1(\beta_n)\varepsilon_n - \ldots \\ &\quad - \eta_{n-1}\omega_{n-1}(\beta_{n-1})\varepsilon_1 + \eta_{n-1}\omega_{n-2}(\beta_{n-1})\varepsilon_2 + \cdots + \eta_{n-1}\omega_1(\beta_{n-1})\varepsilon_{n-1}.\end{aligned} \tag{4.34}$$

In this study, we have attempted to obtain the unknown parameters, E, θ, and β_k, from Eq. 4.34. However, this equation involves handling numerous unknowns simultaneously. To show the problem more clearly, investigating the first three points of the stress-strain data is enough to portray how hard it is to determine the unknown parameters. The first three stress values corresponding to the strain values the material is subjected to are expressed as,

$$\sigma_1 = \eta_1\omega_1(\beta_1)\varepsilon_1, \tag{4.35a}$$

$$\sigma_2 = \eta_2\omega_2(\beta_2)\varepsilon_1 + \eta_2\omega_1(\beta_2)\varepsilon_2, \tag{4.35b}$$

$$\sigma_3 = \eta_3\omega_3(\beta_3)\varepsilon_1 + \eta_3\omega_2(\beta_3)\varepsilon_2 + \eta_3\omega_1(\beta_3)\varepsilon_3. \tag{4.35c}$$

In Eq. 4.35-a the unknowns are η_1 and β_1. Since the ω_i is a dependent variable, once the β_n sequence is known, all $\omega_i(\beta_n)$ can be determined. Therefore in Eq. 4.35-b $\omega_2(\beta_2)$ and $\omega_1(\beta_2)$ are not two distinct unknowns, but two unknowns dependent on β_2. It means two unknowns still exist in each equation. However, there are still two unknowns for each stress value for each strain. To illustrate this pattern, it is sufficient to examine the first few points. At the first stress increment, the unknowns are η_1 and ω_1. At subsequent increments, the unknowns evolve accordingly: at the second increment, η_2 and ω_2 remain undetermined, and so forth for each subsequent stress increment. This sequence of unknowns continues, with each new increment introducing a new pair of unknowns corresponding to the respective strain and stress values. One may easily distinguish that the sequence of the fractional order does not accept any rule. In other words, the value of the fractional variable order at a particular time step may not be influenced by the preceding history of the fractional

order, thereby impacting the Grünwald coefficients accordingly. The Grünwald coefficients ω_n change at each time increment and for each value of the fractional order β_k. Given that, $\beta_i \neq \beta_{i+1}$, it follows that $\omega_n(\beta_i) \neq \omega_n(\beta_{i+1})$. This lack of correlation in the Grünwald coefficients hinders the derivation of the sequence of fractional orders from the previous steps. This reveals the fact that, it is necessary to solve each equation in Eq. 4.35 separately to determine the unknown fractional order at each particular time increment, as each equation contains two unknowns. Therefore, conducting a parameter estimation study using the above method is not feasible with the available mathematical and numerical methods and, hence remains as an open research question.

CHAPTER 5

USER MATERIAL SUBROUTINE DEVELOPMENT

To the best of our knowledge, the material model developed in this study is not available as a predefined option in any existing finite element analysis software. For users who wish to apply a variable fractional order viscoelastic model to analyze complex structures, it is necessary to implement a `UMAT` (User Material) subroutine. In the present chapter, a detailed derivation of the variable fractional order spring-pot element is provided for the homogeneous and isotropic material.

The methodology outlined here is designed to be flexible and can be extended to accommodate similar material models. This approach offers a valuable tool for researchers and engineers seeking to incorporate advanced viscoelastic models into their finite element analyses.

The user material subroutine (UMAT) is essential for defining the constitutive behavior of materials within finite element analysis software. When a user-defined material model is implemented, UMAT is invoked at each material calculation point within the elements. This subroutine can also accommodate solution-dependent state variables, allowing for dynamic updates based on the current state of the solution. During each increment, the solver updates both the stresses and these state variables to reflect their values at the end of the increment. Additionally, UMAT is required to provide the material Jacobian matrix, $\partial\Delta\sigma/\partial\Delta\varepsilon$, which is crucial for defining the mechanical constitutive model and ensuring accurate numerical analysis.

The Jacobian matrix plays a pivotal role in computing strain measures from the deformation gradient tensor. In the UMAT subroutine, the strain tensor is derived from the deformation gradient, with the Jacobian matrix being essential for this process.

Accurate computation of the strain tensor is crucial for precise modeling of material behavior under deformation. Additionally, UMAT can be used in conjunction with the user subroutine `USDFLD` to redefine field variables before they are processed. However, the integration of `USDFLD` is not covered in this work and falls outside the scope of the current study.

5.1 UMAT Development for Constant Order Scott-Blair Model

The three-dimensional response of a material requires a complete description of the material parameters, including volumetric and deviatoric responses. The stress-strain relation is expressed as in the well-known classical viscoelasticity equation

$$\sigma(t) = \int_0^t R(t)\dot{\varepsilon}(\tau)d\tau, \tag{5.1}$$

where $R(t)$ is the relaxation function. If expressed in the indicial notation, the stress-strain relation takes the form

$$\sigma_{ij}(t) = \int_0^t R_{ijkl}(t-\tau)\dot{\varepsilon}_{kl}(\tau)d\tau, \tag{5.2}$$

where R_{ijkl} is the fourth-order stress relaxation tensor. Alotta et al. [69] described the relaxation modulus in terms of its volumetric and deviatoric counterparts

$$R_{ijkl}(t) = \left[K_R(t) - \frac{2}{3}G_R(t)\right]\delta_{ij}\delta_{kl} + G_R(t)\left[\delta_{ik}\delta_{jl} + \delta_{il}\delta_{jk}\right], \tag{5.3}$$

where K_R corresponds to volumetric (bulk) and G_R corresponds to the deviatoric (shear) relaxation modulus. The bulk modulus and shear modulus in the linear elasticity convert to fractional bulk modulus function and fractional shear modulus function as follows

$$K_R(t) = \frac{K_\beta t^{-\beta}}{\Gamma(1-\beta)}, \qquad G_R(t) = \frac{G_\alpha t^{-\alpha}}{\Gamma(1-\alpha)}. \tag{5.4}$$

One may notice tilde, in the most generalized form, the bulk modulus and shear modulus are functions of time and fractional parameters, α and β. The fractional parameters in the bulk response and deviatoric response are not necessarily equal. However, to the best of our knowledge, no such material shows different relaxation behaviors in volumetric and deviatoric responses reported in the literature. Furthermore, from a theoretical point of view, equating the fractional order parameters corresponding to

volumetric and bulk behavior does not violate any physical law. Therefore, they will be assumed to be identical to each other in our further investigations.

It is necessary to underline a notation difference in this chapter. In the finite element routine, we prefer to denote Grünwald coefficients by λ, differently from the Chapter 3. The notation difference is necessary to distinguish it from ω which corresponds to the numerical solution.

When Eq. 5.3 and Eq. 5.1 are combined and expanded, normal and shear stress responses are obtained in terms of their fractional volumetric and fractional deviatoric functions,

$$\begin{aligned} \sigma_{ij}(t) &= 2G_\alpha(D^\alpha \tilde{\varepsilon}_{ij})(t) + 3K_\beta(D^\beta \bar{\varepsilon})(t)\ , \qquad i = j\ ; \quad \{1,2,3\}\ , \\ \tau_{ij}(t) &= G_\alpha(D^\alpha \gamma_{ij})(t)\ , \qquad\qquad\qquad\qquad i \neq j\ ; \quad \{1,2,3\}, \end{aligned} \tag{5.5}$$

where $\bar{\varepsilon} = \sum_1^3 \varepsilon_{ii}/3$ is mean strain and $\tilde{\varepsilon}_{ij}(t) = \varepsilon_{ij}(t) - \bar{\varepsilon}(t)\delta_{ij}$ is deviatoric strain.

The time discretization of the constant fractional order derivative operator is defined by the Grünwald-Letnikov derivative in Eq. 5.6

$$({}^{GL}D^\alpha f)(t) = ({}^{GL}D^\alpha f)(k\Delta t) = \lim_{\Delta t \to 0} \Delta t^{-\alpha} \sum_{j=1}^{k+1} \lambda_j^{(\alpha)} f^{(k-j+2)}. \tag{5.6}$$

The binomial coefficients in the Grünwald-Letnikov derivative is described as,

$$\lambda_{j+1}^{(\alpha)} = \frac{j-1-\alpha}{j}\lambda_j^{(\alpha)}\ ; \qquad \lambda_1^{(\alpha)} = 1. \tag{5.7}$$

Returning to Eq. 5.5, the time discretization of the normal and shear components is performed as follows:
At the increment $k+1$,

$$\begin{aligned} \sigma_{ij}^{(k+1)} &= 2G_\alpha \Delta t^{-\alpha} \sum_{j=1}^{k+1} \lambda_j^{(\alpha)} \tilde{\varepsilon}_{ij}^{(k-j+2)} + 3K_\beta \Delta t^{-\beta} \sum_{j=1}^{k+1} \lambda_j^{(\beta)} \bar{\varepsilon}^{(k-j+2)} \qquad ; i = j, \\ \tau_{ij}^{(k+1)} &= G_\alpha \Delta t^{-\alpha} \sum_{j=1}^{k+1} \lambda_j^{(\alpha)} \gamma_{ij}^{(k-j+2)} \qquad\qquad\qquad\qquad\qquad\qquad ; i \neq j. \end{aligned} \tag{5.8}$$

The normal and shear stress increments can then be formulated as

$$\Delta\sigma_{ii}^{(k+1)} = \sigma_{ii}^{(k+1)} - \sigma_{ii}^{(k)}, \qquad \Delta\tau_{ij}^{(k+1)} = \tau_{ij}^{(k+1)} - \tau_{ij}^{(k)}. \tag{5.9}$$

To find the stress increments, the summation upper limits should be adjusted. Rearranging Eq. 5.8 to perform the calculations between the two subsequent time increments,

$$\begin{aligned}\sigma_{ij}^{(k+1)} &= 2G_\alpha \Delta t^{-\alpha} \sum_{j=1}^{k} \lambda_j^{(\alpha)} \tilde{\varepsilon}_{ij}^{(k-j+2)} + 2G_\alpha \Delta t^{-\alpha} \lambda_{k+1}^{(\alpha)} \tilde{\varepsilon}_{ij}^{(1)}, \\ &\quad + 3K_\beta \Delta t^{-\beta} \sum_{j=1}^{k} \lambda_j^{(\beta)} \bar{\varepsilon}^{(k-j+2)} + 3K_\beta \Delta t^{-\beta} \lambda_{k+1}^{(\beta)} \bar{\varepsilon}^{(1)} \qquad ; i = j \\ \tau_{ij}^{(k+1)} &= G_\alpha \Delta t^{-\alpha} \sum_{j=1}^{k} \lambda_j^{(\alpha)} \gamma_{ij}^{(k-j+2)} + G_\alpha \Delta t^{-\alpha} \lambda_{k+1}^{(\alpha)} \gamma_{ij}^{(1)} \qquad ; i \neq j.\end{aligned} \tag{5.10}$$

Now to find the difference between two subsequent increments by subtracting the stress at $(k)^{th}$ increment from $(k+1)^{th}$ increment,

$$\Delta\sigma_{ii}^{(k+1)} = \sigma_{ii}^{(k+1)} - \sigma_{ii}^{(k)} \tag{5.11}$$

yields to the normal and shear stress increments,

$$\begin{aligned}\Delta\sigma_{ij}^{(k+1)} &= 2G_\alpha \Delta t^{-\alpha} \sum_{j=1}^{k} \lambda_j^{(\alpha)} \Delta\tilde{\varepsilon}_{ij}^{(k-j+2)} + 2G_\alpha \Delta t^{-\alpha} \lambda_{k+1}^{(\alpha)} \tilde{\varepsilon}_{ij}^{(1)} \\ &\quad + 3K_\beta \Delta t^{-\beta} \sum_{j=1}^{k} \lambda_j^{(\beta)} \Delta\bar{\varepsilon}^{(k-j+2)} + 3K_\beta \Delta t^{-\beta} \lambda_{k+1}^{(\beta)} \bar{\varepsilon}^{(1)} \qquad ; i = j, \\ \Delta\tau_{ij}^{(k+1)} &= G_\alpha \Delta t^{-\alpha} \sum_{j=1}^{k} \lambda_j^{(\alpha)} \Delta\gamma_{ij}^{(k-j+2)} + G_\alpha \Delta t^{-\alpha} \lambda_{k+1}^{(\alpha)} \gamma_{ij}^{(1)} \qquad ; i \neq j.\end{aligned} \tag{5.12}$$

Substituting the definitions of the deviatoric and mean strain terms, the difference between the two subsequent time steps at $(k)^{th}$ and $(k+1)^{th}$ becomes,

$$\begin{aligned}\Delta\sigma_{ij}^{(k+1)} &= \frac{4}{3} G_\alpha \Delta t^{-\alpha} \sum_{j=1}^{k} \lambda_j^{(\alpha)} \left(\Delta\varepsilon_{11}^{(k-j+2)} - \frac{\Delta\varepsilon_{22}^{(k-j+2)} + \Delta\varepsilon_{33}^{(k-j+2)}}{2} \right) \\ &\quad + K_\beta \Delta t^{-\beta} \sum_{j=1}^{k} \lambda_j^{(\beta)} \Delta\varepsilon_v^{(k-j+2)} \\ &\quad + [2G_\alpha \Delta t^{-\alpha} \lambda_{k+1}^{(\alpha)} \tilde{\varepsilon}_{ij}^{(1)} + 3K_\beta \Delta t^{-\beta} \lambda_{k+1}^{(\beta)} \bar{\varepsilon}^{(1)}] \qquad ; i = j, \\ \Delta\tau_{ij}^{(k+1)} &= G_\alpha \Delta t^{-\alpha} \sum_{j=1}^{k} \lambda_j^{(\alpha)} \Delta\gamma_{ij}^{(k-j+2)} + [G_\alpha \Delta t^{-\alpha} \lambda_{k+1}^{(\alpha)} \gamma_{ij}^{(1)}] \qquad ; i \neq j.\end{aligned} \tag{5.13}$$

The bracketed terms in the above equations will not contribute to the Jacobian.

Recalling the definitions of the deviatoric and mean stresses,

$$\tilde{\varepsilon}_{ij}(t) = \varepsilon_{ij}(t) - \bar{\varepsilon}(t)\delta_{ij} \ , \quad \bar{\varepsilon} = \sum \frac{\varepsilon_{ii}}{3} \tag{5.14}$$

$$\frac{\partial \Delta\sigma_{ii}^{(k+1)}}{\partial \Delta\varepsilon_{ii}^{(k+1)}} = \frac{4}{3}G_\alpha \Delta t^{-\alpha}\lambda_1^{(\alpha)} + K_\beta \Delta t^{-\beta}\lambda_1^{(\beta)} \ , \tag{5.15}$$

$$\frac{\partial \Delta\sigma_{ii}^{(k+1)}}{\partial \Delta\varepsilon_{jj}^{(k+1)}} = -\frac{2}{3}G_\alpha \Delta t^{-\alpha}\lambda_1^{(\alpha)} + K_\beta \Delta t^{-\beta}\lambda_1^{(\beta)} \ , \tag{5.16}$$

$$\frac{\partial \Delta\sigma_{ij}^{(k+1)}}{\partial \Delta\gamma_{ij}^{(k+1)}} = G_\alpha \Delta t^{-\alpha}\lambda_1^{(\alpha)} \ , \tag{5.17}$$

where $\lambda_1^{(\alpha)} = \lambda_1^{(\beta)} = 1$.

As a side note, the same relations can be directly obtained from the indicial representation of the stress,

$$\sigma_{ij}(t) = \int [(K_R - \frac{2}{3}G_R)\delta_{ij}\delta_{kl} + G_R(\delta_{ik}\delta_{jl} + \delta_{il}\delta_{jk})]\dot{\varepsilon}_{kl}(\tau)d\tau. \tag{5.18}$$

The formulation outlined above is essential for characterizing the constant order fractional material behavior. To benchmark and evaluate the material subroutine, this study selects the ramp-hold relaxation and ramp-hold creep problems for comparative analysis. An analytical solution for these problems is sought to establish a reference against which the performance of the material subroutine can be tested. This approach ensures a rigorous validation of the subroutine by comparing its results with well-established analytical solutions, thereby assessing its accuracy and reliability.

In the parameter estimation study we assume fraction order for the volumetric and shear response of the material is governed by the same fractional order, $\beta(t)$.

5.1.1 Analytical Solution to Ramp-Hold Relaxation

The displacement function is a ramp-hold type characteristic so that the strain function becomes

$$\varepsilon_{xx}(t) = \epsilon[t \cdot H(t) - t \cdot H(t-1) - H(t-1)]. \tag{5.19}$$

Given the stress-strain relationship

$$\sigma_{ij}(t) = \int_0^t R_{ijkl}(t-\tau)\dot{\varepsilon}_{kl}(\tau)d\tau, \tag{5.20}$$

and the relaxation functions

$$K_R(t) = \frac{K_\beta t^{-\beta}}{\Gamma(1-\beta)}, \qquad G_R(t) = \frac{G_\beta t^{-\beta}}{\Gamma(1-\beta)}, \tag{5.21}$$

the derivative of the strain function becomes

$$\dot{\varepsilon}_{kl}(t) = \epsilon(H(t) - H(t-1))\delta_{kl}. \tag{5.22}$$

Furthermore, the relaxation function is expressed as

$$R_{ijkl}(t) = [K_R(t) - \frac{2}{3}G_R(t)]\delta_{ij}\delta_{kl} + G_R(t)(\delta_{ik}\delta_{jl} + \delta_{il}\delta_{jk}). \tag{5.23}$$

Replacing the i, j indices with x and expressing the normal component of the stress in x direction, we obtain

$$\sigma_{xx}(t) = \int_0^t \left[\left(K_\beta - \frac{2}{3}G_\beta \right) \frac{(t-\tau)^{-\beta}}{\Gamma(1-\beta)}\delta_{kl} + 2\frac{G_\beta(t-\tau)^{-\beta}}{\Gamma(1-\beta)}\delta_{xk}\delta_{xl} \right] \dot{\varepsilon}_{kl}(\tau)d\tau. \tag{5.24}$$

Performing the indicial operations, and assuming the applied strain in x direction yield

$$\sigma_{xx}(t) = \int_0^t \left[\frac{K_\beta(t-\tau)^{-\beta}}{\Gamma(1-\beta)} + \frac{4}{3}\frac{G_\beta(t-\tau)^{-\beta}}{\Gamma(1-\beta)} \right] \epsilon(H(\tau) - H(\tau-1))d\tau. \tag{5.25}$$

After integrating, the stress response can then be obtained as,

$$\begin{aligned} \sigma_{xx}(t) = &\left[K_\beta \frac{t^{1-\beta}}{\Gamma(2-\beta)} + \frac{4}{3}G_\beta \frac{t^{1-\beta}}{\Gamma(2-\beta)} \right] \epsilon H(t) \\ &- \left[K_\beta \frac{(t-1)^{1-\beta}}{\Gamma(2-\beta)} + \frac{4}{3}G_\beta \frac{(t-1)^{1-\beta}}{\Gamma(2-\beta)} \right] \epsilon H(t-1). \end{aligned} \tag{5.26}$$

5.1.2 Analytical Solution to Ramp-Hold Creep

In the creep test, the load is kept constant and strain is recorded. Application of the load requires a physical ramp-hold characteristic. Therefore, the stress is imposed as

$$\sigma_{xx}(t) = \sigma(t \cdot H(t) - t \cdot H(t-1) + H(t-1)), \tag{5.27}$$

$$\sigma t H(t) - \sigma t H(t-1) + \sigma H(t-1) = \int_0^t R_{xxkl}(t-\tau)\dot{\varepsilon}_{kl}(\tau)d\tau. \tag{5.28}$$

Laplace transforming yields to,

$$\frac{\sigma}{s^2} - \frac{\sigma e^{-s}}{s^2} - \frac{\sigma e^{-s}}{s^2} + \frac{\sigma e^{-s}}{s^2} = \hat{R}_{xxkl} \cdot s \cdot \hat{\varepsilon}_{kl}. \tag{5.29}$$

Rearranging

$$\frac{\sigma(1-e^{-s})}{s^3} = \hat{R}_{xxkl}\hat{\varepsilon}_{kl} \tag{5.30}$$

and inserting in the viscoelastic stress-strain relationship and Laplace transforming yields

$$\hat{\varepsilon}(s) = \frac{\sigma}{K_\beta + \frac{4}{3}G_\beta}\frac{1-e^{-s}}{s^{2+\beta}}. \tag{5.31}$$

Last, an application of inverse transforming gives us

$$\varepsilon_{xx}(t) = \frac{\sigma}{K_\beta + \frac{4}{3}G_\beta}\frac{t^{\beta+1} - (t-1)^{\beta+1}H(t-1)}{\Gamma(2+\beta)}. \tag{5.32}$$

5.1.3 Benchmark Studies for the FE Simulation and Analytical Results

We have already derived Eqs. 5.26 and 5.32 in an effort to extract the analytical solutions to the ramp-hold type stress relaxation and creep problems. The COF viscoelastic model can also be applied to more comprehensive load/deformation problems by assuming the proper mathematical formulations of the description of the load or displacement.

Generic material properties are assumed to show the correspondence between the derived analytical and developed numerical solutions.

Eq. 5.15, Eq. 5.16, and Eq. 5.17 are coded as UMAT (user material) subroutine in `FORTRAN` language. The subroutine code is called externally in the commercial Abaqus finite element analysis software. The routine calculates the material response as formulated in Eqs. 5.15, 5.16, 5.17. For the FE model and the analysis, the SI-metric consistent unit system is chosen as [m, N, kg, s, Pa, J, kg/m^3].

To test the UMAT routine, a side length of $0.1\ m$ cubical part is generated and meshed as a single element. An eight-noded hexahedral solid element (C3D8) is created in Abaqus for the fast track of the problem. A step time of 10 seconds with 0.1 seconds increment size is chosen, see Fig. 5.2. Therefore the analysis time is planned to be completed in 101 increments of equal time intervals, see Fig. 5.1. Simultaneously, the analytical solutions to the investigated problems are implemented in MATLAB according to the specifications outlined in the finite element model.

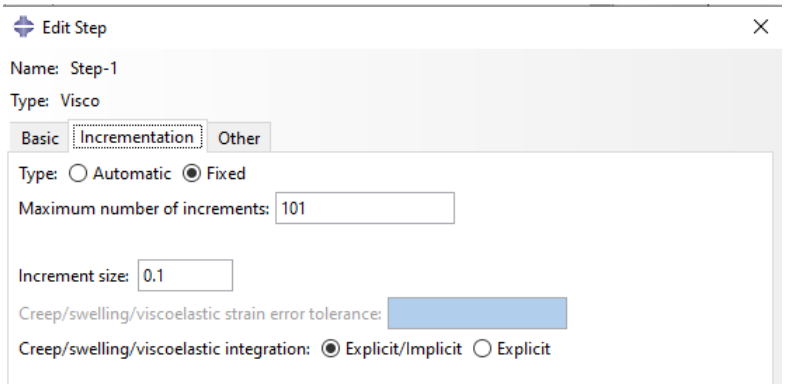

Figure 5.1: Definition of the Load Step

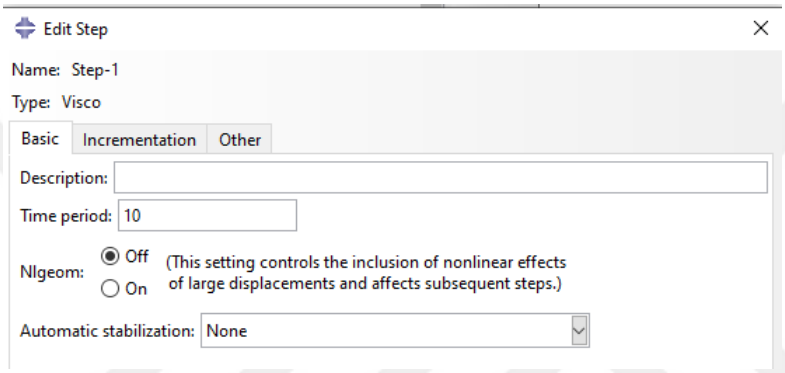

Figure 5.2: Definition of Total Analysis Time

The material parameters K_β, G_β, and α are specified in the material definition menu in Abaqus as shown in Fig. 5.3. The bulk modulus and shear modulus are selected to be $5 \cdot 10^9$ Pa and $3.75 \cdot 10^9$ Pa, respectively. The fractional order is selected to be as $\beta = 0.3$.

For the creep test $1 \cdot 10^7$ Pa surface pressure is applied on the free surface of the cubical element as shown in Fig. 5.4. The opposing face of the cubical element is assigned as XSym boundary condition. In the Abaqus, the ramp-hold type stress or displacement is defined by the proper definition of load characteristics in the Amplitude feature. In our runs, the ramp of the load/displacement is defined between 0-1 seconds and 1-10 seconds the load/displacement is kept the same in the hold time. The target hold stress and the hold displacement are selected as 10^7 Pa and 0.01 m, respectively.

The analyses are conducted on a personal computer equipped with the following hardware configuration: an Intel Core i7 3.4 GHz processor, 16 GB of RAM, an SSD

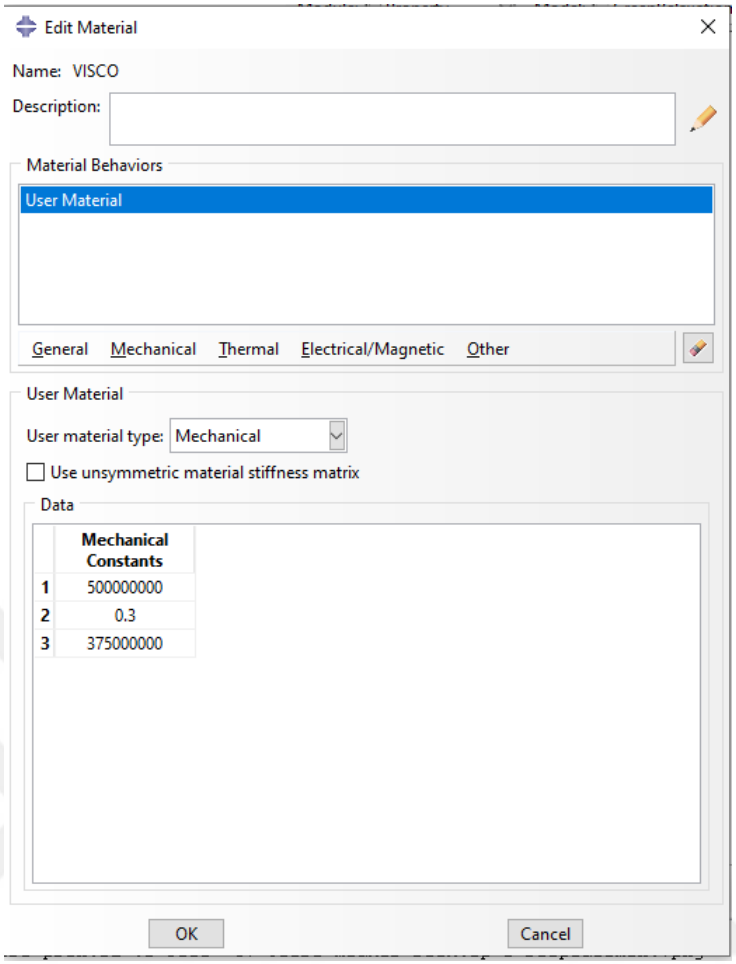

Figure 5.3: Definition of the Material Properties

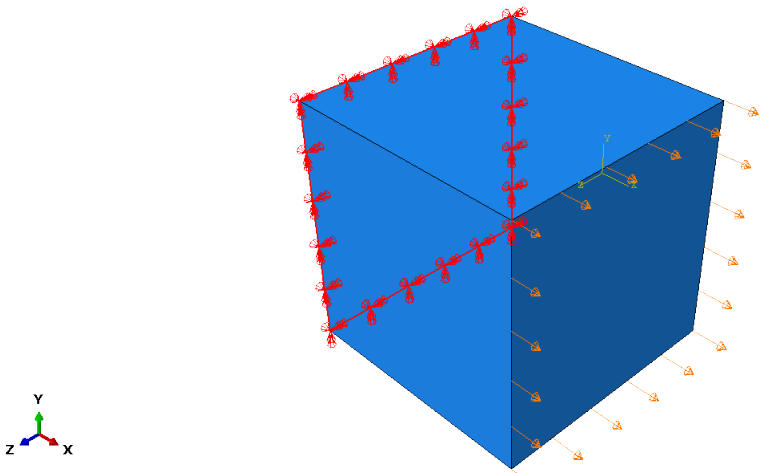

Figure 5.4: XSym Boundary Condition

utilizing the SATA III communication protocol, and storage performance metrics of 468.51 MB/s for sequential read and 410.21 MB/s for write operations. A typical analysis requires 1.8 seconds of CPU time, which is equivalent to the time needed for analyzing the built-in viscoelastic model with the solver using the one-term Prony series approximation.

The ramp-hold stress and ramp-hold displacement results are calculated both analytically and numerically by using the Abaqus. The responses are presented in Fig. 5.5 and Fig. 5.6. The applied strain history is plotted in Fig. 5.5 as the dashed-dotted line. The right axis shows the applied strain while the left axis shows the stress response of the material using the CO-UMAT code. It is clear from the figure that, at the early stages of the loading, the analytical result and the FE result deviate with a small error. The source of the error stems from the fact that the Grünwald-Letnikov derivative is an approximation rather than an exact representation. This approximation can introduce discrepancies between the theoretical model and practical observations. Consequently, the accuracy of the derived results may be affected. Therefore increasing the time or decreasing the time steps reduces the error.

The same observation is valid for Fig. 5.6. This time, the CO-UMAT code has been tested using a ramp-hold creep test, which simulates mechanical creep testing. Although the FE results and the analytical solution exhibit discrepancies at the initial stages of loading, they swiftly converge to the same value at later stages of the analysis.

The comparison between the subroutine (FEA) results and the analytical results reveals that both methods yield comparable estimations. The minor discrepancy observed between the numerical and analytical outcomes is attributed to the use of a finite difference approach for calculating the Grünwald-Letnikov derivative. This method represents a numerical approximation rather than an exact differentiation of the constant fractional order derivative of the function in question.

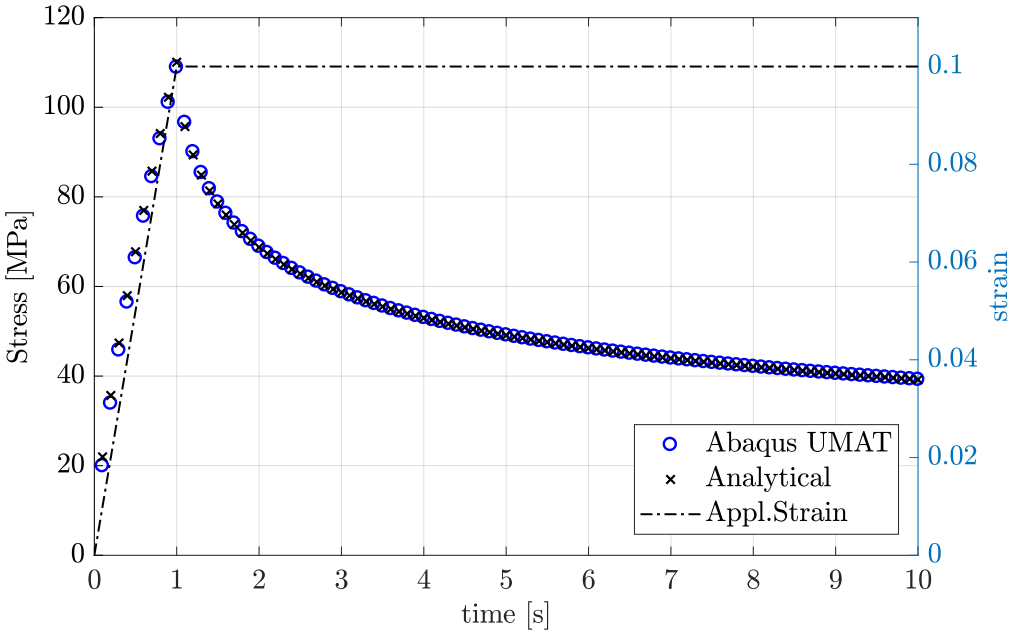

Figure 5.5: COFSB Model Response Against Ramp-Hold Strain

5.2 UMAT Development for Variable Order Model

The stress-strain relationship is presented in the previous section. In this section, derivations for the variable order fractional viscoelasticity will be presented. As discussed before the stress-strain relationship for a viscoelastic continuum is given as

$$\sigma_{ij}(t) = \int_0^t \tilde{R}_{ijkl}(t-\tau)\dot{\varepsilon}_{ij}(\tau)d\tau, \tag{5.33}$$

where $\tilde{R}_{ijkl}$ denotes the fourth order variable order fractional relaxation tensor function. The relaxation function has been shown as R_{ijkl} without a tilde, previously. We intend to emphasize the relaxation function constituted of variable fractional order. Here the description of the variable order fractional relaxation tensor function is expressed by its variable order (VO) bulk modulus, $\tilde{K}_R(t)$, and VO shear modulus, $\tilde{G}_R(t)$:

$$\tilde{R}_{ijkl}(t) = [\tilde{K}_R(t) - \frac{2}{3}\tilde{G}_R(t)]\delta_{ij}\delta_{kl} + \tilde{G}_R(t)[\delta_{ik}\delta_{jl} + \delta_{il}\delta_{jk}]. \tag{5.34}$$

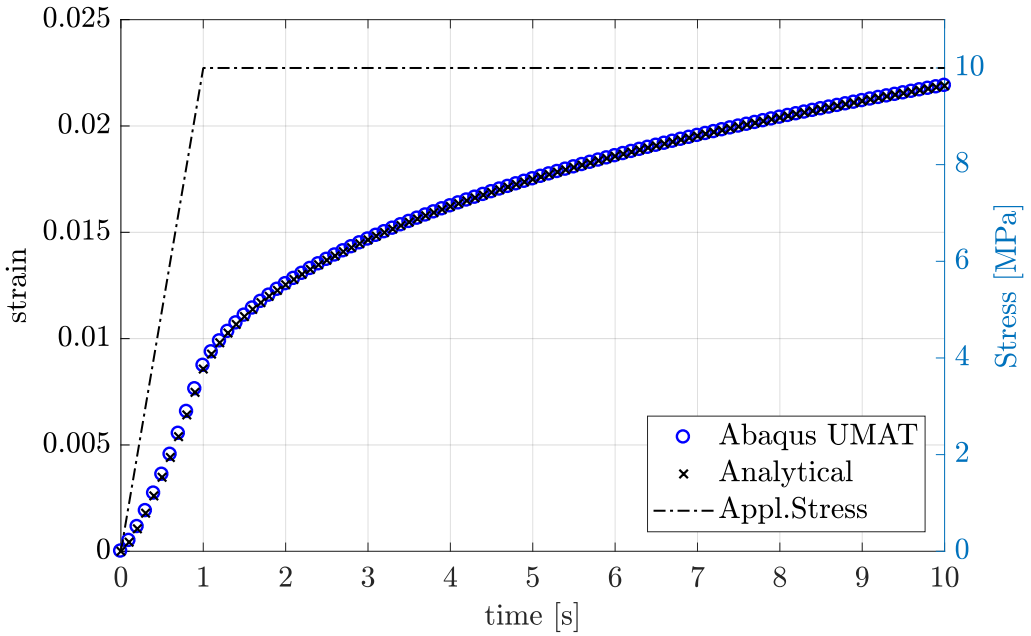

Figure 5.6: COFSB Model Response Against Ramp-Hold Stress

Assuming the fractional order depends only on the time variable, the VO bulk modulus and the VO shear modulus at every time increment are then expressed as

$$\tilde{K}_R(t) = \tilde{K}_{R_i} = \frac{K_\beta t^{-\beta_i}}{\Gamma(1-\beta_i)}, \qquad \tilde{G}_R(t) = \tilde{G}_{R_i} = \frac{G_\beta t^{-\beta_i}}{\Gamma(1-\beta_i)}. \tag{5.35}$$

In Eq. 5.35, K_β, and G_β are bulk modulus and shear modulus constants, respectively. Now, the necessary definitions are complete to express the normal and shear stress formulations. When the above are combined and expanded, normal and shear stress responses of the VO fractional viscoelastic continuum are obtained in terms of their VO fractional volumetric and VO fractional deviatoric functions,

$$\begin{aligned} \sigma_{ij}(t) &= 2\tilde{G}_\beta(D^{\beta(t)}\tilde{\varepsilon}_{ij})(t) + 3\tilde{K}_\beta(D^{\beta(t)}\bar{\varepsilon})(t) \qquad ; i = j, \\ \tau_{ij}(t) &= \tilde{G}_\beta(D^{\beta(t)}\gamma_{ij})(t) \qquad ; i \neq j, \end{aligned} \tag{5.36}$$

where $\tilde{\varepsilon}_{ij}(t) = \varepsilon_{ij}(t) - \bar{\varepsilon}(t)\delta_{ij}$ and $\bar{\varepsilon} = \sum_1^3 \varepsilon_{ii}/3$. The time discretization of the variable order fractional derivative operator can be expressed as Grünwald-Letnikov definition of the fractional derivative using the finite difference method,

$$({}^{VO-GL}D^{\beta(t)}f)(t) = ({}^{VO-GL}D^{\beta(t)}f)(k\Delta t) = \lim_{\Delta t \to 0} \sum_{j=1}^{k+1} \Delta t^{-\beta_j} \tilde{\lambda}_j^{(\beta_j)} f^{(k-j+2)}. \tag{5.37}$$

The binomial coefficients of a variable order are expressed [43, 147] as $\tilde{\lambda}_j^{(\beta_j)}$. For each particular time increment, the fractional order takes its j^{th} value, and the whole sequence of variable order binomial coefficients is calculated corresponding to that order value. Therefore, the binomial coefficients for the variable order fractional derivative are expressed as,

$$\tilde{\lambda}_{j+1}^{(\beta_{j+1})} = \frac{j-1-\beta_j}{j}\tilde{\lambda}_j^{(\beta_j)} \qquad \text{with} \qquad \tilde{\lambda}_1^{(\beta_j)} = 1. \tag{5.38}$$

The calculation method of the variable order binomial coefficients is already presented in Alg.1.

The above definitions constitute the foundation of the VO stress formulations. Then, the stress formulation of variable order fractional continuum is expressed as for the $(k+1)^{\text{th}}$ time increment

$$\begin{aligned}
\sigma_{ij}^{(k+1)} &= 2\sum_{j=1}^{k+1}\tilde{G}_{\beta_j}^{(j)}\Delta t^{-\beta_j}\tilde{\lambda}_j^{(\beta_j)}\tilde{\varepsilon}_{ij}^{(k-j+2)} + 3\sum_{j=1}^{k+1}\tilde{K}_{\beta_j}^{(j)}\Delta t^{-\beta_j}\tilde{\lambda}_j^{(\beta_j)}\bar{\varepsilon}^{(k-j+2)}, \\
\tau_{ij}^{(k+1)} &= \sum_{j=1}^{k+1}\tilde{G}_{\beta_j}^{(j)}\Delta t^{-\beta_j}\tilde{\lambda}_j^{(\beta_j)}\gamma_{ij}^{(k-j+2)}.
\end{aligned} \tag{5.39}$$

As we have done in the constant order model, the upper bound of the finite summations in the stress formulations should be made equal to perform calculations.

Rearranging by expanding the $(k+1)^{(\text{th})}$ term in the summation 5.39, we get

$$\begin{aligned}
\sigma_{ij}^{(k+1)} &= 2\sum_{j=1}^{k}\tilde{G}_{\beta_j}^{(j)}\Delta t^{-\beta_j}\tilde{\lambda}_j^{(\beta_j)}\tilde{\varepsilon}_{ij}^{(k-j+2)} + 2\tilde{G}_{\beta_j}^{(k+1)}\Delta t^{-\beta_{k+1}}\tilde{\lambda}_{k+1}^{(\beta_{k+1})}\tilde{\varepsilon}_{ij}^{(1)} \\
&\quad + 3\sum_{j=1}^{k}\tilde{G}_{\beta_j}^{(j)}\Delta t^{-\beta_j}\tilde{\lambda}_j^{(\beta_j)}\bar{\varepsilon}^{(k-j+2)} + 3\tilde{K}_{\beta_j}^{(k+1)}\Delta t^{-\beta_{k+1}}\tilde{\lambda}_{k+1}^{(\beta_k+1)}\varepsilon_{ij}^{(1)}, \\
\tau_{ij}^{(k+1)} &= \sum_{j=1}^{k}\tilde{G}_{\beta_j}^{(j)}\Delta t^{-\beta_j}\tilde{\lambda}_j^{(\beta_j)}\gamma_{ij}^{(k-j+2)} + \tilde{G}_{\beta_j}^{(k+1)}\Delta t^{-\beta_{k+1}}\tilde{\lambda}_{k+1}^{(\beta_{k+1})}\gamma_{ij}^{(1)}.
\end{aligned} \tag{5.40}$$

If the two subsequent stresses are written in the form,

$$\begin{aligned}
\Delta\sigma_{ii}^{(k+1)} &= \sigma_{ii}^{(k+1)} - \sigma_{ii}^{(k)}, \\
\Delta\tau_{ii}^{(k+1)} &= \tau_{ii}^{(k+1)} - \tau_{ii}^{(k)},
\end{aligned} \tag{5.41}$$

then the stress increment is obtained. To obtain the stress increment at two subsequent stress increments, the deviatoric and mean strains should be written in open form to

perform the calculations.

$$\begin{aligned}\Delta\sigma_{ij}^{(k+1)} &= 2\sum_{j=1}^{k}\tilde{G}_{\beta_j}\Delta t^{-\beta_j}\tilde{\lambda}_j^{(\beta_j)}\Delta\tilde{\varepsilon}_{ij}^{(k-j+2)} + 2\tilde{G}_{\beta_j}^{(k+1)}\Delta t^{-\beta_{k+1}}\tilde{\lambda}_{k+1}^{(\beta_{k+1})}\tilde{\varepsilon}_{ij}^{(1)} \\ &\quad + 3\sum_{j=1}^{k}\tilde{K}_{\beta_j}\Delta t^{-\beta_j}\tilde{\lambda}_j^{(\beta_j)}\Delta\bar{\varepsilon}^{(k-j+2)} + 3\tilde{K}_{\beta_j}^{(k+1)}\Delta t^{-\beta_{k+1}}\tilde{\lambda}_{k+1}^{(\beta_{k+1})}\epsilon_{ij}^{(1)}, \\ \Delta\tau_{ij}^{(k+1)} &= \sum_{j=1}^{k}\tilde{G}_{\beta_j}\Delta t^{-\beta_j}\tilde{\lambda}_j^{(\beta_j)}\Delta\gamma_{ij}^{(k-j+2)} + \tilde{G}_{\beta_j}\Delta t^{-\beta_{k+1}}\tilde{\lambda}_{k+1}^{(\beta_{k+1})}\gamma_{ij}^{(1)}.\end{aligned} \tag{5.42}$$

Expanding the deviatoric and mean strains yields to,

$$\begin{aligned}\Delta\sigma_{ij}^{(k+1)} &= \frac{4}{3}\sum_{j=1}^{k}\tilde{G}_{\beta_j}\Delta t^{-\beta_j}\tilde{\lambda}_j^{(\beta_j)}\left(\Delta\varepsilon_{11}^{(k-j+2)} - \frac{\Delta\varepsilon_{22}^{(k-j+2)} + \Delta\varepsilon_{33}^{(k-j+2)}}{2}\right) \\ &\quad + \sum_{j=1}^{k}\tilde{K}_{\beta_j}\Delta t^{-\beta_j}\tilde{\lambda}_j^{(\beta_j)}\Delta\varepsilon_v^{(k+1)} \\ &\quad + [2\tilde{G}_{\beta_j}\Delta t^{-\beta_j}\tilde{\lambda}_{k+1}^{(\beta_j)}\tilde{\varepsilon}^{(1)} + 3\tilde{K}_{\beta_j}\Delta t^{-\beta_j}\tilde{\lambda}_{k+1}^{(\beta_j)}\bar{\varepsilon}^{(1)}], \\ \Delta\tau_{ij}^{(k+1)} &= \sum_{j=1}^{k}\tilde{G}_{\beta_j}\Delta t^{-\beta_j}\tilde{\lambda}_j^{(\beta_j)}\Delta\gamma_{ij}^{(k-j+2)} + [\tilde{G}_{\beta_j}\Delta t^{-\beta_j}\tilde{\lambda}_{k+1}^{(\beta_{k+1})}\gamma_{ij}^{(1)}].\end{aligned} \tag{5.43}$$

The bracketed terms in the above equations will not contribute to the Jacobian. Hence we obtain

For $k = 0$, $\tilde{\lambda}_0 = 1$,

$$\begin{aligned}\frac{\partial\Delta\sigma_{ii}^{(k+1)}}{\partial\Delta\varepsilon_{ii}^{(k+1)}} &= \frac{4}{3}\tilde{G}_{\beta_j}\Delta t^{-\beta_j}\tilde{\lambda}_1^{(\beta_j)} + \tilde{K}_{\beta_j}\Delta t^{-\beta_j}\tilde{\lambda}_1^{(\beta_j)}, \\ \frac{\partial\Delta\sigma_{ii}^{(k+1)}}{\partial\Delta\varepsilon_{jj}^{(k+1)}} &= -\frac{2}{3}\tilde{G}_{\beta_j}\Delta t^{-\beta_j}\tilde{\lambda}_1^{(\beta_j)} + \tilde{K}_{\beta_j}\Delta t^{-\beta_j}\tilde{\lambda}_1^{(\beta_j)}, \\ \frac{\partial\Delta\sigma_{ij}^{(k+1)}}{\partial\Delta\gamma_{ij}^{(k+1)}} &= \tilde{G}_{\beta_j}\Delta t^{-\beta}\tilde{\lambda}_1^{(\beta_j)}.\end{aligned} \tag{5.44}$$

5.2.1 Benchmark Studies for Variable Order UMAT (VO-UMAT) Code

CO-UMAT benchmark test with the ramp-hold stress and ramp-hold strain has shown that the maximum error is observed during the ramp of the load. Loading for the creep and the stress relaxation causes fast convergence of the solution. The efficiency of the

code should be tested in the worst possible scenario. Because of this motivation, the benchmarking of the VO-UMAT code is done for ramp loading only.

The generic material parameters are selected to test the code. The bulk modulus and shear modulus constants are selected as 500 MPa and 375 MPa, respectively. The rate of displacement is applied as 0.01 mm/s for the single cubical element that has a side length of 0.1 mm.

The code is constructed so flexibly that by imposing the history of the fractional order as a vector array in the `FORTRAN` environment the whole theoretical domain of the fractional viscoelastic continuum can be analyzed for load and displacement responses. This corresponds to the fractional order can be varied from 0 to 1. At marginal values of the fractional order, the model should portray purely elastic and purely viscous behaviors, respectively.

To assess the efficiency of the VO-UMAT code, eight distinct cases are investigated. A summary of these cases is provided in the Table 5.1. The VO-UMAT code is tested across a spectrum ranging from purely elastic to purely viscous behaviors. Additionally, the efficiency of the VO-UMAT code is evaluated for both the CO and VO cases.

Table 5.1: Summary of Investigated Cases for Definition of the Fractional Order

Case	**Behavior Type**	**Equation for $\beta(t)$**	**Figure**
1	Purely Elastic	$\beta(t) = 0$	Fig. 5.7
2	Purely Viscous	$\beta(t) = 1$	Fig. 5.8
3	COF Viscoelastic	$\beta(t) = 0.3$	Fig. 5.9
4	COF Viscoelastic	$\beta(t) = 0.5$	Fig. 5.10
5	COF Viscoelastic	$\beta(t) = 0.8$	Fig. 5.11
6	VOF Viscoelastic	$\beta(t) = 0.04tH(t)$	Fig. 5.12
7	VOF Viscoelastic	$\beta(t) = (0.4 - 0.04t)H(t)$	Fig. 5.13
8	VOF Viscoelastic	$\beta(t) = 0.4H(t) - 0.06(t-5)H(t-5)$	Fig. 5.14

The cases from 1-5 correspond to the constant fractional order material models. Cases 6-8 represent four different possibilities that the fractional order may vary. The VO

fractional models are selected to yield hardening and the softening behavior of the material. The analytical solutions corresponding to the FEA results calculated using the VO-UMAT code are compared in Figs. 5.7—5.14. The maximum error calculated between the analytical solution and FEA results is printed on the plot for each case. Also, the trend of the fractional order is printed as a subplot in the main plot area in each case.

The perfectly elastic case is illustrated in Fig. 5.7. For a fractional order of $\beta(t) = 0$, the analytical solution corresponds to Hooke's law. The analytical solution presented in Chapter 3 is compared with the VO-UMAT result, demonstrating excellent agreement between the two methods.

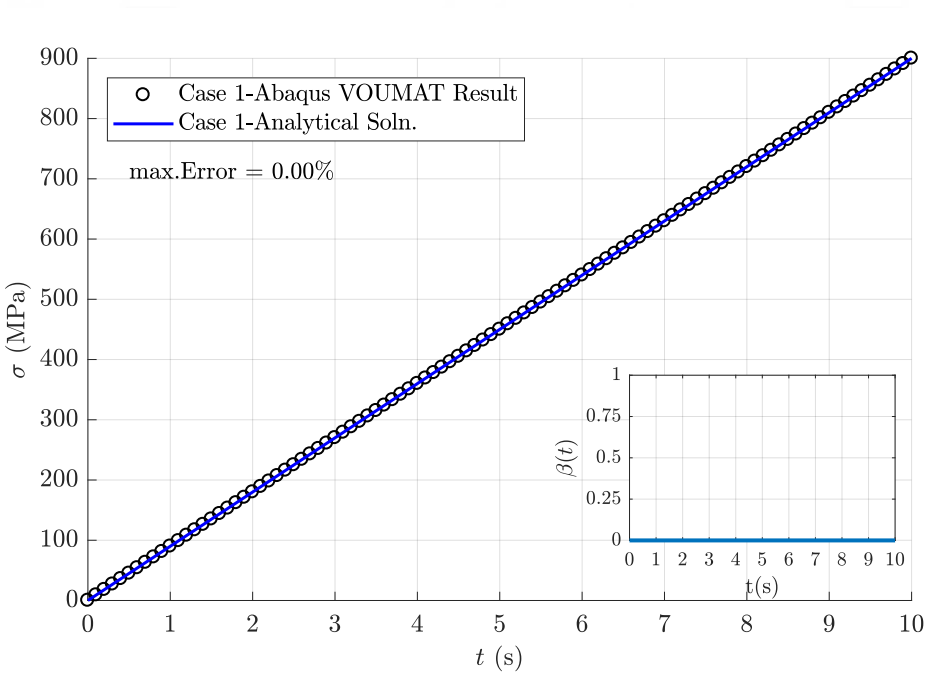

Figure 5.7: Case-1 VO-UMAT Benchmark Result

The UMAT code also accurately simulates the dashpot behavior. The dashpot behavior is also simulated in Abaqus. Fig. 5.8 presents a comparison between the analytical and VO-UMAT results for Case 2. When the fractional order is set to unity for the entire time period, $\beta(t) = 1$, the stress response aligns perfectly with the analytical solution.

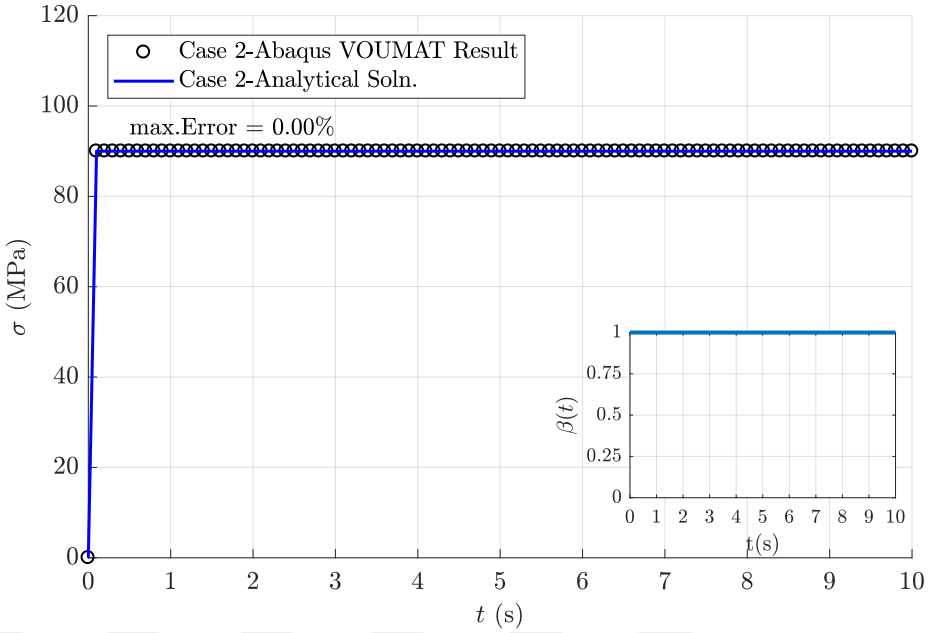

Figure 5.8: Case-2 VO-UMAT Benchmark Result

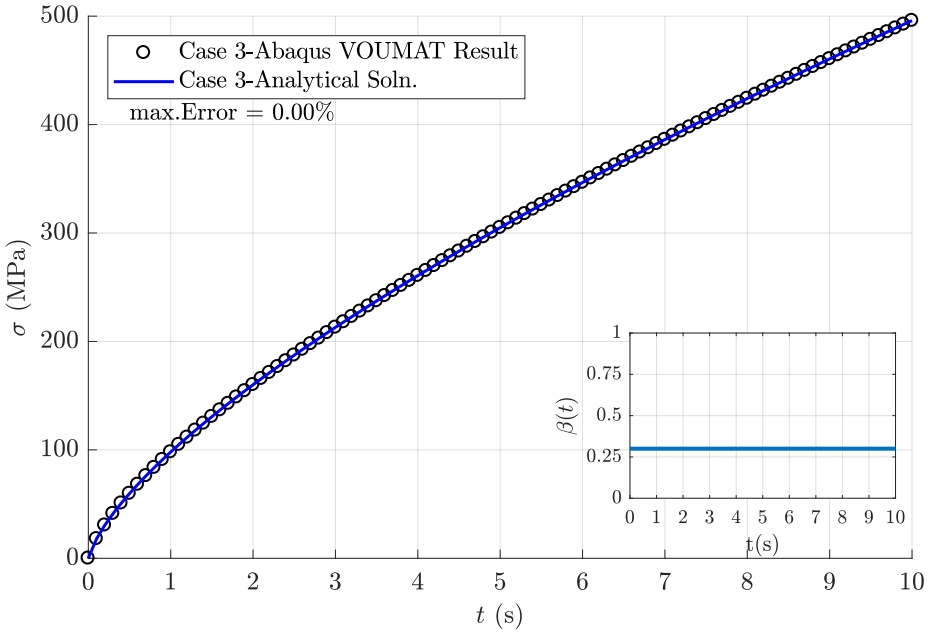

Figure 5.9: Case-3 VO-UMAT Benchmark Result

Cases 3, 4, and 5 examine the efficiency of the method for constant fractional-order scenarios. In the benchmarking study, fractional orders of 0.3, 0.5, and 0.8 are selected. Each case exhibits excellent agreement with the corresponding analytical solution as shown in Figs. 5.9, 5.10, and 5.11.

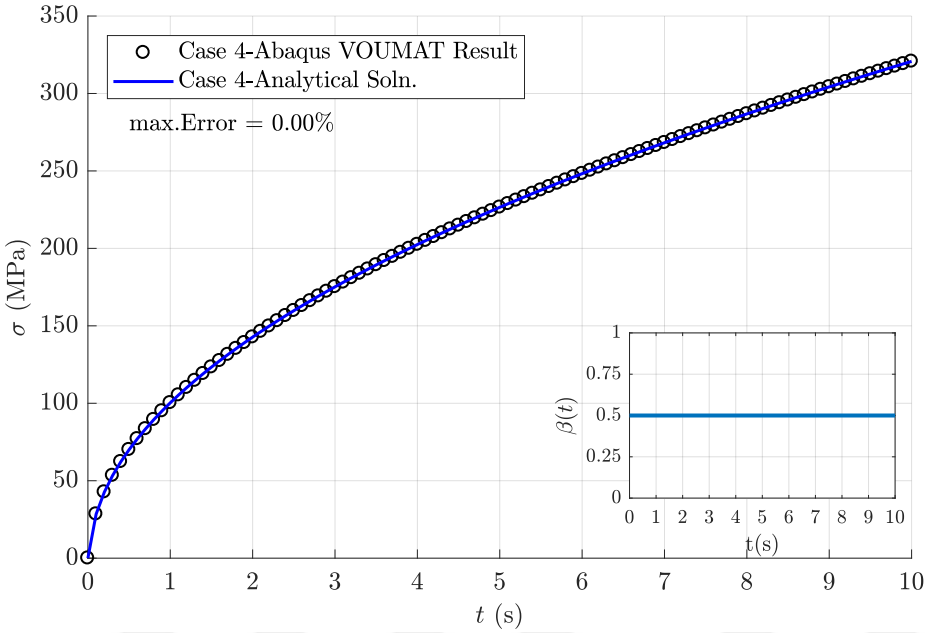

Figure 5.10: Case-4 VO-UMAT Benchmark Result

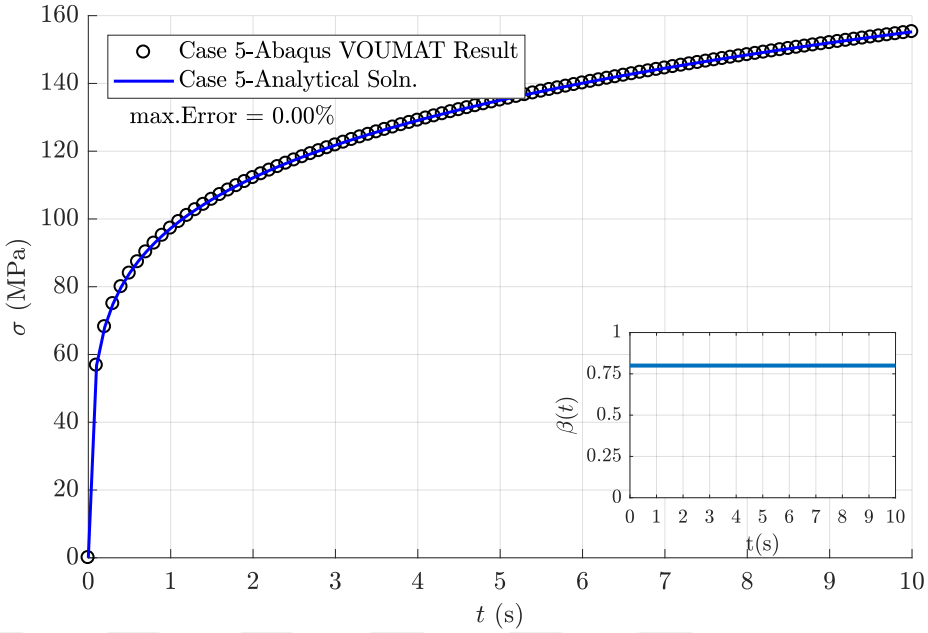

Figure 5.11: Case-5 VO-UMAT Benchmark Result

Cases 1 to 5 represent the constant fractional order cases where Case-1 and Case-2 have special meaning. Case-1 represents the ideal Hookean solid ($\beta(t) = 0$, Fig. 5.7), while Case-2 represents the Newtonian liquid ($\beta(t) = 1$, Fig. 5.8). The VO-UMAT code is capable of calculating the material response with great agreement with the analytical solution for the ramp displacement.

The computed stress error between the VO-UMAT result and analytical solution is calculated as:

$$\text{Error} = \left|\sigma_{\text{Analytical Solution}} - \sigma_{\text{VO-UMAT Result}}\right|. \tag{5.45}$$

Case 6 represents the softening behavior of the fractional viscoelastic material. The fractional order linearly increases starting from the purely elastic case as shown in Fig. 5.12.

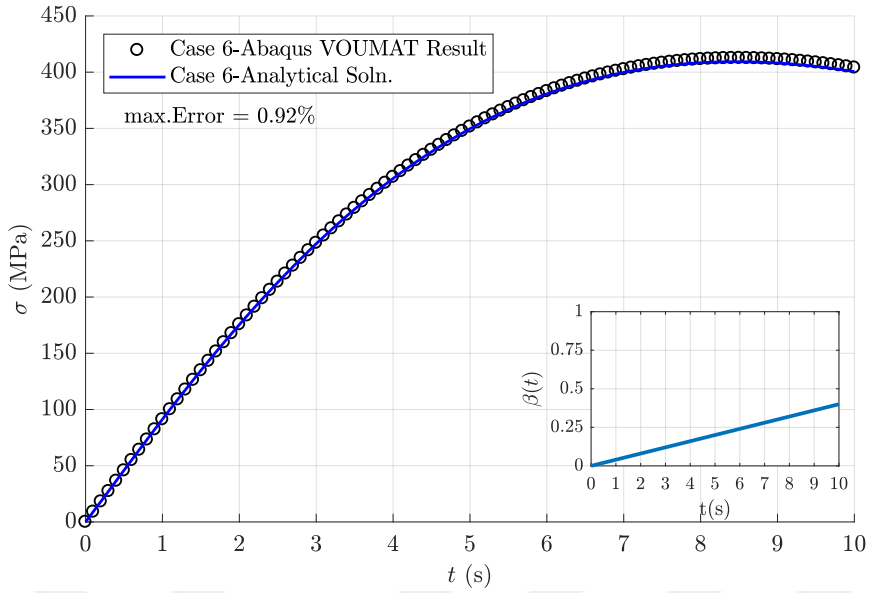

Figure 5.12: Case-6 VO-UMAT Benchmark Result

Case 7 and Case 8 represent two different hardening behavior. For the former, the fractional order and the time are directly inverse proportional as shown in Fig. 5.13. The latter represents the hardening behavior that is triggered after some time. In other words, the fractional order remains constant at 0.4 until the 5 s, then gradually reduces to 0.1.

In cases 6, 7, and 8 the amount of error between the analytical solution and the FEA result is calculated at around 1%.

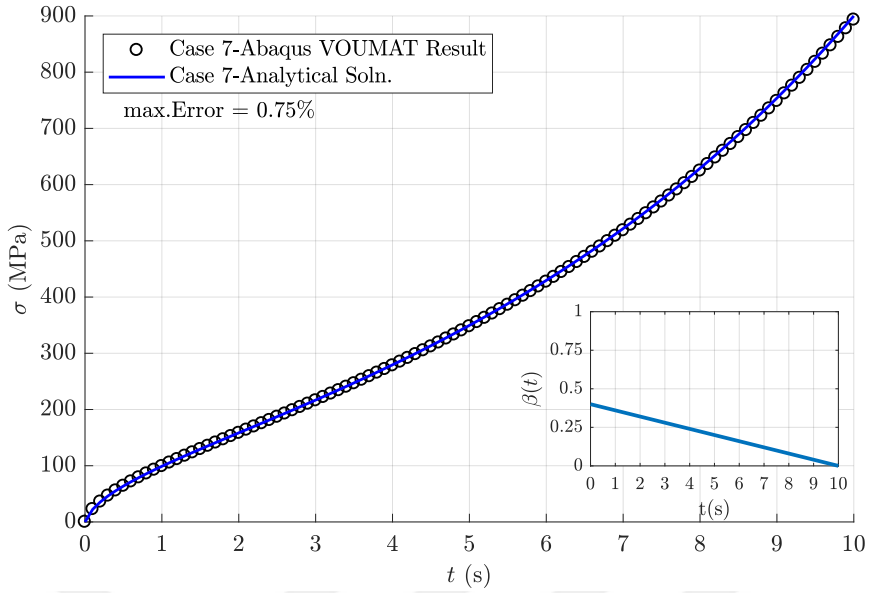

Figure 5.13: Case-7 VO-UMAT Benchmark Result

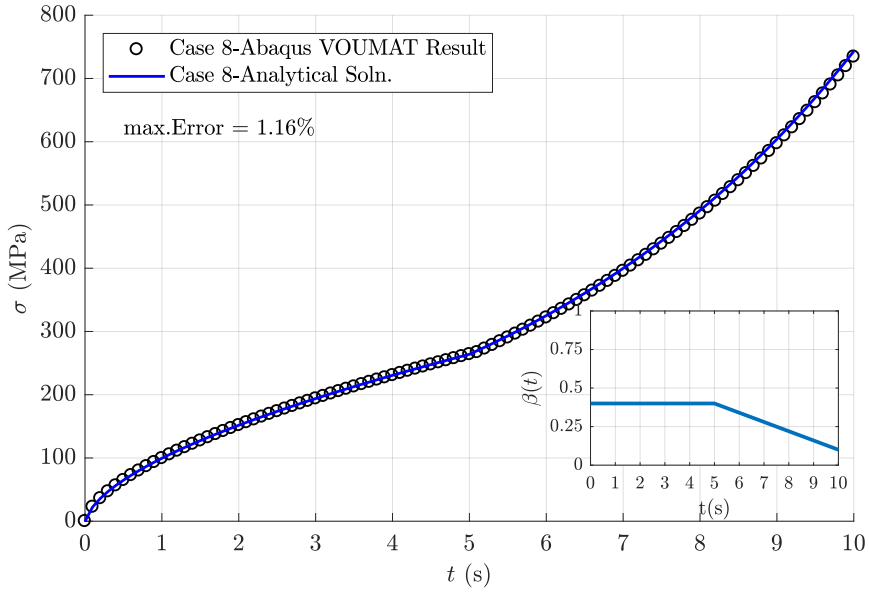

Figure 5.14: Case-8 VO-UMAT Benchmark Result

CHAPTER 6

EXPERIMENTAL VERIFICATION

In Chapter 4 the efficiency of the parameter estimation method is shown with the synthetic test data. The models assumed in Chapter 4 have sudden changes in the fractional order trend. From the mechanical engineering perspective, such abrupt changes are not anticipated. Therefore, the developed model is expected to predict the material parameters with an even improved uncertainty.

In this chapter, the experimental validation of fractional viscoelastic materials is investigated through a systematic two-stage approach. The primary objective is to assess the mechanical response of these materials under controlled loading conditions and to establish a reliable correlation with the proposed material model.

In the first stage, tensile tests are conducted on the specimens using a universal tensile testing machine without any specialized auxiliary equipment. This initial phase provides fundamental stress-strain data, serving as a baseline for further analysis. However, a more comprehensive validation requires additional experimental insights.

In the second stage, the focus shifts towards correlating the material model with the estimated material parameters and the user-defined material subroutine (UMAT) code. A key aspect of this correlation is the determination of the instantaneous Poisson's ratio, which is crucial for an accurate definition of the material behavior. To fully characterize the material properties, both bulk and shear properties must be extracted, necessitating the simultaneous measurement of lateral contraction and axial elongation.

A significant challenge in this context arises from the limitations of conventional strain gauges. Since most strain gauges are restricted to measuring strains below ap-

proximately $\varepsilon \leq 3\%$, they are unsuitable for tests involving higher strain levels. Given that the test strain exceeds this limit, a contactless strain measurement method is employed to ensure accurate and reliable data acquisition. This approach enables precise strain evaluation without the constraints imposed by contact type sensor limitations, thereby enhancing the fidelity of the experimental results. However, contactless measurement methods do inherently carry certain measurement uncertainties as well. In the upcoming section, we will discuss these uncertainties in detail.

By adopting this rigorous methodology, the study aims to provide a robust experimental foundation for the validation of fractional viscoelastic models, ultimately contributing to the broader understanding of the mechanical behavior of such materials.

6.1 Experimental Studies with Simple Tension Test

Experimental investigations have been performed using a Zwick/Roell Z020 uniaxial tension testing apparatus, as depicted in Fig. 6.1. PTFE, PE300, and Ethylene Vinyl Acetate (EVA) which is commercially known as hot glue silicone are selected as the tensile test materials. Their glass transition temperature is well below the room temperature according to the literature and supplier data. The test samples are prepared from either sheet material or round bars. To remove residual stresses from the surface of the bulk material, a machining process is applied to remove at least 60% of the initial thickness from all sides of the material. The dimensions of the specimens are specified according to ASTM D638-14 standards [148]. Following the machining, the specimens are conditioned in a laboratory environment at a temperature of $23 \pm 2^{\circ}$ for a duration exceeding 96 hours before testing, in accordance with Procedure A described in ASTM D618 [149].

The specimens are subjected to predetermined constant strain rate deformations by configuring the test equipment to operate in displacement-controlled loading mode.

Figure 6.1: Uniaxial Tension Test Equipment Zwick/Roell Z020

PE300, PTFE, and EVA uniaxial tension test specimens are fabricated in order to obtain the material parameters. The PE300 and EVA specimens are round-shaped standard test specimens with a gage length of 158 mm and 20 mm, respectively. Their crossectional diameters are 9.97 mm and 11.05 mm. The crosshead displacement velocity is set for each specimen according to its initial gage length so that the rate of strain value is to be as specified in Table 6.1 for each specimen. PTFE specimens are dogbone shaped with a cross-sectional area of 41.9 mm^2 and 41.15 mm^2, a gage length of 38.6 mm and 38.75 mm. PTFE specimens are subjected to two different strain rates to see the effect of strain rate. Round and dogbone shape specimens and

the tension test environment are presented in Fig. 6.2 and Fig. 6.3.

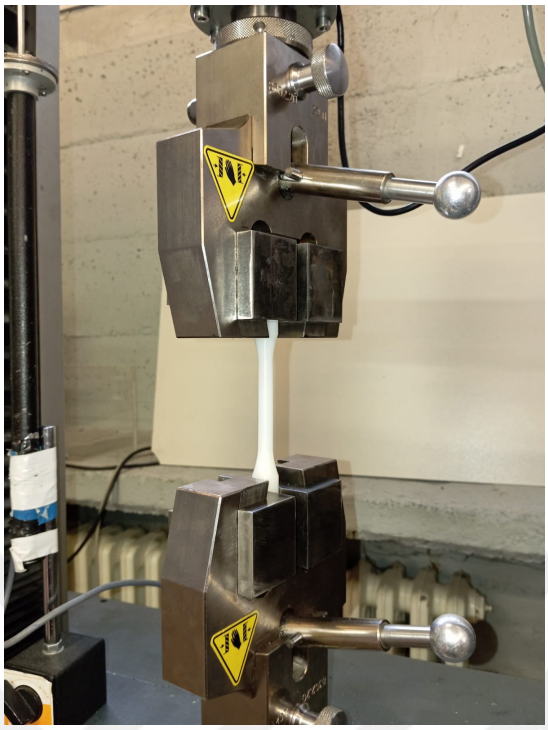

Figure 6.2: PE300 Round Specimen

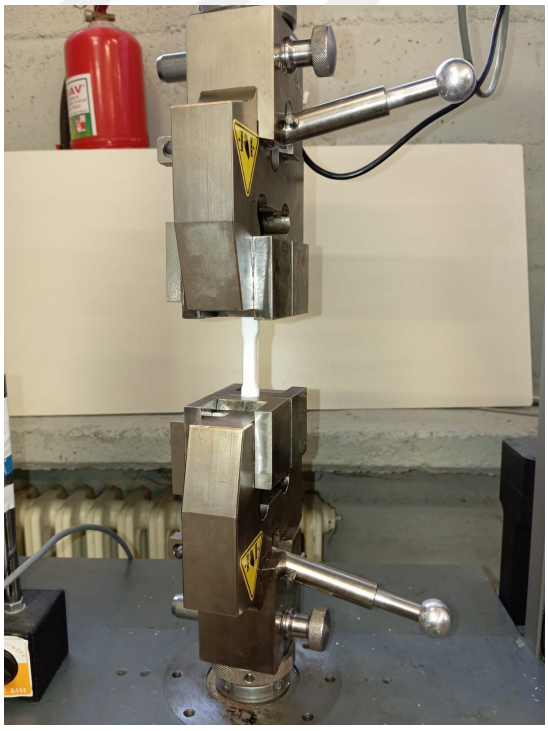

Figure 6.3: PTFE Dogbone Specimen

The estimated pattern of the fractional order against strain is plotted for each of PE300, PTFE, and EVA. PE300 shows linear elastic behavior until 0.018 strain level. The linear elastic behavior can be distinguished from Fig. 6.4. Obviously, the fractional order being zero portrays the linear elastic behavior which is evident in Fig. 6.4 and Fig. 6.5.

The fitted material parameters are presented in Table 6.1. Using the estimated material parameters and the variable-order fractional constitutive equation, the stress-strain responses for each specimen are computed.

To validate the material parameter estimation process, the coefficient of determination, commonly known as R-squared (R^2), is computed using Eq. 6.1. The R^2 metric quantifies the goodness of fit between the experimental data and the model predictions.

$$R^2 = 1 - \frac{\text{sum squared regression (SSR)}}{\text{total sum of squares (SST)}} = 1 - \frac{\sum_{i=1}^{n}(y_i - \hat{y}_i)^2}{\sum_{i=1}^{n}(y_i - \bar{y})^2}, \tag{6.1}$$

where y_i represents the actual measured values of the dependent variable y at each data point, $\bar{y}$ is the mean of the observed values, and $\hat{y}_i$ denotes the predicted values derived from the regression model based on the independent variables.

Table 6.1: Estimated Material Properties

Material	E **(MPa)**	θ **(s**$^{-\beta_i}$**)**	$\dot{\varepsilon}$ **(s**$^{-1}$**)**
PE300	745.57	0.023784	0.2
PTFE-1	129.83	0.000796	0.1
PTFE-2	198.81	0.0426	1.0
EVA	2.44	0.1344	0.2

The stress response of the material is computed from the estimated parameters, and the experimental stress-strain data are plotted together for a comprehensive verification study. To evaluate the accuracy of the material parameter estimation, discrep-

ancies between the calculated and measured stress responses are presented in the corresponding stress-strain diagrams (see Figs. 6.5, 6.7, 6.9, and 6.11). Furthermore, for each test instance, the R-squared values are computed to quantify the goodness of fit. Additionally, the estimation error in the stress measurements is illustrated on the right axis of the diagrams. The analysis reveals that the error remains consistently below 1 MPa across all tested instances, highlighting the reliability of the estimation process.

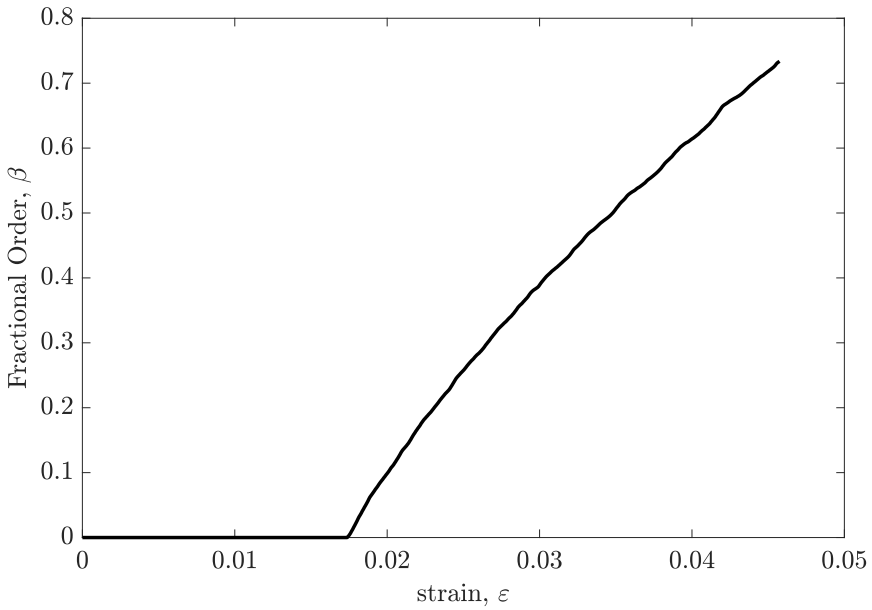

Figure 6.4: PE300 Order-Strain Relation

As observed from Fig. 6.5, PE300 exhibits an initial toeing region. In the initial toeing region, the model generates negative fractional orders, which are approximated to zero for the alignment with the initial assumption. In the absence of such a constraint, the fractional order tends to be affected by significant noise at the early stages of the application of the deformation. By disregarding the negative fractional order, in alignment with our initial assumption, more consistent and reliable results are achieved.

The estimated stress error in PE300 remains below 1 MPa, with the greatest discrepancy observed in the initial toeing region, as illustrated in Fig. 6.5. In the regions located outside the initial toeing zone, the relative error between the measured and

estimated stresses demonstrates a high level of confidence.

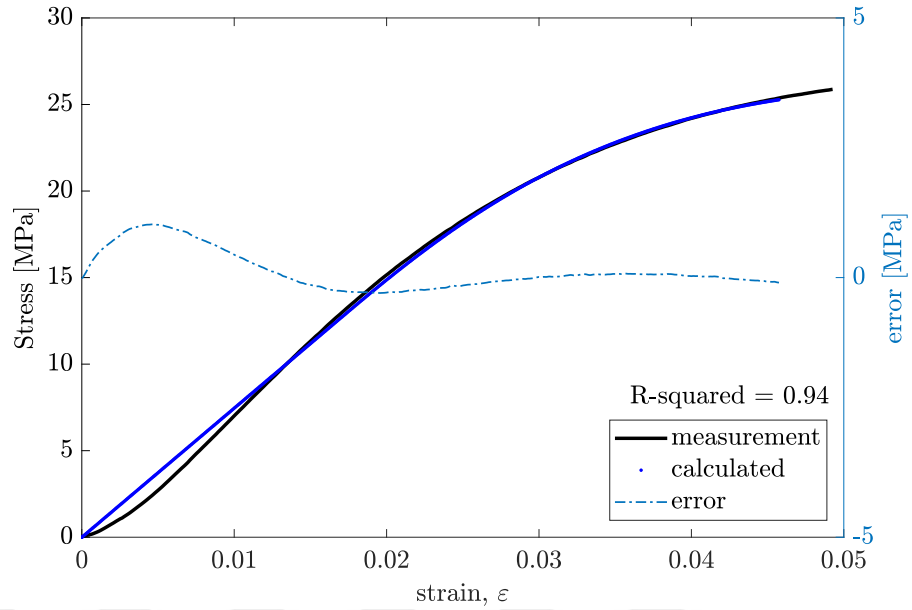

Figure 6.5: PE300 Experimental and Calculated Stress Strain

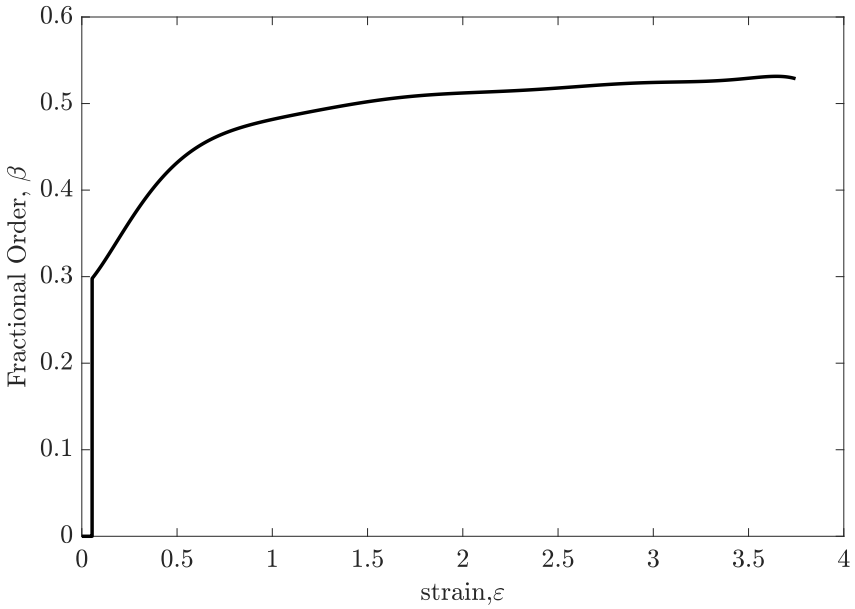

Figure 6.6: PTFE-1 Order-Strain Relation

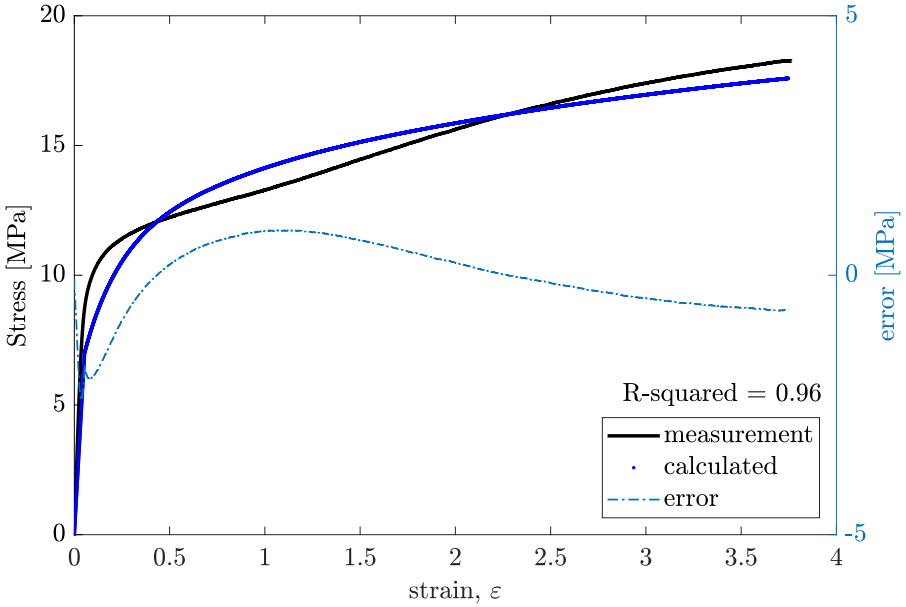

Figure 6.7: PTFE-1 Experimental and Calculated Stress Strain

The PTFE-1 specimen is tested to assess the large deformation performance of the developed model. Compared to PTFE-2, PTFE-1 is subjected to a slower deformation rate. The strain rate is $\dot{\varepsilon} = 1.0\ \mathrm{s}^{-1}$ for the PTFE-1 specimen, which is ten times higher than that of the PTFE-2 specimen ($\dot{\varepsilon} = 0.1\ \mathrm{s}^{-1}$).

Another key difference between the two specimens is that PTFE-1 is pulled up to a strain of $\varepsilon = 3.7$, whereas PTFE-2 is deformed only up to $\varepsilon = 0.18$. In both cases, the specimens exhibit nearly perfect linear elastic behavior up to approximately $\varepsilon = 0.05$. These observations are derived from the data presented in Figs. 6.7 and 6.9.

The estimated fractional orders indicate that the change in fractional order for PTFE-1 is less pronounced than for PTFE-2, see Figs. 6.6 and 6.8. The error in the estimated response of the PTFE-1 specimen is higher than that observed for PTFE-2. This discrepancy may arise due to the large deformation experienced by the PTFE-1 specimen during loading.

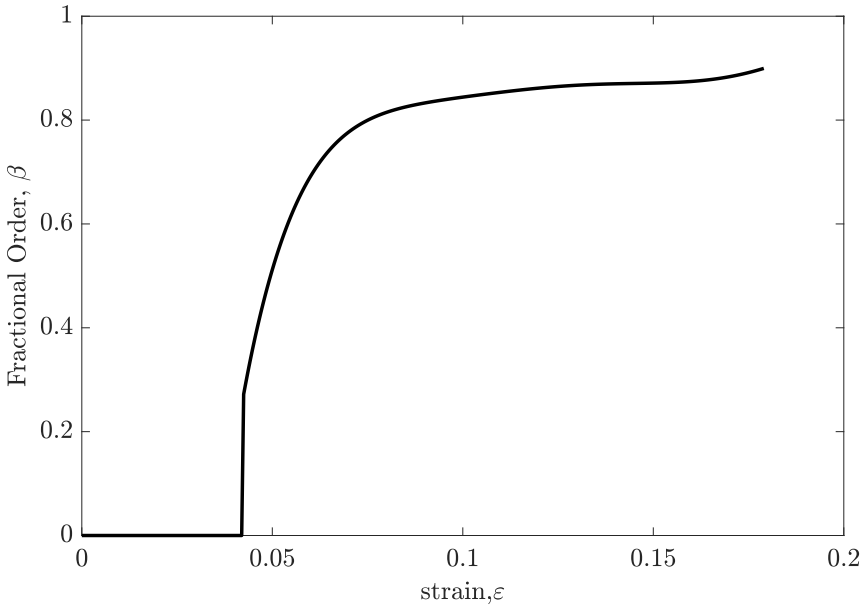

Figure 6.8: PTFE-2 Order-Strain Relation

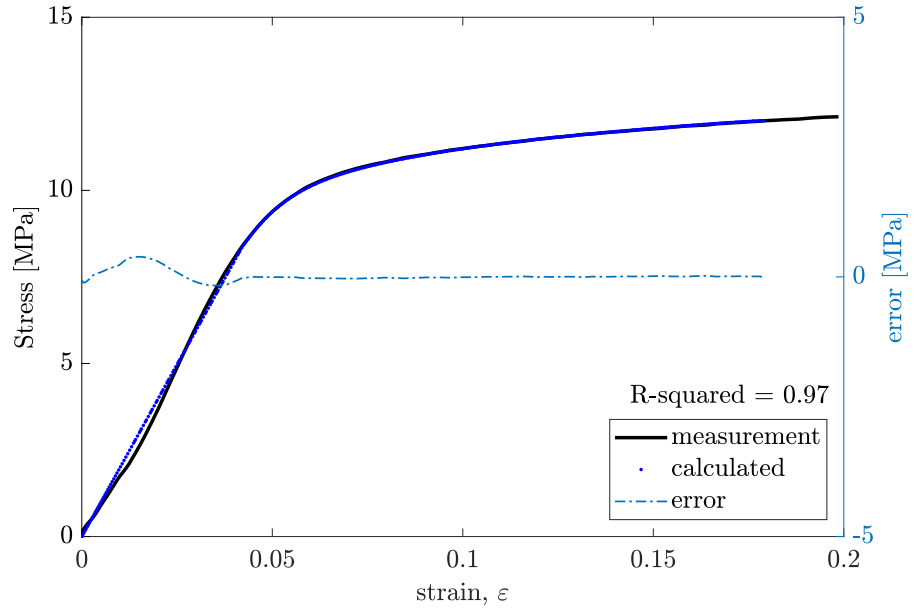

Figure 6.9: PTFE-2 Experimental and Calculated Stress-Strain

The hot glue material test demonstrates excellent agreement between the measured and calculated stresses, with an overall error of less than 0.001 MPa. The model effectively estimates the fractional orders. Notably, a unique conclusion drawn from

the testing of this material is the near absence of a purely elastic region. This observation implies that the material exhibits significant time-dependent behavior even at the onset of deformation.

Especially, Fig. 6.10 clearly illustrates minor noise-like deviations in the fractional order, particularly at strains below $\varepsilon = 0.5$. A similar phenomenon is barely observable in the PE300 specimen, as seen in Fig. 6.4, but it is more pronounced and dramatic in Fig. 6.10.

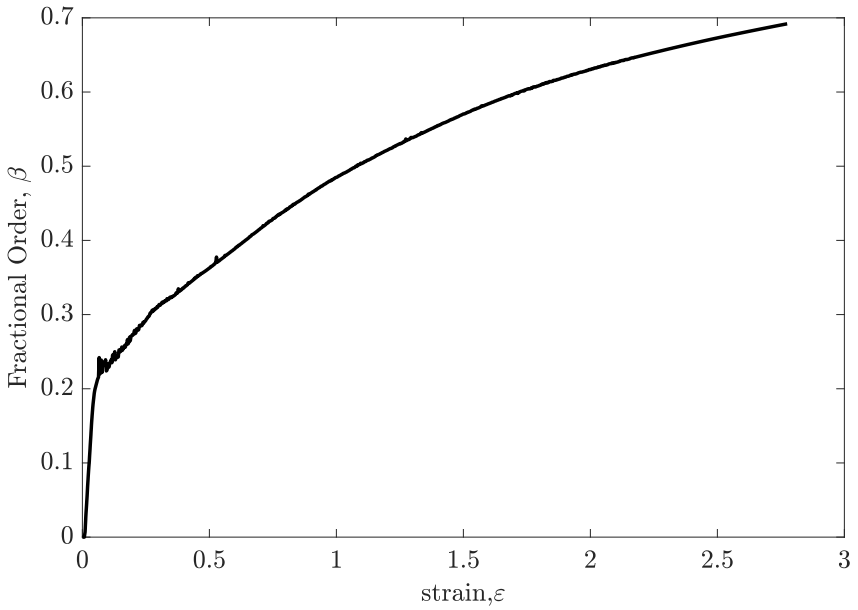

Figure 6.10: EVA Order-Strain Relation

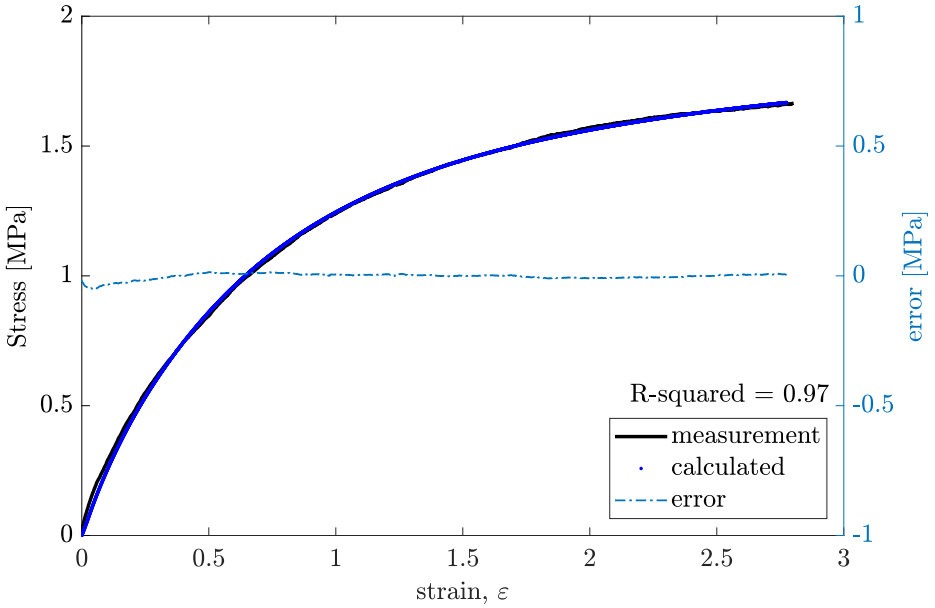

Figure 6.11: EVA Experimental and Calculated Stress-Strain

PTFE-1 and PTFE-2 specimens exhibit a distinct pattern when the fractional order is examined. Initially, the PTFE specimens display linear elastic behavior during the early stages of deformation; however, the fractional order subsequently exhibits an abrupt jump to a higher value, followed by a gradual increase over deformation. In contrast, the fractional order versus strain diagrams for PE300 and EVA materials do not show such sudden jumps, indicating a more continuous evolution of the fractional order with strain.

Overall, the proposed method shows significant promise in accurately estimating real material parameters. It remains effective even in the presence of small, nonsystematic deviations in the fractional order. This approach appears to outperform the method employed by authors in [5]. A major advantage of the current method is that it does not require a predetermined functional form for the fractional order. In contrast, much of the existing literature on parameter identification in fractional viscoelasticity relies on the assumption of a predefined form for this variable order [79, 104, 109, 150, 151].

Next, we extend our experimental test campaign by incorporating the instantaneous material properties derived from the measurements taken from the longitudinal and transverse deformation.

6.2 Experimental Studies with Video Equipment

In the preceding section, the sequence of the fractional order and the material parameters are determined based on a one-dimensional simple tension test. On the other side, the stress-strain response of the VO-UMAT code for the material is evaluated for a single cubical element.

While the tension test provided valuable insights into the material behavior under uniaxial stress, it does not account for the volumetric response of the material, which is crucial for a more comprehensive understanding of its mechanical properties. This section, however, presents the parameter estimation studies that incorporate the volumetric behavior of the material, specifically addressing the influence of transverse strain and therefore the instantaneous Poisson's ratio. This more complete approach allows for a better approximation of the mechanical behavior of the material and enables a deeper analysis of its response under various loading states.

PE300 is selected as the test material for this experimental campaign due to its favorable manufacturability in the form of a standard dogbone-shaped flat specimen. The flat shape is a natural requirement for video measurement of the specimens. The rationale behind this selection lies in the challenges encountered in manufacturing the specimen coupons with alternative materials such as PTFE and EVA. Given their lower stiffness compared to PE300, fabricating ASTM E8-compliant test specimens with precise tolerances proved to be difficult. In contrast, PE300 exhibits sufficient rigidity to allow successful machining within the tolerances specified by the standards [152], ensuring reliable specimen geometry and consistency in mechanical testing. The specimen has a thickness of 5 mm, a width of 12.5 mm, and a gage length of 140 mm conforming to the dimensional requirements outlined in ASTM E8.

Two different uniaxial tensile testing machines are employed in the experimental studies. Although both machines were manufactured by Instron, they differ in terms of load capacity and auxiliary equipment. Specifically, each machine is designed to accommodate different levels of force. Strain measurements are conducted using a Video Extensometer (V-Ext) in one machine, while the other utilized a Digital Image Correlation (DIC) system, depending on the specific test configuration.

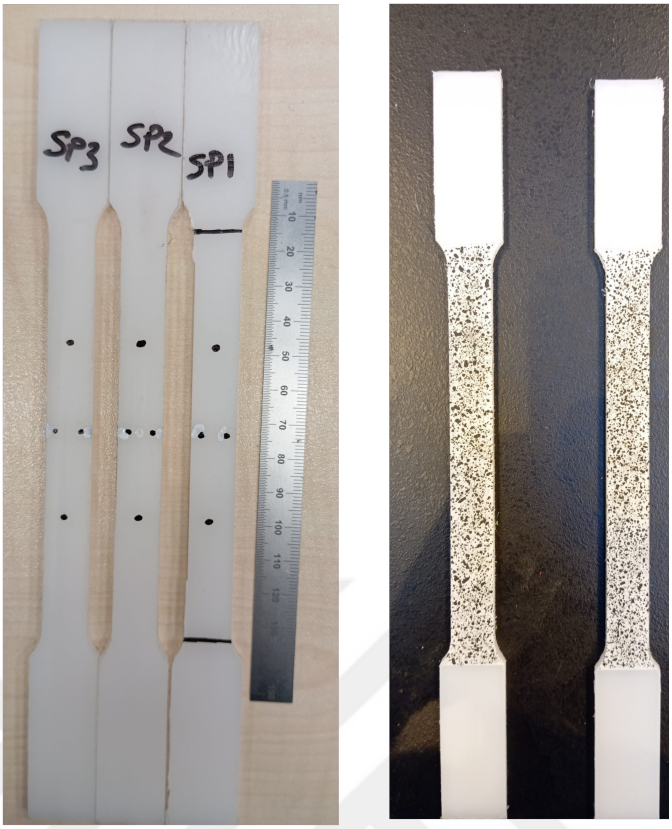

Figure 6.12: Specimens for V-Ext (Left) and DIC (Right) Tests

The crosshead velocity for the specimens is adjusted according to the values shown in Table 6.2. The tensile tests are conducted at three different strain rates.

The V-Ext machine is equipped with a 350 kN load cell, whereas the DIC machine is equipped with a 100 kN load cell. The V-Ext machine is also equipped with a wide-angle view camera and integrated software that uses gauge markers as reference points to track their positions throughout the test. In contrast, the DIC machine utilizes two Dantec wide-angle view cameras, each dedicated to capturing the specimen surface deformation for the longitudinal and transverse directions separately. The DIC system pre-processes the speckle patterns applied to the specimen surface, identifies the grid points, and records their displacements in longitudinal and transverse directions over time. This tracking process is supported by an external software, Is-

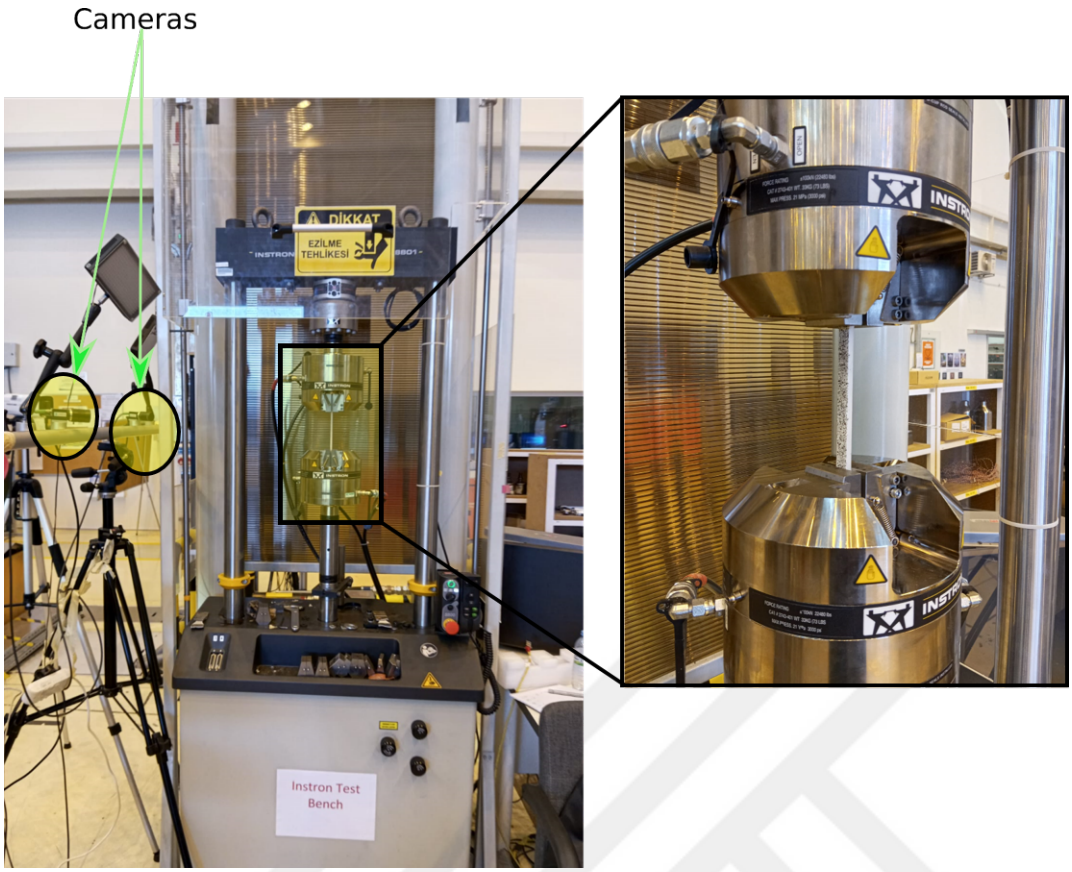

Figure 6.13: DIC Test Setup

tra4D.v4.10, which facilitates the analysis of the captured data. The DIC test setup is shown in Fig. 6.13.

For clarity, the specimen tested in the machine equipped with V-Ext will be referred to as V-Ext, while the specimens tested in the machine equipped with DIC equipment will be denoted as DIC-1, DIC-2, and DIC-3. This notation is adopted to ensure consistency and ease of reference throughout the analysis.

A total of four specimens are tested in the V-Ext and DIC test setup. The V-Ext specimen is subjected to a strain rate of $0.01\ s^{-1}$, while the three DIC specimens are tested at strain rates of $0.01\ s^{-1}$, $0.001\ s^{-1}$, and $0.005\ s^{-1}$, respectively. Table 6.2 provides a detailed summary of these strain rates.

Table 6.2: Strain Rates Used in the Experimental Study

Specimen	**Strain Rate** (s^{-1})
V-Ext	0.01
DIC-1	0.01
DIC-2	0.001
DIC-3	0.005

Regarding data collection, in the V-Ext test, both video sampling and data acquisition occur at intervals of 0.1 s. In contrast, the DIC test machine records load data at the same interval of 0.1 s, but images are captured at a frequency of two frames per second.

The applied stress is calculated using the load data obtained from the load cell for both experiments. In the V-Ext test, strain in both the longitudinal and transverse directions is determined from the displacement data of the gauge marks. In the DIC test, the region of interest for longitudinal and transverse strain measurements is manually selected within the Istra software. The software then computes the strain values along with the associated uncertainties in the calculations.

Using the applied stress and the longitudinal video extensometer data, the parameter estimation study is performed for each specimen as described in Chapter 4. Subsequently, the estimated parameters are substituted back into the constitutive equation, Eq. 3.41, to compute the stress-strain response via an inverse calculation.

Furthermore, an Abaqus model is developed to evaluate the performance of the VO-UMAT code. During the development process, several technical challenges have emerged, which offer valuable lessons and help refine our approach. A comprehensive discussion of the model, along with an in-depth analysis of the encountered challenges, is provided in a dedicated section.

6.2.1 Abaqus Model and VO-UMAT Implementation

For the finite element analysis, the tensile test specimen exhibits pronounced geometrical symmetry, which we exploited to reduce computational costs. Fig. 6.14 illustrates the orthogonal symmetry planes in the half-model of the specimen. Consequently, only one-quarter of the model as depicted in Figure 6.14 is used for mesh generation. The remaining partitions are excluded from the model to ensure an efficient use of computational resources. The controlled displacement and the symmetry boundary conditions are imposed on the reduced model.

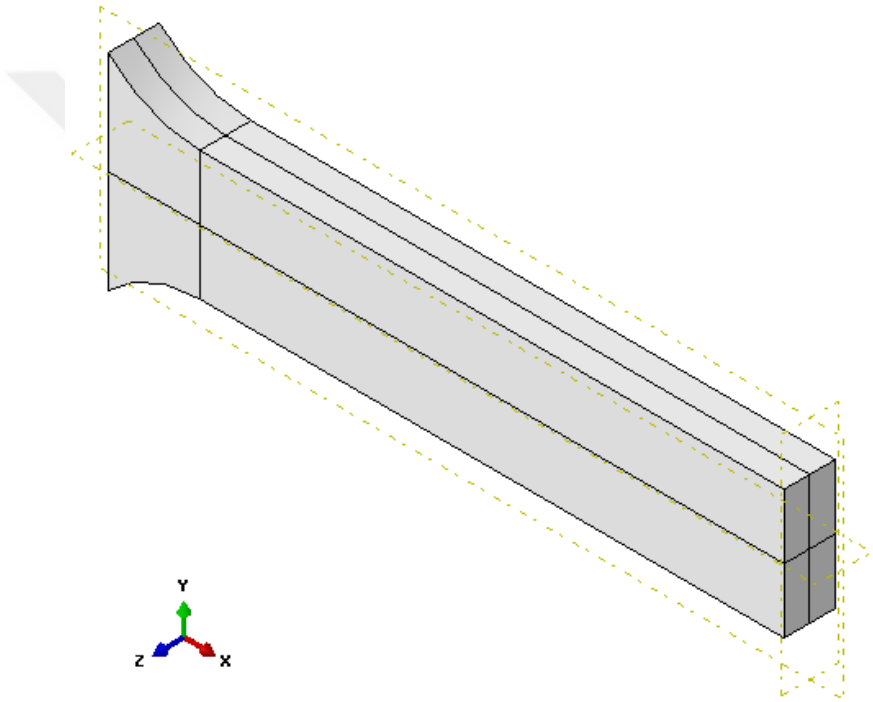

Figure 6.14: Orthogonal Symmetry Planes of the Model

For the mesh structure of the model, we employ cubical elements, namely first-order constant strain elements (C3D8) and second-order linear strain elements (C3D20R), to investigate the impact of element type on the computational results. Fig. 6.15 illustrates an example mesh structure of the analyzed model, along with the mirror image of the elements used to complete the domain in the half model. This approach not only clarifies the element configuration but also ensures that the full domain is accurately represented, thereby enhancing the reliability of the simulation outcomes.

To fully define the problem, symmetry boundary conditions corresponding to the XY, YZ, and XZ symmetry planes are imposed simultaneously on the model. This ensures that the computational domain accurately reflects the inherent symmetries of the problem, thereby simplifying the analysis and reducing computational costs.

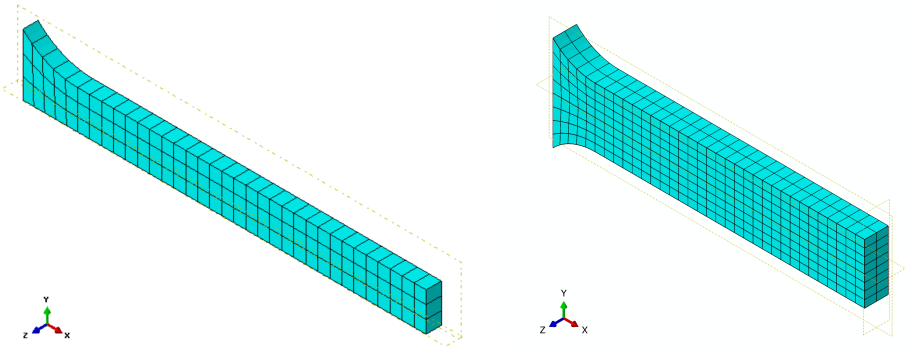

Figure 6.15: Comparison of Mesh Structures: 1/8 Model (Left) versus 1/2 Model (Right)

At this point, we would like to highlight a challenge encountered during the implementation of the VO-UMAT code. Instantaneous bulk and shear modulus terms appear in the VO-UMAT formulation, as shown in Eq. 5.44. Therefore, the instantaneous Poisson's ratio needs to be computed for each data point for the VO-UMAT code.

Instantaneous bulk and shear modulus are computed from the calculated sequence of the Poisson's ratio by extending the relations commonly used in elastic material properties:

$$K(t) = \frac{E_f(t)}{3(1-2\nu(t))} \qquad G(t) = \frac{E_f(t)}{2(1+\nu(t))}. \tag{6.2}$$

Due to uncertainties inherent in non-contact video measurement methods, as well as other experimental uncertainties, the instantaneous Poisson's ratio is computed to exceed its physically plausible limit, especially in the V-Ext test. Consequently, these calculated values are initially set to a constant value of 0.48 to perform the Abaqus VO-UMAT implementation of the V-Ext data. However, abrupt fluctuations in the instantaneous Poisson's ratio led to convergence errors, causing the analysis to terminate prematurely. To overcome this issue, a curve-fitting approach is employed for

the instantaneous Poisson's ratio for V-Ext and DIC specimens, thereby enhancing the stability of the simulation. The experimentally computed Poisson's ratio is fitted to a power function of time. In addressing the convergence problem, the motivation for fitting Poisson's ratio to a power function stems from the constitutive model we initially assumed. Since this model exhibits a strong dependence on a power function of time and the calculated Poisson's ratio follows a similar trend, we adopt a power function of time for Poisson's ratio. For each experimental time data point, the Poisson's ratio entered into the VO-UMAT model is recalculated.

Subsequently, the fitted values are manually entered into the designated section of the VO-UMAT code (see Appendix-A), where they are used to calculate the instantaneous bulk and shear moduli. This approach overcome the stability problems.

After addressing these issues and incorporating the definition of the instantaneous Poisson's ratio within the VO-UMAT code, we proceed to evaluate the mesh dependence of the model. This analysis is performed to ensure that the numerical results are robust and not unduly influenced by the finite element discretization.

A mesh convergence study is performed to assess the mesh sensitivity of the problem by systematically refining the mesh. The characteristic element size is gradually reduced from 5 mm to 0.5 mm, and the impact on the analysis results is summarized in Table 6.3. For post-processing purposes, the node corresponding to the centroidal node of the full model is selected. Table 6.3 summarizes the element sizes, number of elements, computed axial stress at the centroidal node, and computational time.

Table 6.3: Comparison of Element Types and Sizes in the VO-UMAT Analyses

Element Type	**Element Size (mm)**	**No. of Elements**	σ_{11}**(MPa)**	**CPU Time (s)**
C3D20R	5	13	25.33	0.3
	4	34	25.50	1.6
	3	44	25.97	2.0
	2	136	26.27	4.2
	1	1407	26.50	40.0
	0.5	9380	26.53	383.3
C3D8	5	13	23.60	0.7
	4	34	23.70	0.9
	3	44	24.10	1.1
	2	136	24.60	1.2
	1	1407	25.36	6.6
	0.5	9380	25.49	48.4

The characteristic element size and the convergence of the axial stress result, σ_{11}, are plotted as a function of CPU time in Fig. 6.16. The mesh convergence test is conducted using the test parameters of the DIC-2 test. As a reference, the axial stress measured in the DIC-2 test at a strain level of 0.08 is 27.29 MPa. The difference between the measured and stress calculated by VO-UMAT using C3D20R elements of size 0.5 mm is 0.76 MPa.

In addition, Fig. 6.17 presents a comparison based on the number of elements used in the analysis.

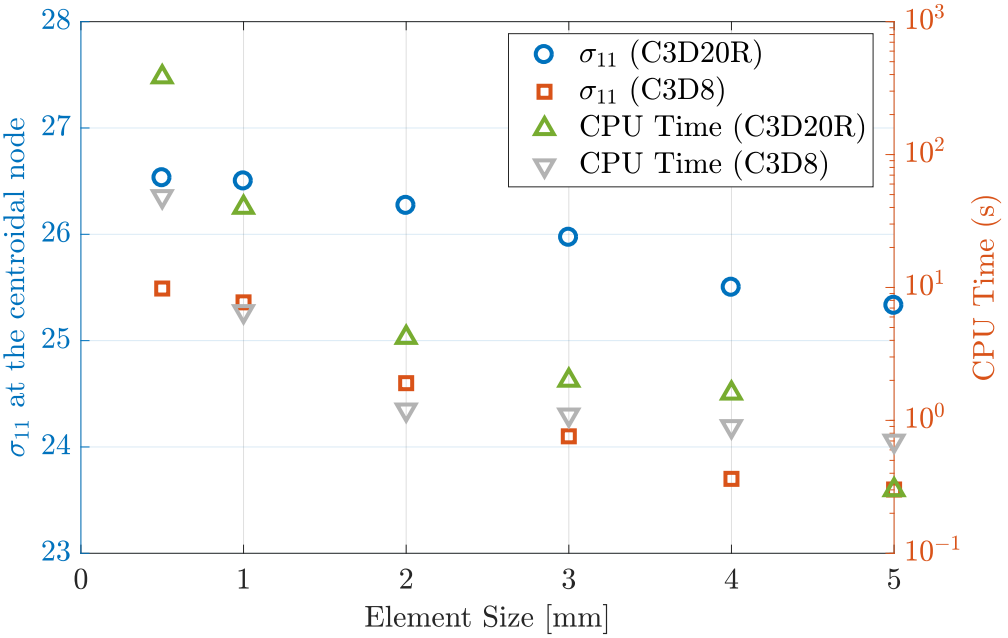

Figure 6.16: Mesh Convergence Study by Element Size

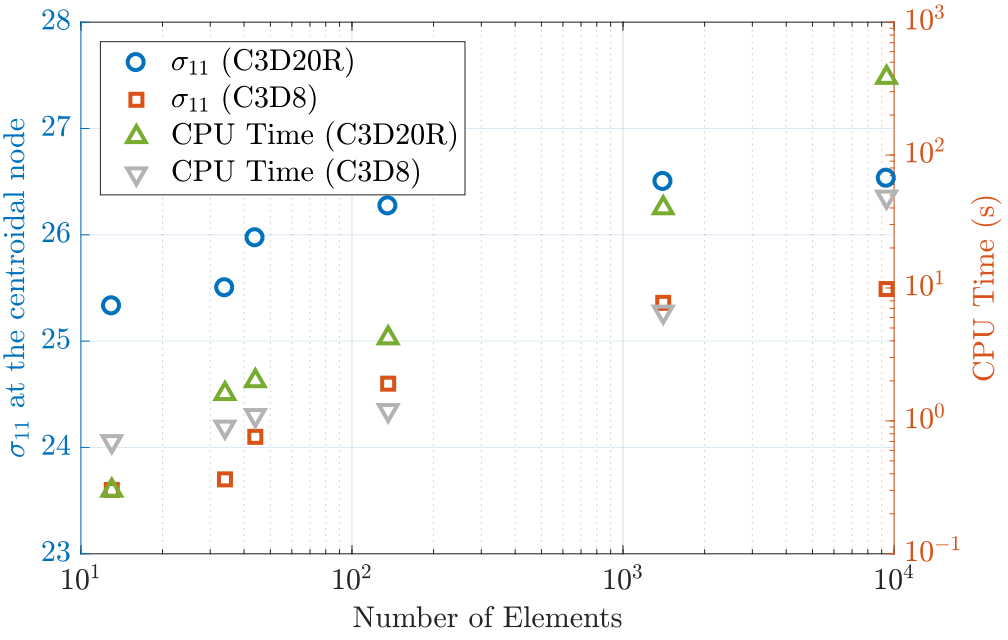

Figure 6.17: Mesh Convergence Study by the Number of Elements

It is evident from these figures that reducing the element size beyond 1 mm does not result in a significant change in the calculated stress, but it does lead to a dramatic increase in computational effort. This trend is observed for both element types, C3D8 and C3D20R.

Moreover, the mesh convergence study indicates that the C3D8 elements tend to produce slightly less stress. C3D20R elements yield results that more closely approximate the experimental data.

A typical result is presented in Fig. 6.18. In the figure, both deformed and undeformed configurations of the reduced model are illustrated. A uniform stress distribution is clearly observed around the gauge zone of the specimen.

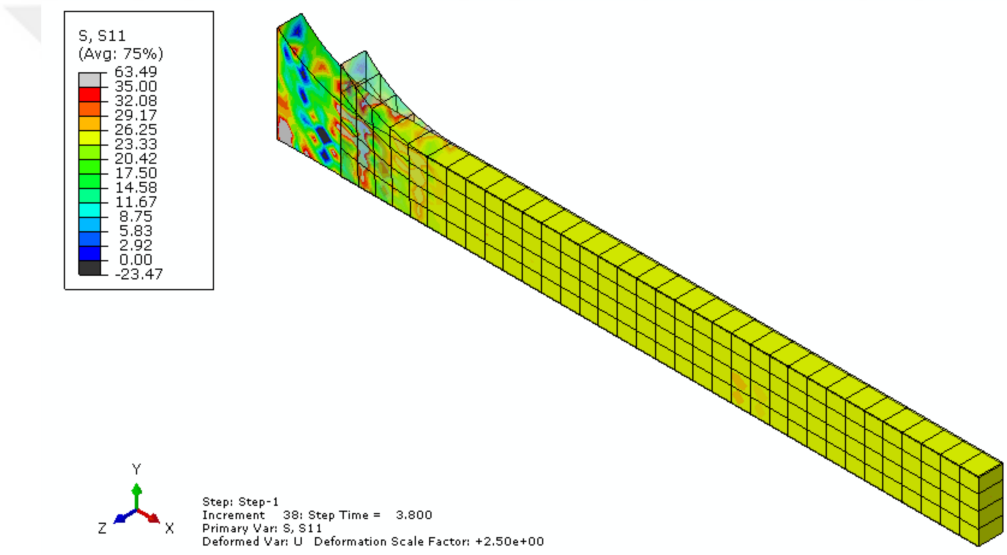

Figure 6.18: Stress Distribution on the Reduced Model

6.2.2 Comparison of Analytical, UMAT, and Experimental Results

For all test cases, the stress-strain responses obtained from the machine travel data, as well as from either the video extensometer or digital image correlation results, are plotted in Figs. 6.19, 6.25, 6.28, and 6.32. For improved visualization, absolute values are used when plotting the transverse strain in all test cases. Similarly, V-Ext and DIC test data are presented in Figs. 6.20, 6.26, 6.29, and 6.33, respectively.

The stress-strain response of the V-Ext test is plotted in Fig. 6.19. The strain in the longitudinal and the transverse directions are plotted in Fig. 6.20.

Among the four tests, the least noise in the calculated Poisson's ratio is observed in the V-Ext data. However, during the early stages of the V-Ext test, the computed Poisson's ratio exhibits physically implausible values. As the test progresses, the Poisson's ratio values stabilize and follow a power-law decay trend. Fig. 6.22 shows the correlation between the video extensometer data, model fit calculation, and VO-UMAT calculation. At the onset of loading, a deviation is observed between the model fit and the VO-UMAT calculations compared to the extensometer data. This discrepancy may be attributed to initial measurement uncertainty, Poisson's ratio estimation, or transient effects in the material response. In higher strains, VO-UMAT overshoots the video extensometer data.

The maximum stress error between the video extensometer data and the VO-UMAT result is approximately 1.35 MPa. The variable fractional orders exhibit a linear elastic response at the onset of deformation. At higher strain levels, small deviations from the general trend become clearly noticeable, as illustrated in Fig. 6.22.

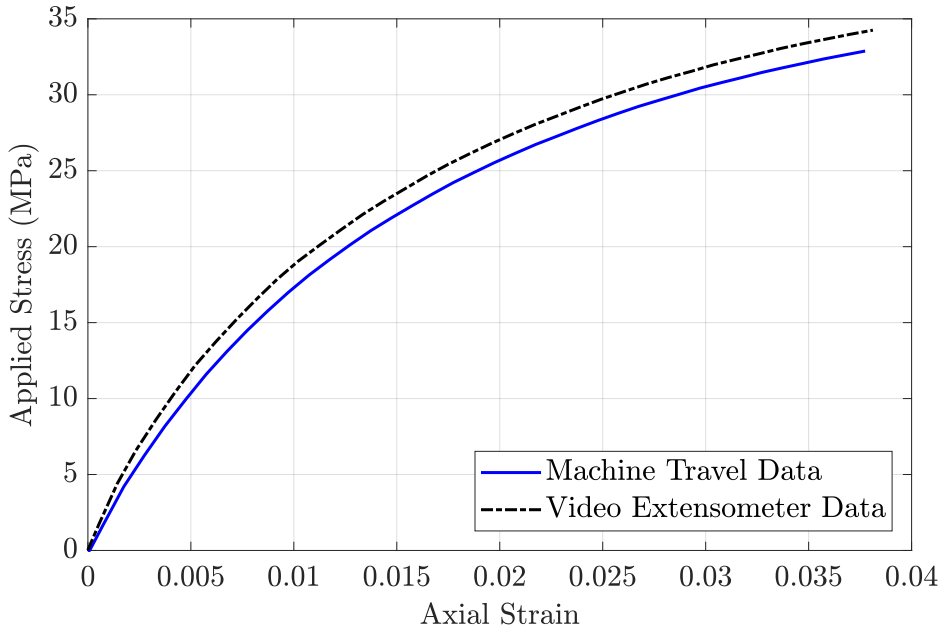

Figure 6.19: V-Ext Test Stress-Strain Response

The applied stress is determined by dividing the instantaneous load by the initial cross-sectional area of the specimen. The axial strain is computed either from the crosshead displacement or from the displacement of gauge points along the load axis, as recorded by a video extensometer. Fig. 6.19 demonstrates that the strain measured using the V-Ext method is consistently higher than the strain calculated from the machine travel data. This discrepancy is commonly observed in the experimental studies that employ an extensometer.

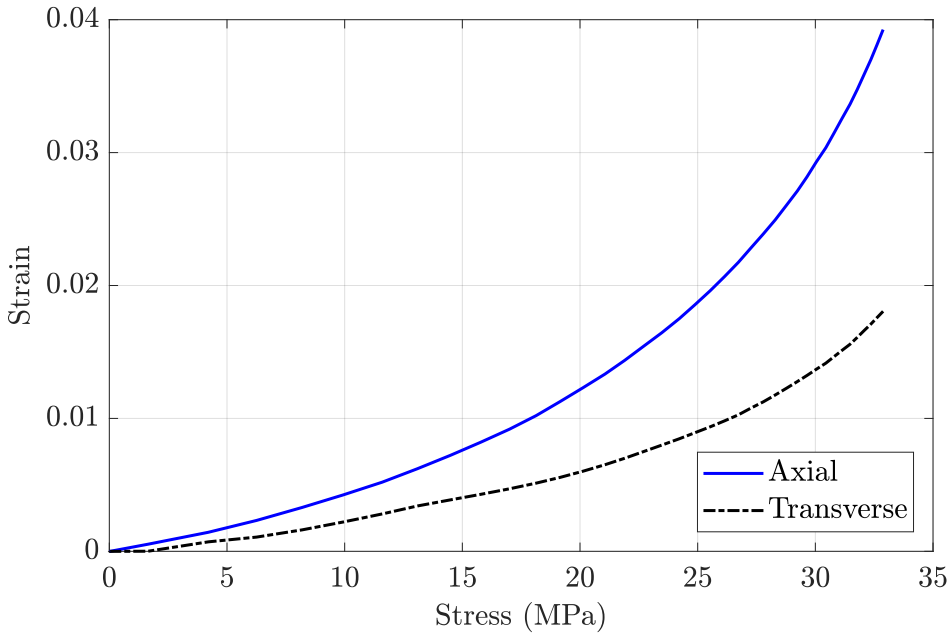

Figure 6.20: V-Ext Test Longitudinal Strain vs Transverse Strain

The longitudinal and transverse strain values are calculated from the corresponding displacement results measured by video extensometer. Fig. 6.20 presents the absolute value of the transverse strain for better demonstration purposes. The slope of the transverse strain does not correspond to the general trend observed in the longitudinal strain at the onset of loading. It becomes more evident when the Poisson's ratio is calculated using the strains derived from the video extensometer data. The computed values of Poisson's ratio up to 1.2 s exceed 0.5, which suggests the presence of measurement errors in the video extensometer data. However, after approximately 1 s from the start of the test, a consistent trend in Poisson's ratio is observed as shown

in Fig. 6.21. However, the uncertainty in the measurements in the longitudinal and transverse directions could not be evaluated in the video extensometer test setup.

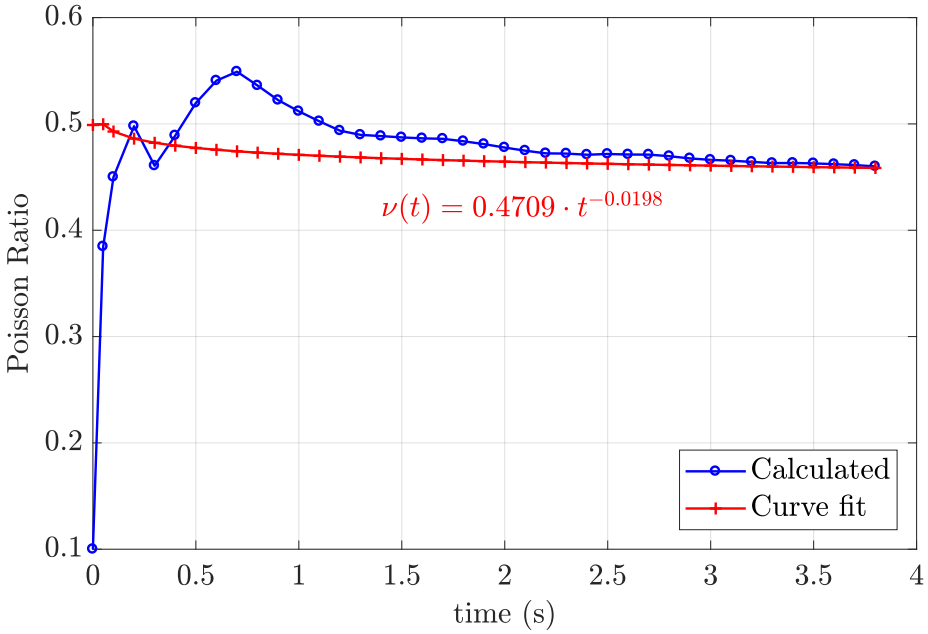

Figure 6.21: V-Ext Test Poisson's Ratio

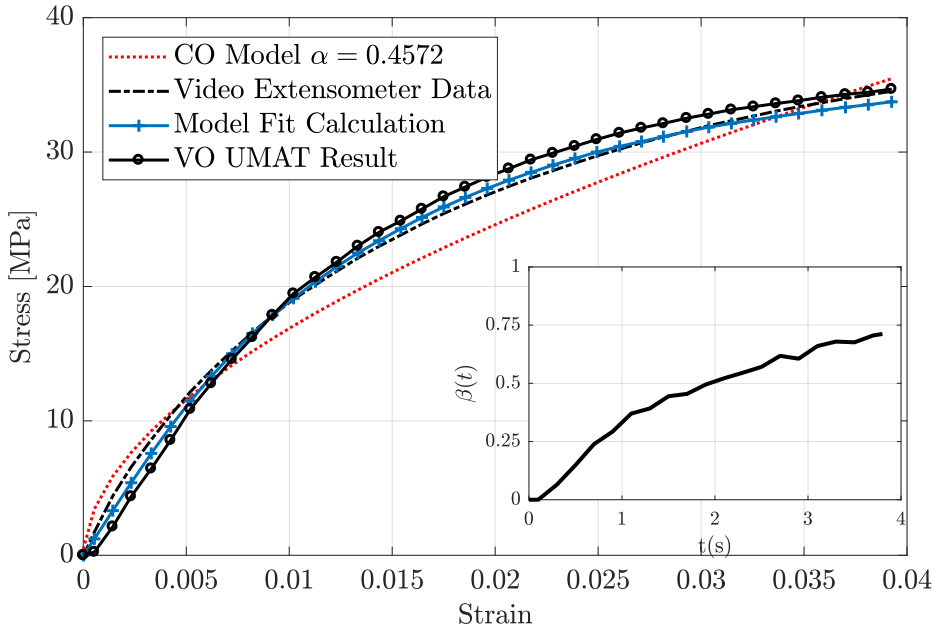

Figure 6.22: V-Ext Test, Stress-Strain Responses Comparison Study

Unlike the V-Ext data, the DIC method also provided strain uncertainty in longitudinal and transverse directions. For the DIC-1 test the strain uncertainty in the transverse direction is around 1300 $\mu\varepsilon$, and stabilized during the course of the test. In the longitudinal direction data uncertainty drops to around 500 $\mu\varepsilon$, and seems to approach 600 $\mu\varepsilon$ as the test advances. The strain uncertainty is calculated by Istra software as shown in Fig. 6.23.

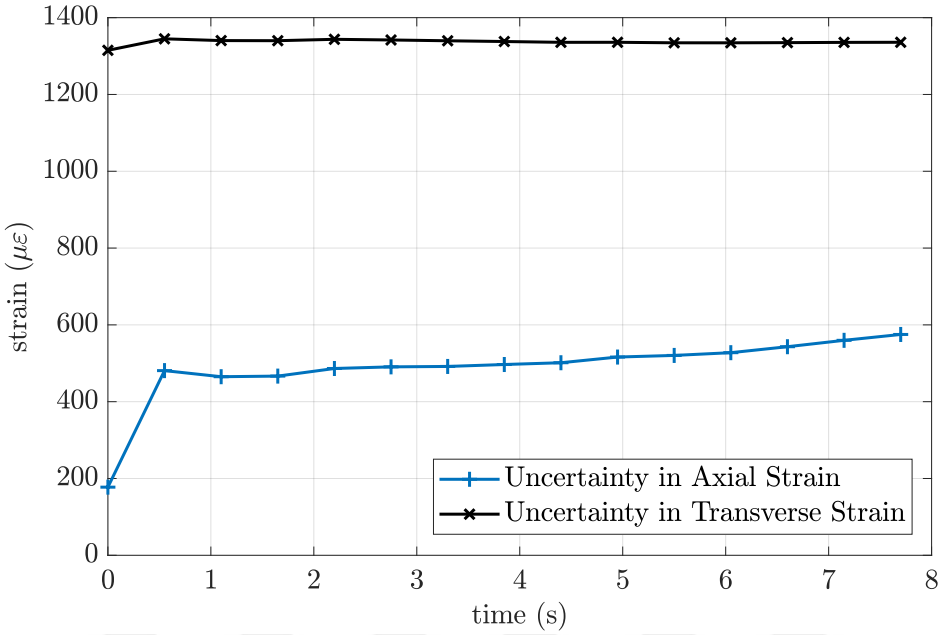

Figure 6.23: DIC-1 Test Strain Uncertainty

The DIC method estimates the Poisson's ratio with noticeable noise, as seen in Fig. 6.24, but all values remain within a physically reasonable range. A power-law decay curve fit is applied to the calculated Poisson's ratio. As mentioned earlier, the fitted values are then used as input for the VO-UMAT model to enhance the stability and accuracy of the numerical simulations.

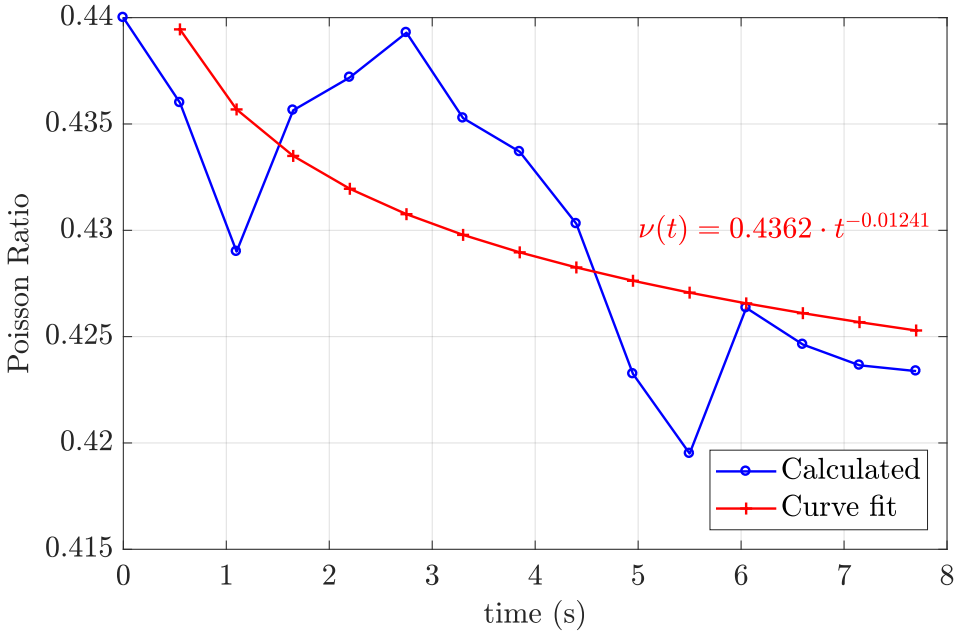

Figure 6.24: DIC-1 Test Poisson's Ratio

The maximum stress error between the DIC-1 data and the VO-UMAT result is found approximately 1.13 MPa from Fig. 6.27.

Although the strain rates applied to the V-Ext and DIC-1 specimens are the same, Figs. 6.19 and 6.25 clearly reveal a deviation in the stress responses between the DIC-1 and V-Ext tests. Notably, the V-Ext specimen exhibits a stiffer behavior. This discrepancy can be attributed to a violation of the prescribed thermal conditioning protocol as per ASTM. The V-Ext specimen is not allowed to stay long enough in the laboratory environment before testing but is immediately subjected to the test after staying in the cold environment prior to the test. This observation underscores the significant impact that proper thermal conditioning has on the test results.

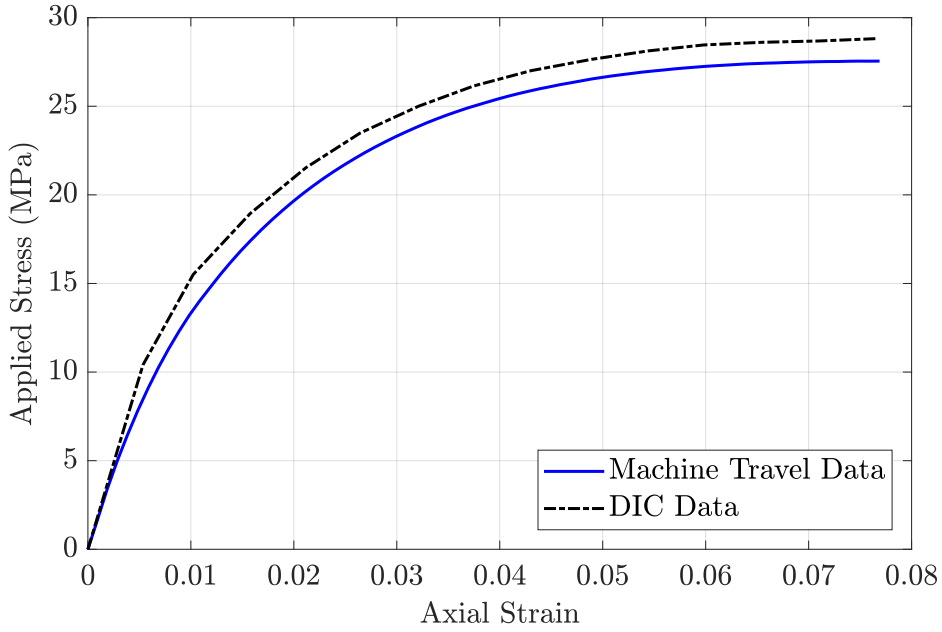

Figure 6.25: DIC-1 Test Stress-Strain Response

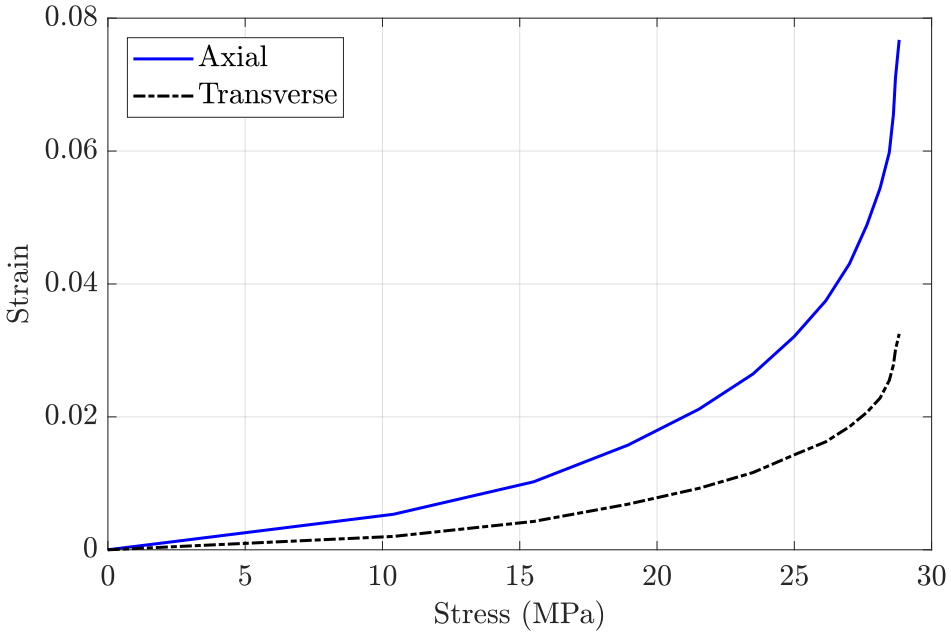

Figure 6.26: DIC1 Test Longitudinal Strain vs Transverse Strain

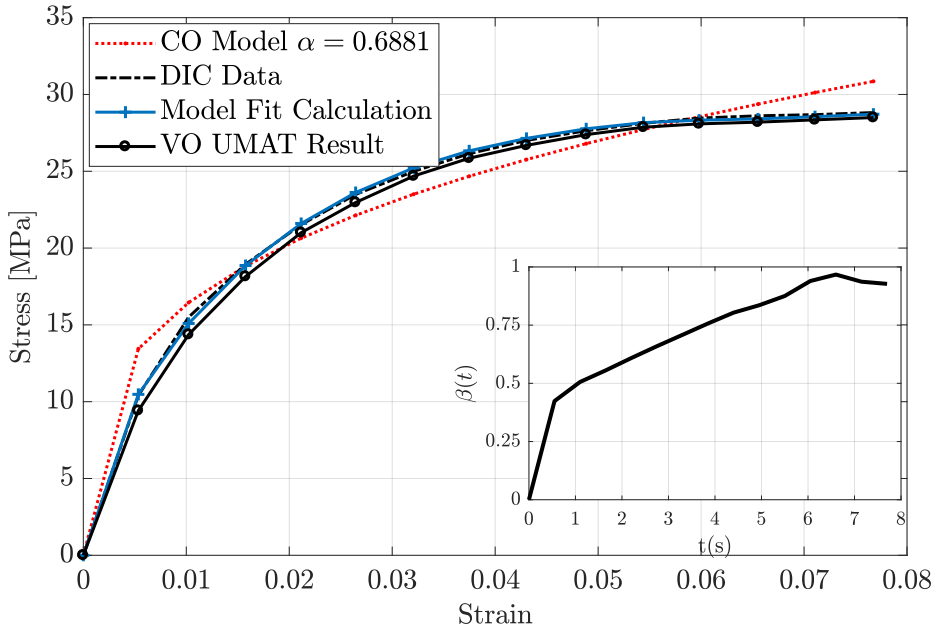

Figure 6.27: DIC-1 Test, Stress-Strain Responses Comparison Study

Although the stress-strain plot in Fig. 6.28 and the longitudinal-transverse strain plots do not show any noisy trend as shown in Fig. 6.29, a high experimental noise measured in the calculated Poisson's ratio.

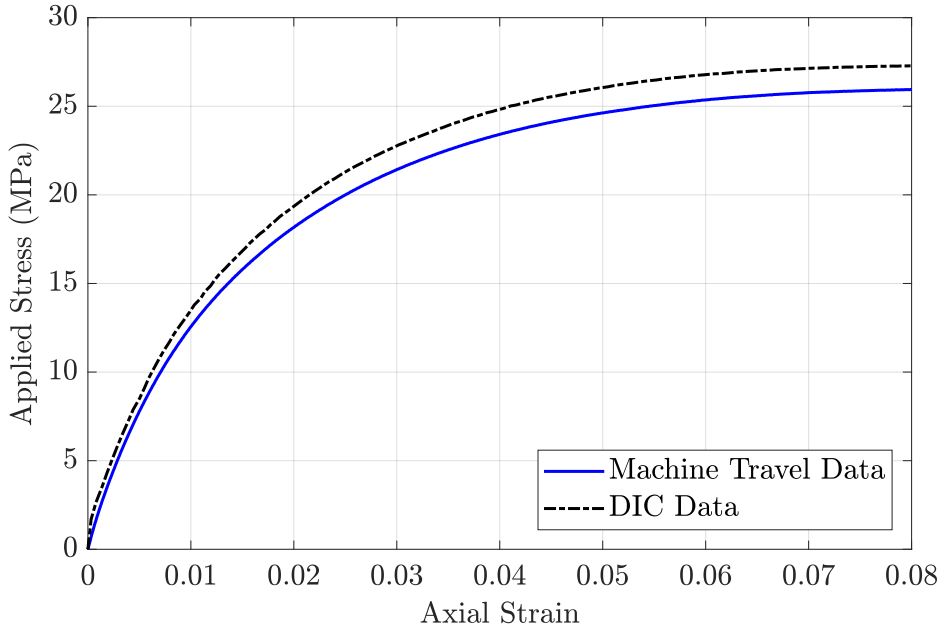

Figure 6.28: DIC-2 Test Stress-Strain Response

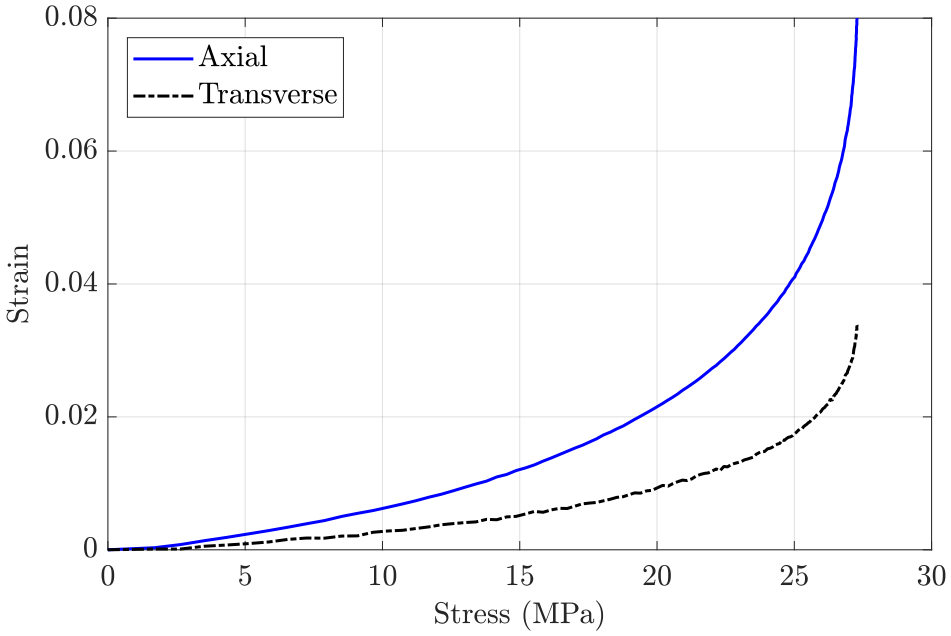

Figure 6.29: DIC-2 Test Longitudinal Strain vs Transverse Strain

In contrast to the other tests, the first several data points of the DIC-2 test exhibit a significantly noisy behavior in the calculated Poisson's ratio. Nevertheless, the overall trend is consistent with a power-law decay function. The maximum stress error between the DIC data and the VO-UMAT result is found less than 1.0 MPa from Fig. 6.31

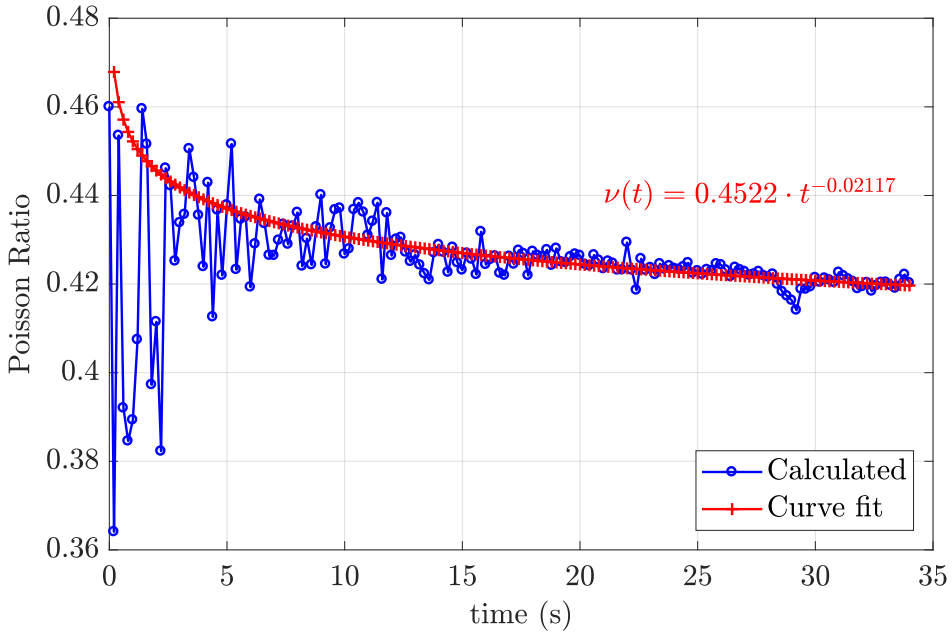

Figure 6.30: DIC-2 Test Poisson's Ratio

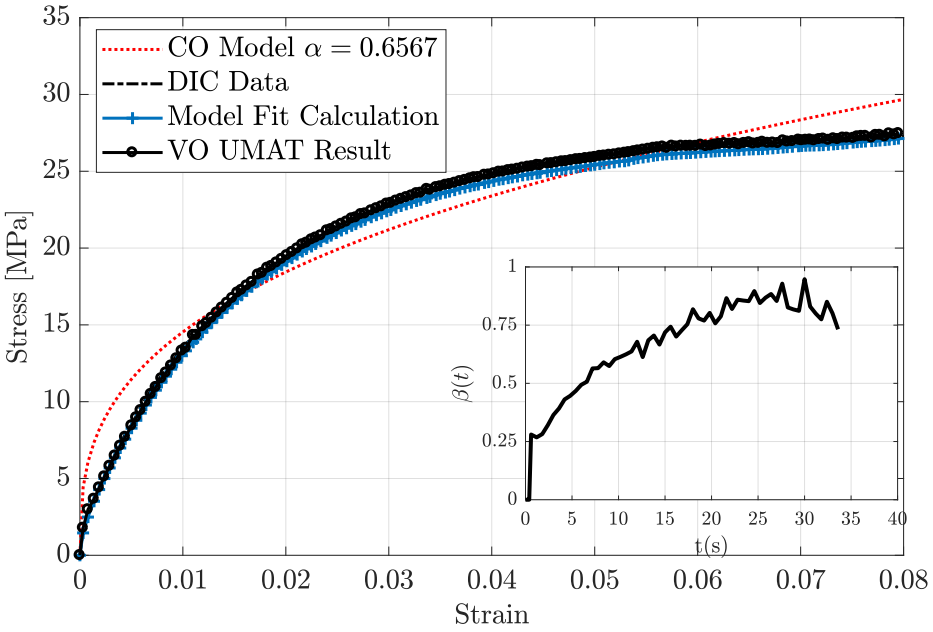

Figure 6.31: DIC-2 Test, Stress-Strain Responses Comparison Study

The stress-strain response derived from the DIC-3 data deviates from both the VO-UMAT result and the model estimate at the early stages of the test. This discrepancy is potentially attributable to the use of the approximated Poisson's ratio value. The fractional order estimated by the model contains less noisy data as shown in Fig. 6.35 compared to the DIC-2 test, in Fig. 6.31.

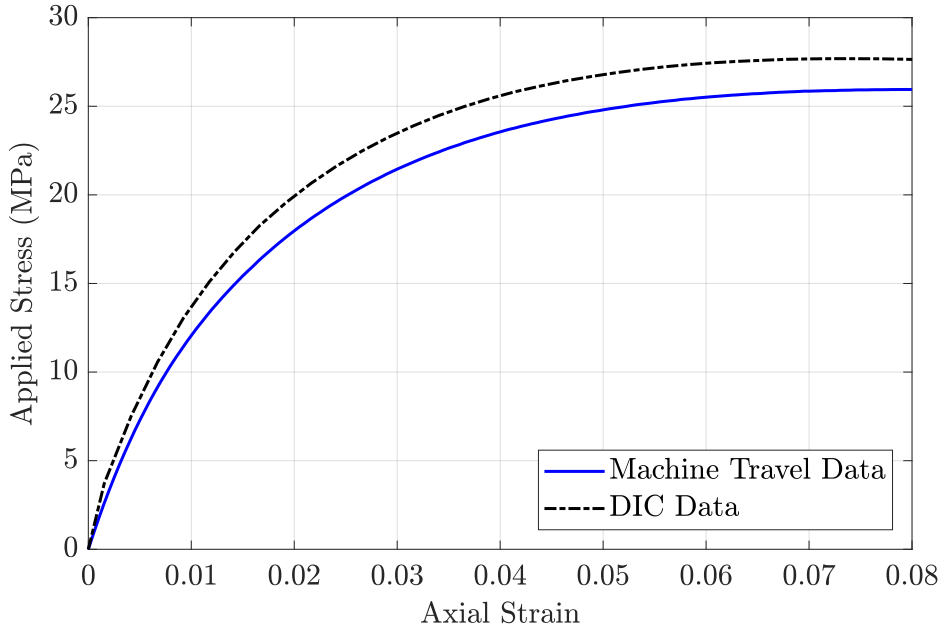

Figure 6.32: DIC-3 Test Stress-Strain Response

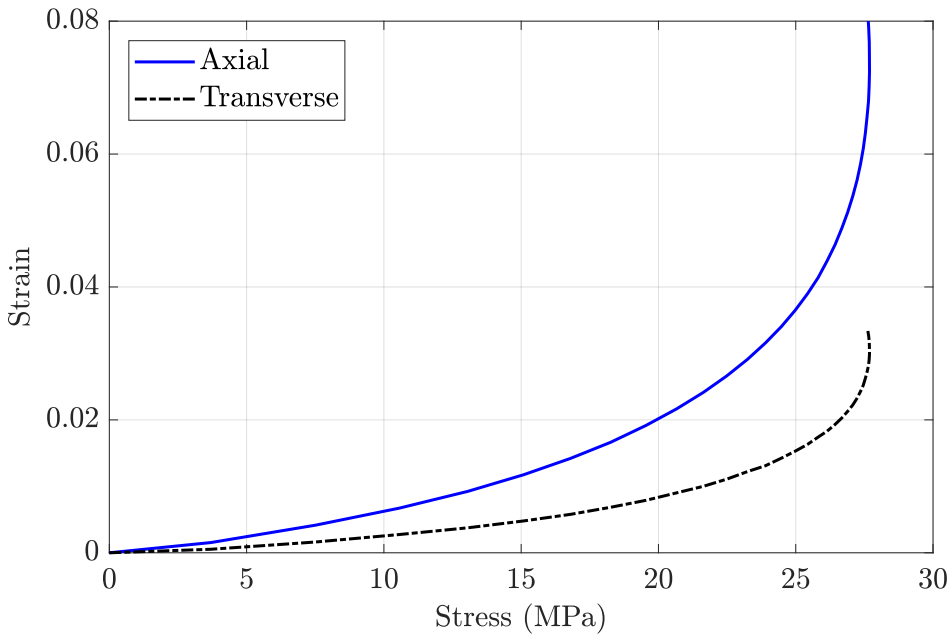

Figure 6.33: DIC3 Test Longitudinal Strain vs Transverse Strain

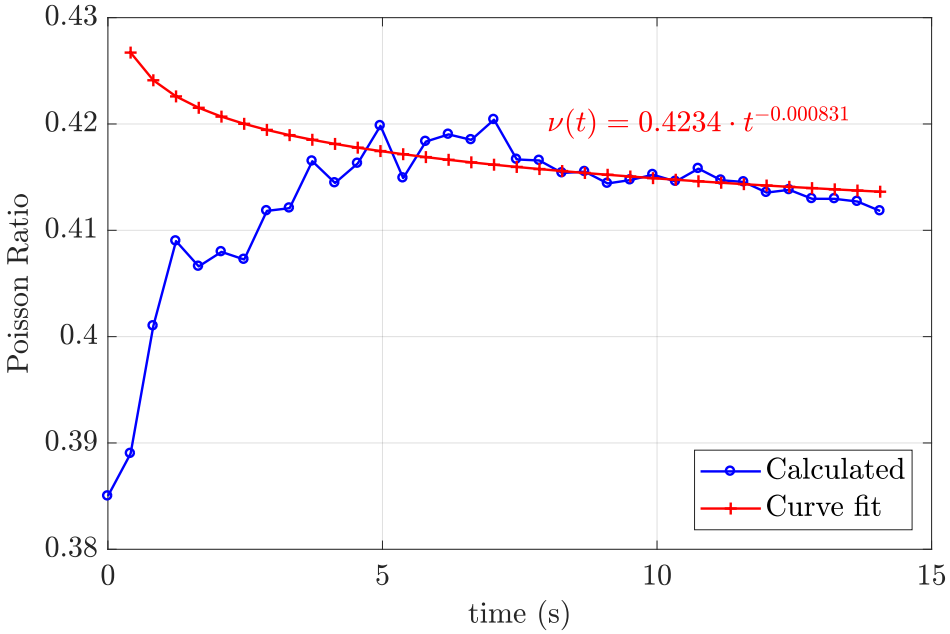

Figure 6.34: DIC-3 Test Poisson's Ratio

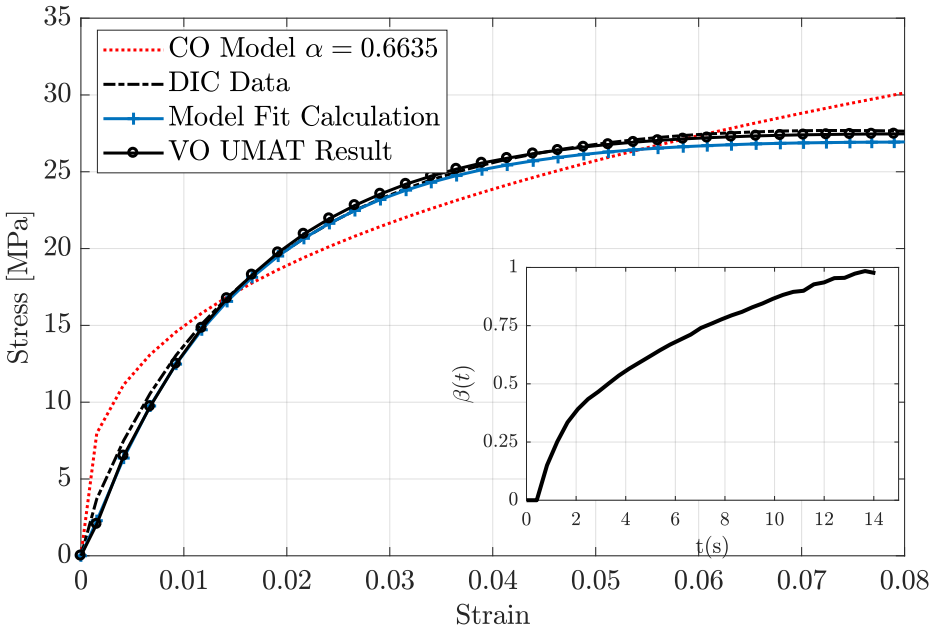

Figure 6.35: DIC-3 Test, Stress-Strain Responses Comparison Study

For comparison purposes, stress-strain data obtained from both the V-Ext and DIC tests are employed to determine the material parameters when modeled using the constant fractional order viscoelastic Scott-Blair's spring-pot (COFSB) model. In reference to the analytical approach we have already derived in Eq. 4.6, for determining the stress response of the material under constant strain rate loading, the stress-strain data from each test are utilized to derive the material parameters. To achieve this, the stress-strain data are fitted to Eq. 4.6 using the least-squares method in conjunction with the Levenberg-Marquardt algorithm, facilitating the determination of the fractional characteristic number, E_f, and the constant fractional order, α. Figures 6.22, 6.27, 6.31, and 6.35 show the performance of constant order compared to variable order modeling the viscoelastic behavior.

By analyzing Figs. 6.22, 6.27, 6.31, and 6.35, it is evident that the COFSB model estimates exhibit a significant estimation error in comparison to the variable-order viscoelastic model. Model comparison studies further indicate that the relative error between the CO model and the VO model reflects the divergence behavior as deformation progresses. Additionally, the CO model exhibits a stiffer response at the initial stages of deformation, leading to a higher relative error.

As a concluding remark for this section, the VO-UMAT model shows a strong correlation with the experimental data. Also, the variable-order fractional viscoelastic model is superior to the constant fractional viscoelastic model. Furthermore, using the curve-fit values for the Poisson's ratio at each increment did not lead to significant deviations from the experimental measurements.

CHAPTER 7

CONCLUSIONS AND DISCUSSIONS

The studies presented in this thesis primarily focus on two specific aspects that represent original contributions to the field of fractional viscoelasticity:

- Variable order fractional spring-pot model parameter estimation studies,
- User material subroutine code in Abaqus for the variable order fractional spring-pot model.

Initially, we have approached the parameter estimation problem by seeking an analytical method of determination of the fractional order sequence. However, the parameter estimation studies conducted with the analytical tools have not consistently provided a reliable solution under the specified loading conditions. Given the ambiguity regarding whether the fractional order is dependent on strain rate for particular viscoelastic materials, it is essential to determine the sequence of the fractional variable order under just one constant strain rate deformation. Nevertheless, some researchers [77, 113] suggest that the fractional order may not be entirely independent of strain rate, which limits the available mathematical tools for determining the fractional order sequence. Alternative to determining the fractional order sequence analytically, we have proposed using an approach of combined use of least squares curve fitting and nonlinear constrained optimization to determine the elastic constant, viscous constant, and the sequence of the fractional order.

The effectiveness of the VO model is demonstrated through a comparison with the CO model estimates. The superiority of the VO fractional viscoelastic model is highlighted in the comparative study of the V-Ext and DIC test methods in Chapter 6.

Although our proposed method effectively estimates the fractional order sequence, its validity is limited to constant rate deformations. Employing a constant rate of deformation is indeed the most convenient approach for determining material parameters experimentally, but extending this method to parameter estimation under stress relaxation and creep behavior would necessitate complex formulations and its experimental validation would require specialized experimental setups. For instance, to study stress relaxation in a variable order fractional viscoelastic model, the specimen would need to be subjected to a constant strain, which implies that temperature variations during stress relaxation would be necessary due to the absence of strain dependence in such cases. This type of experiment would require a uniaxial tension test with specific tooling in a thermal chamber. For this reason, we have identified these scenarios as potential areas for further research and excluded them from the scope of this work. An extensive experimental campaign could be beneficial for a complete description of the fractional viscoelastic behavior.

The studies on the constant order parameter estimation using synthetic test data reveal that the incorporation of Grünwald constants hinders the estimation of the fractional orders instantly. A convergence period is always required for the solution. When there is a sudden change in the fractional order, the model cannot adapt well, resulting in errors near the points of fractional order change. Additionally, for harmonic variations in fractional order, the error is slightly higher compared to models with linearly changing orders.

Studying with real experimental data revealed us hardening and softening behavior of the material can be well estimated by the variable order fractional spring-pot element. The inverse calculation of the stress response, derived from the applied strain history, demonstrates a remarkable agreement with the empirical data. This correspondence not only validates the accuracy of our inverse analysis methodology but also reinforces the reliability of the stress-strain model we have employed. The strong alignment between the predicted stress responses and the actual measurements underscores the effectiveness of our approach and enhances the credibility of our results. Such consistency provides a solid foundation for future research and applications in this domain.

One of the significant contributions of this study is the development of user material subroutine codes. These two subroutines are developed for both constant fractional order and variable fractional order spring-pot models. Their formulations are detailed in Chapter 5. The VO-UMAT formulation and its associated code represent the most comprehensive form of fractional viscoelasticity, encompassing the full spectrum of fractional viscoelastic behaviors, including both purely elastic and pure viscous responses. The VO-UMAT subroutine code provided in Appendix A effectively captures both constant and variable fractional order behaviors. The results from both the approximate solution and the Abaqus analysis, incorporating the VO-UMAT model, show a high degree of agreement, further validating the reliability and accuracy of the formulation developed for the VO-UMAT subroutine. Such consistency between different analytical approaches to variable order patterns reinforces the credibility of our findings and provides a strong foundation for further investigation in this area.

The volumetric behavior of PE300 is closely approximated by the VO-UMAT model, even when the Poisson's ratio values are replaced by the curve-fit values. Experimental studies have demonstrated that the Poisson's ratio is not constant over time. In particular, if both the bulk and shear moduli are defined using the same fractional order, the Poisson's ratio would either remain constant or vary linearly with time. This behavior becomes evident upon recalling Eq. 5.4:

$$K_R(t) = \frac{K_{\beta(t)} t^{-\beta(t)}}{\Gamma(1-\beta(t))} \quad , \quad G_R(t) = \frac{G_{\alpha(t)} t^{-\alpha(t)}}{\Gamma(1-\alpha(t))}.$$

The observed trend in the Poisson ratio suggests that the definition of the fractional order for shear and bulk terms should be distinct. Previously, we have assumed that $\beta(t) = \alpha(t)$. However, despite the noise in the calculated Poisson's ratio and the inherent uncertainty in the data, the overall trend indicates that defining two separate fractional orders would better align with the experimental results. These distinct fractional orders should independently govern the bulk and shear moduli, ultimately yielding the experimentally observed power-law behavior of Poisson's ratio.

When the definitions of the bulk and shear moduli (given in Eq. 6.2) are substituted into Eq. 7.1 under the assumption of a common fractional order, the terms containing the fractional order becomes a common factor, therefore, will cancel each other out.

$$\nu(t) = \frac{3K(t) - 2G(t)}{2(3K(t) + G(t))} \tag{7.1}$$

As a result, Poisson's ratio loses its dependence on the fractional order. However, the Poisson's ratio estimated in this study exhibits a strong correlation with time, indicating that it retains significant time-dependent terms.

This finding indirectly points to the necessity of employing distinct fractional orders for the bulk and shear moduli in order to accurately capture the material behavior.

7.1 Future Directions

The studies presented in this work offer a novel perspective on the parameter estimation method of fractional viscoelastic modeling of materials. The parameter estimation method proposed in this study can be further developed by systematically evaluating the discrepancy between the estimated and measured stress responses at each time step. Incorporating a correction loop into the estimation process can help reduce this discrepancy by allowing for real-time adjustments to the estimated fractional order. This iterative approach aims to minimize the error and enhance the accuracy of the parameter estimation.

As discussed in the text, using a constant strain rate deformation is likely the most convenient method for parameter estimation. However, a more comprehensive approach is required to address a wider range of loading conditions. Our methodology is valid only for the constant rate of deformation case. A convenient parameter estimation method could be developed to address arbitrary or random loading conditions.

Moreover, alternative parameter estimation methods have been explored, but could not be fully addressed in this research. Further research is required to advance the development of potential parameter estimation methods. Additionally, while not covered in the current study, random variations in the fractional order due to external or internal factors represent another important area for future research. A dedicated investigation is needed to examine how randomness on the fractional order influences material response and its parameter estimation study.

The proposed parameter estimation method shows promise for real-time application, suggesting its potential utility in in-situ scenarios.

Our primary hypothesis states that the mechanical response of a viscoelastic material could be effectively captured using the variable-order fractional spring-pot model. The developed user material subroutine for the Abaqus model is readily extendable to more complex variable-order fractional viscoelastic models, such as the variable-order fractional Kelvin-Voigt model or the variable-order Maxwell model.

REFERENCES

[1] W. Smit and H. de Vries, "Rheological models containing fractional derivatives," *Rheologica Acta*, vol. 9, no. 4, pp. 525–534, 1970.

[2] S. Müller, M. Kästner, J. Brummund, and V. Ulbricht, "A nonlinear fractional viscoelastic material model for polymers," *Computational Materials Science*, vol. 50, no. 10, pp. 2938–2949, 2011.

[3] D. Lei, Y. Liang, and R. Xiao, "A fractional model with parallel fractional Maxwell elements for amorphous thermoplastics," *Physica A: Statistical Mechanics and its Applications*, vol. 490, pp. 465–475, Jan. 2018.

[4] C. Fang, X. Shen, K. He, C. Yin, S. Li, X. Chen, and H. Sun, "Application of fractional calculus methods to viscoelastic behaviours of solid propellants," *Philosophical Transactions of the Royal Society A: Mathematical, Physical and Engineering Sciences*, vol. 378, no. 2172, p. 20190291, 2020.

[5] S. S. Tabatabaei, H. Talebi, and M. Tavakoli, "A novel adaptive order/parameter identification method for variable order systems application in viscoelastic soft tissue modeling," *Chaos, Solitons & Fractals*, vol. 102, pp. 447–455, Sept. 2017.

[6] M. Hossain, R. Navaratne, and D. Perić, "3D printed elastomeric polyurethane: Viscoelastic experimental characterizations and constitutive modelling with nonlinear viscosity functions," *International Journal of Non-Linear Mechanics*, vol. 126, p. 103546, Nov. 2020.

[7] "Abaqus/CAE User's Manual," 2016.

[8] R. M. Christensen, *Theory of Viscoelasticity: An Introduction*. New York: Academic Press, 2nd ed ed., 1982.

[9] W. Flügge, *Viscoelasticity*. Berlin, Heidelberg: Springer-Verlag Berlin Heidelberg GmbH, 2nd ed., 1975.

[10] C. Zener, "Anelasticity of metals," *Del Nuovo Cimento*, vol. 7, no. 10, p. 25, 1958.

[11] F. Mainardi and G. Spada, "Creep, relaxation and viscosity properties for basic fractional models in rheology," *The European Physical Journal Special Topics*, vol. 193, no. 1, pp. 133–160, 2011.

[12] H. Schiessel and A. Blumen, "Hierarchical analogues to fractional relaxation equations," *Journal of Physics A: Mathematical and General*, vol. 26, no. 19, pp. 5057–5069, 1993.

[13] D. G. Fesko and N. W. Tschoegl, "Time-temperature superposition in thermorheologically complex materials," *Journal of Polymer Science Part C: Polymer Symposia*, vol. 35, no. 1, pp. 51–69, 2007.

[14] N. Demirci, "Formulation and implementation of a fractional order viscoelastic material model into finite element software and material model parameter identification using in-vivo indenter experiments for soft biological tissues," Master's thesis, Middle East Technical University, 2012.

[15] M. Sasso, G. Palmieri, and D. Amodio, "Application of fractional derivative models in linear viscoelastic problems," *Mechanics of Time-Dependent Materials*, vol. 15, no. 4, pp. 367–387, 2011.

[16] P. Nutting, "A new general law of deformation," *Journal of the Franklin Institute*, vol. 191, pp. 679–685, 1920.

[17] J. H. Snoeijer, A. Pandey, M. A. Herrada, and J. Eggers, "The relationship between viscoelasticity and elasticity," *Proceedings of the Royal Society A: Mathematical, Physical and Engineering Sciences*, vol. 476, p. 20200419, Nov. 2020.

[18] J. Long, R. Xiao, and W. Chen, "Fractional viscoelastic models with non-singular kernels," *Mechanics of Materials*, vol. 127, pp. 55–64, Dec. 2018.

[19] R. C. Koeller, "Applications of fractional calculus to the theory of viscoelasticity," *Journal of Applied Mechanics*, vol. 51, no. 2, pp. 299–307, 1984.

[20] M. Caputo and M. Fabrizio, "Applications of New Time and Spatial Fractional Derivatives with Exponential Kernels," *Progress in Fractional Differentiation and Applications*, vol. 2, pp. 1–11, Jan. 2016.

[21] W. N. Findley, J. S. Lai, and K. Onaran, *Creep and Relaxation of Nonlinear Viscoelastic Materials, with an Introduction to Linear Viscoelasticity*. North-Holland Series in Applied Mathematics and Mechanics v. 18, Amsterdam ; New York: North-Holland Pub. Co. : sole distributors for the U.S.A. and Canada, Elsevier/North Holland, 1976.

[22] M. Di Paola, R. Heuer, and A. Pirrotta, "Fractional visco-elastic Euler–Bernoulli beam," *International Journal of Solids and Structures*, vol. 50, pp. 3505–3510, Oct. 2013.

[23] M. Di Paola, A. Pirrotta, and A. Valenza, "Visco-elastic behavior through fractional calculus: An easier method for best fitting experimental results," *Mechanics of Materials*, vol. 43, no. 12, pp. 799–806, 2011.

[24] A. Gemant, "A method of analyzing experimental results obtained from elasto-viscous bodies," *Physics*, vol. 7, pp. 311–317, Aug. 1936.

[25] D. Ingman, J. Suzdalnitsky, and M. Zeifman, "Constitutive dynamic-order model for nonlinear contact phenomena," *Journal of Applied Mechanics*, vol. 67, no. 2, pp. 383–390, 2000.

[26] M. Caputo and F. Mainardi, "Linear models of dissipation in anelastic solids," *Rivista Del Nuovo Cimento*, vol. 1, no. 2, p. 38, 1971.

[27] A. Pipkin and T. Roger, "A non-linear integral representation for viscoelastic behaviour," *Journal of Mechanical Physics and Solids*, vol. 16, pp. 59–72, 1968.

[28] A. Freed, K. Diethelm, and Y. Luchko, "Fractional-Order Viscoelasticity (FOV): Constitutive development using the fractional calculus: First annual report," *Fractional Calculus*, p. 138, 2002.

[29] K. D. Papoulia, V. P. Panoskaltsis, N. V. Kurup, and I. Korovajchuk, "Rheological representation of fractional order viscoelastic material models," *Rheologica Acta*, vol. 49, no. 4, pp. 381–400, 2010.

[30] M. Enelund and P. Olsson, "Damping described by fading memory—analysis and application to fractional derivative models," *International Journal of Solids and Structures*, vol. 36, no. 7, pp. 939–970, 1999.

[31] G. W. Scott Blair, B. C. Veinoglou, and J. E. Caffyn, "Limitations of the Newtonian time scale in relation to non-equilibrium rheological states and a theory of quasi-properties," *Proceedings of the Royal Society of London. Series A, Mathematical and Physical Sciences*, vol. 189, no. 1016, pp. 69–87, 1947.

[32] G. L. Slonimsky, "Laws of mechanical relaxation processes in polymers," *Journal of Polymer Science Part C: Polymer Symposia*, vol. 16, no. 3, pp. 1667–1672, 1967.

[33] M. Caputo and F. Mainardi, "A new dissipation model based on memory mechanism," *Pure and Applied Geophysics PAGEOPH*, vol. 91, no. 1, pp. 134–147, 1971.

[34] L. Debnath, "Recent applications of fractional calculus to science and engineering," *International Journal of Mathematics and Mathematical Sciences*, vol. 2003, no. 54, pp. 3413–3442, 2003.

[35] R. L. Bagley and P. J. Torvik, "Fractional calculus - A different approach to the analysis of viscoelastically damped structures," *AIAA Journal*, vol. 21, pp. 741–748, May 1983.

[36] N. Heymans, "Fractional calculus description of non-linear viscoelastic behaviour of polymers," *Nonlinear Dynamics*, vol. 38, no. 1-4, pp. 221–231, 2004.

[37] P. J. Torvik and R. L. Bagley, "On the appearance of the fractional derivative in the behavior of real materials," *Journal of Applied Mechanics*, vol. 51, no. 2, pp. 294–298, 1984.

[38] A. Lion, "On the thermodynamics of fractional damping elements," *Continuum Mechanics and Thermodynamics*, vol. 9, no. 2, pp. 83–96, 1997.

[39] M. A. Ezzat, A. S. El-Karamany, A. A. El-Bary, and M. A. Fayik, "Fractional calculus in one-dimensional isotropic thermo-viscoelasticity," *Comptes Rendus Mécanique*, vol. 341, pp. 553–566, July 2013.

[40] M. Ezzat, A. El-Karamany, and A. El-Bary, "Thermo-viscoelastic materials with fractional relaxation operators," *Applied Mathematical Modelling*, vol. 39, pp. 7499–7512, Dec. 2015.

[41] H. Schiessel, R. Metzler, A. Blumen, and T. F. Nonnenmacher, "Generalized viscoelastic models: Their fractional equations with solutions," *Journal of Physics A: Mathematical and General*, vol. 28, pp. 6567–6584, Dec. 1995.

[42] N. Heymans and J. C. Bauwens, "Fractal rheological models and fractional differential equations for viscoelastic behavior," *Rheologica Acta*, vol. 33, no. 3, pp. 210–219, 1994.

[43] I. Podlubny, "Matrix approach to discrete fractional calculus," *Fractional Calculus and Applied Analysis*, vol. 3, no. 4, 2000.

[44] H. Sun, W. Chen, H. Wei, and Y. Chen, "A comparative study of constant-order and variable-order fractional models in characterizing memory property of systems," *The European Physical Journal Special Topics*, vol. 193, no. 1, pp. 185–192, 2011.

[45] X. Su, D. Yao, and W. Xu, "A new method for formulating linear viscoelastic models," *International Journal of Engineering Science*, vol. 156, p. 103375, Nov. 2020.

[46] X. Su, W. Xu, W. Chen, and H. Yang, "Fractional creep and relaxation models of viscoelastic materials via a non-Newtonian time-varying viscosity: Physical interpretation," *Mechanics of Materials*, vol. 140, p. 103222, 2020.

[47] S. G. Samko and B. Ross, "Integration and differentiation to a variable fractional order," *Integral Transforms and Special Functions*, vol. 1, no. 4, pp. 277–300, 1993.

[48] L. Li, R. Lin, and T. Y. Ng, "A fractional nonlocal time-space viscoelasticity theory and its applications in structural dynamics," *Applied Mathematical Modelling*, vol. 84, pp. 116–136, Aug. 2020.

[49] S. Patnaik, J. P. Hollkamp, and F. Semperlotti, "Applications of variable-order fractional operators: A review," *Proceedings of the Royal Society A: Mathe-*

matical, Physical and Engineering Sciences, vol. 476, no. 2234, p. 20190498, 2020.

[50] M. Di Paola, G. Alotta, A. Burlon, and G. Failla, "A novel approach to nonlinear variable-order fractional viscoelasticity," *Philosophical Transactions of the Royal Society A: Mathematical, Physical and Engineering Sciences*, vol. 378, p. 20190296, May 2020.

[51] C. F. Lorenzo and T. T. Hartley, "Variable order and distributed order fractional operators," *Nonlinear Dynamics*, vol. 29, pp. 57–98, 2002.

[52] C. S. Drapaca and S. Sivaloganathan, "A fractional model of continuum mechanics," *Journal of Elasticity*, vol. 107, pp. 105–123, Apr. 2012.

[53] W. Sumelka and T. Blaszczyk, "Fractional continua for linear elasticity," *Archive of Applied Mechanics*, vol. 66, no. 3, pp. 147–172, 2014.

[54] W. Sumelka, K. Szajaek, and T. Lodygowski, "Plane strain and plane stress elasticity under fractional continuum mechanics," *Archive of Applied Mechanics*, 2014.

[55] W. Sumelka, "Fractional calculus for continuum mechanics – anisotropic non-locality," *Bulletin of the Polish Academy of Sciences Technical Sciences*, vol. 64, pp. 361–372, June 2016.

[56] R. Xiao, H. Sun, and W. Chen, "A finite deformation fractional viscoplastic model for the glass transition behavior of amorphous polymers," *International Journal of Non-Linear Mechanics*, vol. 93, pp. 7–14, July 2017.

[57] K. Adolfsson and M. Enelund, "Fractional derivative viscoelasticity at large deformations," *Nonlinear Dynamics*, vol. 33, pp. 301–321, 2003.

[58] W. Malesza, M. Macias, and D. Sierociuk, "Analytical solution of fractional variable order differential equations," *Journal of Computational and Applied Mathematics*, vol. 348, pp. 214–236, 2019.

[59] N. Makris, "Time-response functions of fractional derivative rheological models," *Rheol Acta*, vol. 59, pp. 846–873, 2020.

[60] L. Eldred, W. Baker, and A. Palazotto, "Numerical application of fractional derivative model constitutive relations for viscoelastic materials," *Computers & Structures*, vol. 60, no. 6, pp. 875–882, 1996.

[61] K. Oldham and J. Spanier, *The Fractional Calculus - Theory and Applications of Differentiation and Integration to Arbitrary Order*, vol. 111 of *Mathematics in Science and Engineering*. Elsevier, 1974.

[62] Z. Wei and N. Shimizu, "FE formulation for the viscoelastic body modeled by fractional constitutive law," *Acta Mechanica Sinica*, vol. 17, no. 4, pp. 354–365, 2001.

[63] A. Schmidt and L. Gaul, "Finite element formulation of viscoelastic constitutive equations using fractional time derivatives," *Nonlinear Dynamics*, vol. 29, pp. 37–55, 2002.

[64] N. Colinas-Armijo, S. Cutrona, M. Di Paola, and A. Pirrotta, "Fractional viscoelastic beam under torsion," *Communications in Nonlinear Science and Numerical Simulation*, vol. 48, pp. 278–287, July 2017.

[65] A. Pirrotta, S. Cutrona, S. D. Lorenzo, and A. D. Matteo, "Fractional viscoelastic Timoshenko beam deflection via single equation: Fractional Visco-Elastic Timoshenko Beam Deflection via Single Equation," *International Journal for Numerical Methods in Engineering*, vol. 104, no. 9, pp. 869–886, 2015.

[66] W. Sumelka, T. Blaszczyk, and C. Liebold, "Fractional Euler-Bernoulli beams: Theory, numerical study and experimental validation," *European Journal of Mechanics - A/Solids*, vol. 54, pp. 243–251, 2015.

[67] G. Alotta, O. Barrera, A. C. F. Cocks, and M. D. Paola, "On the numerical implementation of a 3D fractional viscoelastic constitutive model," in *2015 SIMULIA COmmunity Conference*, p. 13, 2015.

[68] G. Alotta and N. Colinas-Armijo, "Analysis of Fractional Viscoelastic Material With Mechanical Parameters Dependent on Random Temperature," *ASCE-ASME J Risk and Uncert in Engrg Sys Part B Mech Engrg*, vol. 3, p. 030906, Sept. 2017.

[69] G. Alotta, O. Barrera, A. Cocks, and M. Di Paola, "The finite element implementation of 3D fractional viscoelastic constitutive models," *Finite Elements in Analysis and Design*, vol. 146, pp. 28–41, July 2018.

[70] M. D. Paola and M. Zingales, "Exact mechanical models of fractional hereditary materials," *Journal of Rheology*, vol. 56, pp. 983–1004, Sept. 2012.

[71] G. Alotta, O. Barrera, A. C. F. Cocks, and M. D. Paola, "On the behavior of a three-dimensional fractional viscoelastic constitutive model," *Meccanica*, vol. 52, pp. 2127–2142, July 2017.

[72] G. Alotta, O. Barrera, and E. C. Pegg, "Viscoelastic material models for more accurate polyethylene wear estimation," *The Journal of Strain Analysis for Engineering Design*, vol. 53, pp. 302–312, July 2018.

[73] W. Glöckle and T. Nonnenmacher, "A fractional calculus approach to self-similar protein dynamics," *Biophysical Journal*, vol. 68, pp. 46–53, Jan. 1995.

[74] W. G. Glöckle and T. F. Nonnenmacher, "Fractional relaxation and the time-temperature superposition principle," *Rheologica Acta*, vol. 33, no. 4, pp. 337–343, 1994.

[75] W. G. Gloeckle and T. F. Nonnenmacher, "Fractional integral operators and Fox functions in the theory of viscoelasticity," *Macromolecules*, vol. 24, no. 24, pp. 6426–6434, 1991.

[76] N. Makris, "Three-dimensional constitutive viscoelastic laws with fractional order time derivatives," *Journal of Rheology*, vol. 41, no. 5, pp. 1007–1020, 1997.

[77] L. Ramirez and C. Coimbra, "A variable order constitutive relation for viscoelasticity," *Annalen der Physik*, vol. 16, no. 7-8, pp. 543–552, 2007.

[78] D.-L. Chen, P.-F. Yang, and Y.-S. Lai, "A review of three-dimensional viscoelastic models with an application to viscoelasticity characterization using nanoindentation," *Microelectronics Reliability*, vol. 52, pp. 541–558, Mar. 2012.

[79] G. Xiang, D. Yin, R. Meng, and C. Cao, "Predictive model for stress relaxation behavior of glassy polymers based on variable-order fractional calculus," *Polymers for Advanced Technologies*, vol. 32, pp. 703–713, Feb. 2021.

[80] J. Sweeney, M. Bonner, and I. Ward, "Modelling of loading, stress relaxation and stress recovery in a shape memory polymer," *Journal of the Mechanical Behavior of Biomedical Materials*, vol. 37, pp. 12–23, Sept. 2014.

[81] K. S. Fancey, "A mechanical model for creep, recovery and stress relaxation in polymeric materials," *Journal of Materials Science*, vol. 40, pp. 4827–4831, Sept. 2005.

[82] R. De Pascalis, I. D. Abrahams, and W. J. Parnell, "On nonlinear viscoelastic deformations: A reappraisal of Fung's quasi-linear viscoelastic model," *Proceedings of the Royal Society A: Mathematical, Physical and Engineering Sciences*, vol. 470, no. 2166, p. 20140058, 2014.

[83] K. L. Troyer, D. J. Estep, and C. M. Puttlitz, "Viscoelastic effects during loading play an integral role in soft tissue mechanics," *Acta Biomaterialia*, vol. 8, pp. 234–243, Jan. 2012.

[84] T. C. Doehring, A. D. Freed, E. O. Carew, and I. Vesely, "Fractional order viscoelasticity of the aortic valve cusp: An alternative to quasilinear viscoelasticity," *Journal of Biomechanical Engineering*, vol. 127, no. 4, pp. 700–708, 2005.

[85] D. O. Craiem, F. J. Rojo, J. M. Atienza, G. V. Guinea, and R. L. Armentano, "Fractional calculus applied to model arterial viscoelasticity," *Latin American Applied Research*, p. 5, 2008.

[86] A. D. Freed and K. Diethelm, "A K-BKZ formulation for soft-tissue viscoelasticity," *NASA*, 2005.

[87] A. D. Freed and K. Diethelm, "Fractional Calculus in Biomechanics: A 3D Viscoelastic Model Using Regularized Fractional Derivative Kernels with Application to the Human Calcaneal Fat Pad," *Biomechanics and Modeling in Mechanobiology*, vol. 5, no. 4, pp. 203–215, 2006.

[88] D. Craiem, F. J. Rojo, J. M. Atienza, R. L. Armentano, and G. V. Guinea, "Fractional-order viscoelasticity applied to describe uniaxial stress relaxation of human arteries," *Physics in Medicine and Biology*, vol. 53, no. 17, pp. 4543–4554, 2008.

[89] N. Grahovac and M. Žigić, "Modelling of the hamstring muscle group by use of fractional derivatives," *Computers & Mathematics with Applications*, vol. 59, pp. 1695–1700, Mar. 2010.

[90] V. Libertiaux and F. Pascon, "Differential versus integral formulation of fractional hyperviscoelastic constitutive laws for brain tissue modelling," *Journal of Computational and Applied Mathematics*, vol. 234, no. 7, pp. 2029–2035, 2010.

[91] F. Meral, T. Royston, and R. Magin, "Fractional calculus in viscoelasticity: An experimental study," *Communications in Nonlinear Science and Numerical Simulation*, vol. 15, no. 4, pp. 939–945, 2010.

[92] L. E. S. Ramirez and C. F. M. Coimbra, "On the selection and meaning of variable order operators for dynamic modeling," *International Journal of Differential Equations*, vol. 2010, pp. 1–16, 2010.

[93] Y. A. Rossikhin and M. V. Shitikova, "Application of fractional calculus for dynamic problems of solid mechanics: Novel trends and recent results," *Applied Mechanics Reviews*, vol. 63, no. 1, p. 010801, 2010.

[94] S. A. Bentil and R. B. Dupaix, "Exploring the mechanical behavior of degrading swine neural tissue at low strain rates via the fractional Zener constitutive model," *Journal of the Mechanical Behavior of Biomedical Materials*, vol. 30, pp. 83–90, Feb. 2014.

[95] E. T. Ali Tolga Petekkaya, "In vivo indenter experiments via ellipsoid indenter tips to determine the personal and local in-plane anisotropic mechanical behavior of soft biological tissues," *Journal of the Faculty of Engineering and Architecture of Gazi University*, pp. 63–72, 2011.

[96] N. Demirci and E. Tönük, "Non-integer viscoelastic constitutive law to model

soft biological tissues to in-vivo indentation," *Acta of Bioengineering and Biomechanics; 04/2014; ISSN 1509-409X*, 2014.

[97] B. Carmichael, H. Babahosseini, S. N. Mahmoodi, and M. Agah, "The fractional viscoelastic response of human breast tissue cells," *Physical Biology*, vol. 12, no. 4, p. 046001, 2015.

[98] Z. Dai, Y. Peng, H. A. Mansy, R. H. Sandler, and T. J. Royston, "A model of lung parenchyma stress relaxation using fractional viscoelasticity," *Medical Engineering & Physics*, vol. 37, pp. 752–758, Aug. 2015.

[99] E. Bologna, M. Di Paola, K. Dayal, L. Deseri, and M. Zingales, "Fractional-order nonlinear hereditariness of tendons and ligaments of the human knee," *Philosophical Transactions of the Royal Society A: Mathematical, Physical and Engineering Sciences*, vol. 378, p. 20190294, May 2020.

[100] J. E. Traver, I. Tejado, E. Mingorance, J. Prieto-Arranz, R. Mayordomo, A. M. Pérez-Pico, and B. M. Vinagre, "Fractional modeling of flexural behavior of toenail plates: First step for clinical purposes," *Medical Engineering & Physics*, vol. 90, pp. 23–32, Apr. 2021.

[101] Y. Peng, J. Zhao, and Y. Li, "A wellbore creep model based on the fractional viscoelastic constitutive equation," *Petroleum Exploration and Development*, vol. 44, pp. 1038–1044, Dec. 2017.

[102] F. Wu, J. F. Liu, and J. Wang, "An improved Maxwell creep model for rock based on variable-order fractional derivatives," *Environmental Earth Sciences*, vol. 73, pp. 6965–6971, June 2015.

[103] X.-B. Xu and Z.-D. Cui, "Investigation of a fractional derivative creep model of clay and its numerical implementation," *Computers and Geotechnics*, vol. 119, p. 103387, 2020.

[104] C. Han, X. Liu, D. Li, and Y. Shao, "Constitutive modeling of rock materials based on variable-order fractional theory," *Mechanics of Time-Dependent Materials*, 2021.

[105] F. Wu, R. Gao, J. Liu, and C. Li, "New fractional variable-order creep model with short memory," *Applied Mathematics and Computation*, vol. 380, p. 125278, Sept. 2020.

[106] H. Xu and X. Jiang, "Creep constitutive models for viscoelastic materials based on fractional derivatives," *Computers & Mathematics with Applications*, vol. 73, pp. 1377–1384, Mar. 2017.

[107] Y. Bouras, D. Zorica, T. M. Atanacković, and Z. Vrcelj, "A non-linear thermo-viscoelastic rheological model based on fractional derivatives for high temperature creep in concrete," *Applied Mathematical Modelling*, vol. 55, pp. 551–568, Mar. 2018.

[108] Z. Li, H. Wang, R. Xiao, and S. Yang, "A variable-order fractional differential equation model of shape memory polymers," *Chaos, Solitons & Fractals*, vol. 102, pp. 473–485, Sept. 2017.

[109] N. Colinas-Armijo, M. Di Paola, and A. Di Matteo, "Fractional viscoelastic behaviour under stochastic temperature process," *Probabilistic Engineering Mechanics*, vol. 54, pp. 37–43, 2018.

[110] H. Esmonde and S. Holm, "Fractional derivative modelling of adhesive cure," *Applied Mathematical Modelling*, vol. 77, pp. 1041–1053, 2020.

[111] R. Meng, D. Yin, C. Zhou, and H. Wu, "Fractional description of time-dependent mechanical property evolution in materials with strain softening behavior," *Applied Mathematical Modelling*, vol. 40, no. 1, pp. 398–406, 2016.

[112] R. Meng, D. Yin, H. Yang, and G. Xiang, "Parameter study of variable order fractional model for the strain hardening behavior of glassy polymers," *Physica A: Statistical Mechanics and its Applications*, vol. 545, p. 123763, May 2020.

[113] R. Meng, D. Yin, and C. S. Drapaca, "A variable order fractional constitutive model of the viscoelastic behavior of polymers," *International Journal of Non-Linear Mechanics*, vol. 113, pp. 171–177, 2019.

[114] R. Meng, D. Yin, and C. S. Drapaca, "Variable-order fractional description of compression deformation of amorphous glassy polymers," *Computational Mechanics*, vol. 64, no. 1, pp. 163–171, 2019.

[115] K. Diethelm, "An algorithm for the numerical solution of differential equations of fractional order," *Electronic Transactions on Numerical Analysis*, vol. 5, pp. 1–6, 1997.

[116] K. Diethelm, N. J. Ford, and A. D. Freed, "A Predictor-Corrector approach for the numerical solution of fractional differential equations," *Nonlinear Dynamics*, vol. 29, no. 3, p. 22, 2002.

[117] K. Adolfsson, M. Enelund, and S. Larsson, "Adaptive discretization of fractional order viscoelasticity using sparse time history," *Computer Methods in Applied Mechanics and Engineering*, vol. 193, no. 42-44, pp. 4567–4590, 2004.

[118] K. Diethelm, N. Ford, A. Freed, and Yu. Luchko, "Algorithms for the fractional calculus: A selection of numerical methods," *Computer Methods in Applied Mechanics and Engineering*, vol. 194, no. 6-8, pp. 743–773, 2005.

[119] D. Valério and J. Sá da Costa, "Variable-order fractional derivatives and their numerical approximations," *Signal Processing*, vol. 91, pp. 470–483, Mar. 2011.

[120] X. Li, "Numerical solution of fractional differential equations using cubic B-spline wavelet collocation method," *Communications in Nonlinear Science and Numerical Simulation*, vol. 17, pp. 3934–3946, Oct. 2012.

[121] I. Podlubny, *Fractional Differential Equations*, vol. 198 of *Academic Press*. Academic Press, 1999.

[122] N. J. Ford and A. C. Simpson, "The numerical solution of fractional differential equations: Speed versus accuracy," *Numerical Algorithms*, vol. 26, pp. 333–346, 2001.

[123] K. Diethelm and A. Freed, "An efficient algorithm for the evaluation of convolution integrals," *Computers & Mathematics with Applications*, vol. 51, pp. 51–72, Jan. 2006.

[124] W. Deng, "Short memory principle and a predictor–corrector approach for fractional differential equations," *Journal of Computational and Applied Mathematics*, vol. 206, pp. 174–188, Sept. 2007.

[125] B. Bagharzadehtvasani, A. H. Refahi Sheikhani, and H. Aminikhah, "A numerical scheme for solving variable order Caputo-Prabhakar fractional integro-differential equation," *International Journal of Nonlinear Analysis and Applications*, vol. 13, Jan. 2022.

[126] A. El Hamidi and A. Tfayli, "Identification of the derivative order in fractional differential equations," *Mathematical Methods in the Applied Sciences*, p. mma.6175, 2020.

[127] A. Beltempo, A. Bonelli, O. S. Bursi, and M. Zingales, "A numerical integration approach for fractional-order viscoelastic analysis of hereditary-aging structures," *International Journal for Numerical Methods in Engineering*, vol. 121, no. 6, pp. 1120–1146, 2020.

[128] R. Du and Z. Liang, "Two new approximations for variable-order fractional derivatives," *Discrete Dynamics in Nature and Society*, vol. 2017, pp. 1–10, 2017.

[129] D. Tavares, R. Almeida, and D. F. Torres, "Caputo derivatives of fractional variable order: Numerical approximations," *Communications in Nonlinear Science and Numerical Simulation*, vol. 35, pp. 69–87, June 2016.

[130] A. H. Bhrawy and M. A. Zaky, "Numerical algorithm for the variable-order Caputo fractional functional differential equation," *Nonlinear Dynamics*, vol. 85, pp. 1815–1823, Aug. 2016.

[131] C.-H. Lai and F. Magoules, *Numerical Methods for Fractional Calculus*. 2015.

[132] G. A. Anastassiou and I. K. Argyros, *Intelligent Numerical Methods: Applications to Fractional Calculus*, vol. 624 of *Studies in Computational Intelligence*. Cham: Springer International Publishing, 2016.

[133] T. A. Surguladze, "On certain applications of fractional calculus to viscoelasticity," *Journal of Mathematical Sciences*, vol. 12, no. 5, 2002.

[134] S. Samko, "Fractional integration and differentiation of variable order: An overview," *Nonlinear Dynamics*, vol. 71, pp. 653–662, Mar. 2013.

[135] H. Sun, A. Chang, Y. Zhang, and W. Chen, "A review on variable-order fractional differential equations: Mathematical foundations, physical models, numerical methods and applications," *Fractional Calculus and Applied Analysis*, vol. 22, no. 1, pp. 27–59, 2019.

[136] X.-J. Yang, *General Fractional Derivatives: Theory, Methods and Applications*. Boca Raton : CRC Press, Taylor & Francis Group, 2019.: Chapman and Hall/CRC, 1 ed., 2019.

[137] A. Bonfanti, J. L. Kaplan, G. Charras, and A. Kabla, "Fractional viscoelastic models for power-law materials," *Soft Matter*, vol. 16, no. 26, pp. 6002–6020, 2020.

[138] X.-J. Yang, F. Gao, and Y. Ju, *General Fractional Derivatives with Applications in Viscoelasticity*. Elsevier, 2020.

[139] G. Scarpi, "Sui Modelli Reologici Intermedi Per Liquidi Viscoelastici," *Accademia Delle Scienze*, 1973.

[140] D. Mozyrska and P. Ostalczyk, "Variable-, fractional-order Grünwald-Letnikov backward difference selected properties," in *2016 39th International Conference on Telecommunications and Signal Processing (TSP)*, (Vienna, Austria), pp. 634–637, IEEE, June 2016.

[141] A. Burlon, G. Alotta, M. Di Paola, and G. Failla, "An original perspective on variable-order fractional operators for viscoelastic materials," *Meccanica*, vol. 56, pp. 769–784, Apr. 2021.

[142] I. Podlubny, A. V. Chechkin, T. Skovranek, Y. Chen, and B. M. V. Jara, "Matrix approach to discrete fractional calculus II: Partial fractional differential equations," *Journal of Computational Physics*, vol. 228, no. 8, pp. 3137–3153, 2009.

[143] S. G. Samko and A. A. Kilbas, *Fractional Integrals and Derivatives*. Gordon and Breach Science Publishers, 1993.

[144] R. Garrappa, A. Giusti, and F. Mainardi, "Variable-order fractional calculus: A change of perspective," *Communications in Nonlinear Science and Numerical Simulation*, vol. 102, p. 105904, Nov. 2021.

[145] A. Giusti, I. Colombaro, R. Garra, R. Garrappa, and A. Mentrelli, "On variable-order fractional linear viscoelasticity," *Fractional Calculus and Applied Analysis*, vol. 27, pp. 1564–1578, Aug. 2024.

[146] T. Nguyen, H. Jerryqi, F. Castro, and K. Long, "A thermoviscoelastic model for amorphous shape memory polymers: Incorporating structural and stress relaxation," *Journal of the Mechanics and Physics of Solids*, vol. 56, no. 9, pp. 2792–2814, 2008.

[147] Y. Gao, D. Yin, and B. Zhao, "A Variable-Order Fractional Constitutive Model to Characterize the Rate-Dependent Mechanical Behavior of Soft Materials," *Fractal and Fractional*, vol. 6, p. 590, Oct. 2022.

[148] D20 Committee, "D638-14 Test Method for Tensile Properties of Plastics," tech. rep., ASTM International.

[149] D. Committee, "D618-13 Standard Practice for Conditioning Plastics for Testing," tech. rep.

[150] R. Meng, L. Cao, and Q. Zhang, "Study on the performance of variable-order fractional viscoelastic models to the order function parameters," *Applied Mathematical Modelling*, vol. 121, pp. 430–444, Sept. 2023.

[151] B. Han, D. Yin, and Y. Gao, "Analysis of the variable-order fractional viscoelastic modeling with application to polymer materials," *Polymers for Advanced Technologies*, vol. 34, no. 8, pp. 2707–2720, 2023.

[152] E28 Committee, "E8-21 Test Methods for Tension Testing of Metallic Materials," tech. rep., ASTM International.

APPENDICES

A. VARIABLE ORDER UMAT SUBROUTINE CODE

```
C Variable order UMAT  code for 3D FRACTIONAL Variable Order Scott Blair Element
C Muhammed Cakir, METU
C Ergin Tonuk (Dr.), METU

      SUBROUTINE UMAT(STRESS,STATEV,DDSDDE,SSE,SPD,SCD,
     1 RPL,DDSDDT,DRPLDE,DRPLDT,
     2 STRAN,DSTRAN,TIME,DTIME,TEMP,DTEMP,PREDEF,DPRED,CMNAME,
     3 NDI,NSHR,NTENS,NSTATV,PROPS,NPROPS,COORDS,DROT,PNEWDT,
     4 CELENT,DFGRD0,DFGRD1,NOEL,NPT,LAYER,KSPT,KSTEP,KINC)
C
      INCLUDE 'ABA_PARAM.INC'
C
      CHARACTER*80 CMNAME
      DIMENSION STRESS(NTENS),STATEV(NSTATV),
     1 DDSDDE(NTENS,NTENS),
     2 DDSDDT(NTENS),DRPLDE(NTENS),
     3 STRAN(NTENS),DSTRAN(NTENS),TIME(2),PREDEF(1),DPRED(1),
     4 PROPS(NPROPS),COORDS(3),DROT(3,3),DFGRD0(3,3),DFGRD1(3,3)
      DIMENSION SVector(NTENS)
      COMMON str(101,1,8,6)
      real*8 bnm,eps,epsvol,Tshr,TBulk,VO(101)
      dimension bnm(kinc+1),eps(kinc+1,ntens),epsvol(kinc+1),
     1 Tshr(3)
C
C The "CommonBlock" must be modified according to the model size (number of elements) and
C the total number of steps.
C For the entries related to the Bulk Modulus, Shear Modulus, and Poisson Ratio,
C the corresponding variables and their dimensions must be defined in the preamble,
C with a suitable variable assigned to each.
C
      str(kinc,noel,npt,1:ntens)=stran(1:ntens)
      eps(1:kinc,1:ntens)=str(1:kinc,noel,npt,1:ntens)

C DEFINITION OF VARIABLE ORDER STARTS HERE ***

                          WRITE(*, *)  'ORDER:', VO(kinc)

C DEFINITION OF VARIABLE ORDER ENDS HERE  ***

      bnm(1)=1
      do k=1,kinc
```

```
          bnm(k+1)=(k-1-VO(kinc))*bnm(k)/(k)
        end do
C
        eps(kinc+1,1:ntens)=eps(kinc,1:ntens)+dstran(1:ntens)
        epsvol=sum(eps(:,1:ndi),dim=2)
C
        TBulk=0.0
        do k1=1,kinc+1
          TBulk=TBulk+props(1)*epsvol(kinc-k1+2)*bnm(k1)/(dtime**VO(kinc))
        end do
C
        do k2=1,ndi
          Tshr(k2)=0.0
          do k1=1,kinc+1
           Tshr(k2)=Tshr(k2)+props(2)*eps(kinc-k1+2,k2)*bnm(k1)/(dtime**VO(kinc))
          end do
        end do
        Tshr=Tshr*4.0/3.0
C
        SumTshr=sum(Tshr)
C
        do k2=1,ndi
          SVector(k2)=TBulk+Tshr(k2)-(SumTshr-Tshr(k2))/2.0
        end do
C
        do k2=1,ndi
          I1=ndi+k2
          SVector(I1)=0.0
         do k1=1,kinc+1
           SVector(I1)=SVector(I1)+props(2)*eps(kinc-k1+2,I1)*bnm(k1)/(dtime**VO(kinc))
         end do
        end do
C
        stress=SVector
C
         term1=props(1)/(dtime**VO(kinc))
         term2=props(2)/(dtime**VO(kinc))
         term3=term1+4.0*term2/3.0
C
        do k1=1,ndi
          ddsdde(k1,k1)=term3
        end do
C
        term4=term1-2.0*term2/3.0
C
        do k1=2,ndi
          do k2=1,k1-1
```

```
            ddsdde(k1,k2)=term4
            ddsdde(k2,k1)=term4
        end do
    end do
C
    do k1=1,ndi
        k2=ndi+k1
        ddsdde(k2,k2)=term2
    end do
C
    RETURN
    END
```

B. CALCULATION OF THE GRÜNWALD CONSTANTS OF ALG.1, EQ. 3.33

```
function [ w ] = VO_wcoeffsU( beta,n )
%   beta is the Variable Order Fractional order at particular time instant
w(1)=1;
if n>1
for j=1:n
     w(j+1)=w(j)*(j-1-beta)/j;
     if j+1>n-1; break
     end
end
end
end
```

C. CALCULATION OF THE STRESS RESPONSE OF A VARIABLE ORDER FRACTIONAL VISCOELASTIC MATERIAL AS PER ALG.2, EQ. 3.34

```
% VO MODEL
% VOF Scott Blair Model

%%% MATERIAL DEFINITION STARTS HERE %%%
% Define material parameters E(1x1), theta(1x1), beta(1xn)
% Define problem dt(1x1), T(1xn), t(1xn), c(1x1)
%%% MATERIAL DEFINITION ENDS HERE %%%

eps = c*t; % Calculate Strain history
n = length(eps);
Ebeta = E*theta.^beta;
w(1)=1;
eta = Ebeta.*dt.^(-beta);
VOUp = zeros(n);
W = zeros(n);
for k = 1:n % row
w = VO_wcoeffsU(beta(k),n); %% Calculation of Grünwald constants
    for i = 1:k % column
         VOUP(k,i) = w(k-i+1)*eta(k);
    end
end
for h = 1:n
    eta(h) = Ebeta(h)*dt.^(-beta(h));
end
S = (VOUp*eps');
```

CURRICULUM VITAE

PERSONAL INFORMATION

Surname, Name : Çakır, Muhammed
Nationality : Turkish (T.C.)

EDUCATION

Degree	Institution	Year of Graduation
M.S.	METU	2017
B.S.	Ege University	2011
High School	Kaman Lisesi	2004

PROFESSIONAL EXPERIENCE

Year	Place	Enrollment
2 years	TUSAS	Design Engineer
8 years	METU	Research Assistant
2 years	Nachi GmBH	Project Engineer

PUBLICATIONS

-